UNIVERSITY OF CALIFORNIA
Los Angeles

Estimating Stochastic Volatility within a Trading Day

A dissertation submitted in partial satisfaction
of the requirements for the degree
Doctor of Philosophy in Economics

by

Sibo Yan

2017

ABSTRACT OF THE DISSERTATION

Estimating Stochastic Volatility within a Trading Day

by

Sibo Yan
Doctor of Philosophy in Economics
University of California, Los Angeles, 2017
Professor Bryan C. Ellickson, Chair

This thesis uses high-frequency data to characterize the volatility of asset prices within a trading day. The estimation procedure applies the generalized method of moments (GMM) to the Heston (1993) model of stochastic volatility. I apply the estimation to SPY in chapter 1 and to other 8 assets in chapter 2. I compare estimation results and discuss the implications and applicability of the model. In Chapter 3 I examine the path behavior of realized volatility and provide evidence that it is important to allow jumps in the Heston model.

The dissertation of Sibo Yan is approved.

Rosa Matzkin

Francis Longstaff

Zhipeng Liao

Bryan C. Ellickson, Committee Chair

University of California, Los Angeles

2017

To my love,

who have been with me every step of the way in my hard days

TABLE OF CONTENTS

LIST OF FIGURES

LIST OF TABLES

ACKNOWLEDGMENTS

I would like to thank first and foremost my advisor Bryan Ellickson, who has been providing guidance and support for me throughout my entire thesis research. I would also like to thank the other members of my committee Francis Longstaff, Rosa Matzkin, and Zhipeng Liao for all of their help. I would especially like to thank my group members Duke Whang, Hongxiang Xu and Miao Sun for their comments and inspiration.

VITA

2011	B.S.c (Mathematics and Economics and Minor in Information Technology), Hong Kong University of Science and Technology.
2013	M.A. (Economics), UCLA, Los Angeles, California.
2013	Ph.D Candidate (Economics), UCLA, Los Angeles, California.
2012–2016	Teaching Fellow, Department of Economics, UCLA.
2017	M.S. (Statistics), UCLA, Los Angeles, California.

CHAPTER 1

Estimating Intraday Stochastic Volatility

1.1 Introduction

Understanding volatility and its dynamics is an important subject in modern finance. As the primary measure of risk, volatility drives the construction of optimal portfolios, the hedging and pricing of options and other derivative securities or the determination of a firm's value while exposing to a variety of risk factors. It also plays a critical role in discovering trading and investment opportunities which provide an attractive risk-return trade-off.

It is therefore not surprising that numerous efforts have been spent on modeling the volatility process. In particular, continuous-time stochastic volatility(SV) models are widely used in the empirical finance literature, surveyed in Part II of *The Handbook of Financial Time Series* (Anderson et al. (2009)). The Heston (1993) is a popular SV model due to its analytical tractability.

Realized volatility is one of the most natural and model-free methods to measure stock price volatility (Anderson and Bollerslev (1997)). It is defined as the cumulative summation of the squared log returns of discretely sampled stock prices over a time interval. The theory of stochastic integration implies that realized volatility (RV) converges uniformly in probability to the quadratic variation (QV) over the same time interval when prices are sampled more and more frequently. Therefore since it became available, using high-frequency trading data to approximate quadratic variation has been viewed optimistically. (Merton (1980) and Nelson (1992)).

However, because of concerns about market microstructure noise, it has become a com-

mon practice to sample prices at most once every five minutes when computing daily RV[1].

Bollerslev and Zhou (2002) is one of the pioneering studies of applying daily RV to the estimation of SV models. They use the stochastic differential equation that characterizes the motion of the continuous-time volatility process of the Heston model to derive moment conditions for the sequence of daily QV. These moment conditions allow estimation of the three parameters of the Heston model using the generalized method of moments (GMM). Because QV is latent, Bollerslev and Zhou (2002) replace QV with RV using prices sampled every 5 minutes to reduce the measurement error.

Bollerslev and Zhou (2002) estimate their model using Deutsch Mark U.S. Dollar spot exchange rates. I found three papers citing Bollerslev and Zhou (2002) that apply their methodology to stocks and ETFs. Corradi and Distaso (2006) test their model with General Electric, Intel and Microsoft stocks. Garcia, Lewis, Pastorello and Renault (2011) and Bergantini (2013) use the $S\&P$ 500 stock index. All of these studies focus on quadratic variation over the trading day and sample prices once every five minutes. In contrast, we focus on the behavior of quadratic variation over short intervals (100 seconds) within the trading day.

The analytical framework used in this thesis builds on Sun (2016), which differs from Bollerslev and Zhou (2002) in several important aspects:

- Realized volatility is computed for each 100-second interval which allows us to examine the path behavior of stochastic volatility within a trading day.

- Concerned about market microstructure noise, Bollerslev and Zhou (2002) assume prices are sampled with error. They decrease the sampling frequency of stock prices to once every five minutes to reduce the effects of this measurement error. We assume instead that realized volatility measure quadratic variation with error, and introduce an assumption that justify replacing quadratic variations with realized volatilities. The 100-second RVs behave better than the literature suggests. Figure 1.1 plots the

[1]See chapter 7, Figure 7.1: "Volatility Signature Plots" in Aït-Sahalia and Jacod (2014) and Aït-Sahalia, Mykland and Zhang (2005, 2006)

daily integrated realized volatility using SPY sampled at 5-minute frequency on the horizontal axis and the daily average of 100-second RV using prices sampled every second on the vertical axis. The average 100 second RV is noisy but lie reasonably close to the daily RV except for a few outliers.

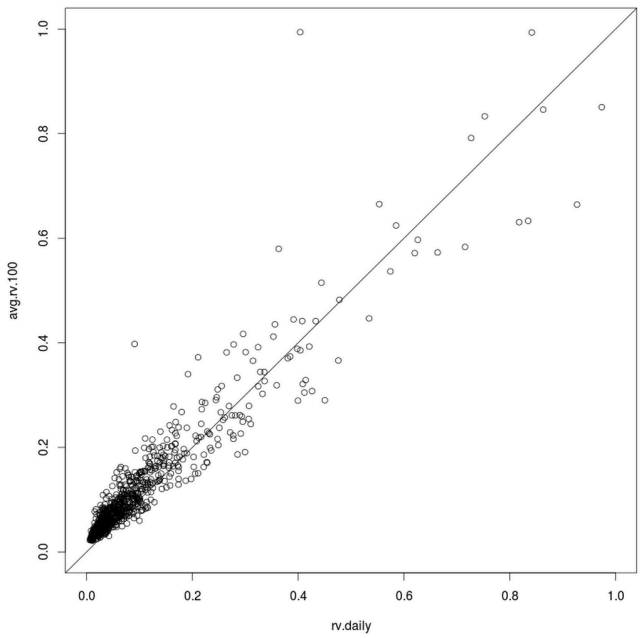

Figure 1.1: Daily RV versus the average of 100-sec RV

- Bollerslev and Zhou (2002) develop a moment condition for the conditional second moment of quadratic variation, using nuisance parameters to deal with measurement error associated with replacing quadratic variations by realized volatility. Instead, we provide explicit formulas for the asymptotic autocovariances of quadratic variation which we use to derive second order moment conditions to estimate volatility of volatility that are unaffected by measurement error.

This chapter makes several important modifications to Sun (2016) that bolsters the reliability of our estimation framework. First, Sun (2016) uses the first order moment condition

for realized volatility to estimate the speed of mean reversion and asymptotic mean of the Heston model for SPY, an exchange traded fund tracking the S&P 500 index. He substitutes estimates of these two parameters into the second-moment conditions for lag 1 and lag 2 autocorrelations in order to estimate the volatility-of-volatility parameter of the Heston model. In contrast, I estimate all three parameters simultaneously with all the moment conditions to insure the standard errors of parameter estimates are correct. Second, I take advantage of the fact that we can freely choose the time scale to pick the time unit to be a year. In this way, I increase the magnitude of realized volatility over a 100-second interval, which avoids computational errors in the GMM estimation.

To put my research into practice, I estimate the Heston model using daily RVs with prices sampled once every 5 minutes. I compare the results with Bollerslev and Zhou (2002) which clarifies the differences between their approach and ours. I found 67 days missing in the data sample used in Sun (2016), which I added to the data set. I also verified that every trading day in the entire 8 years of the data sample is now included.

The time frame of my study, 2007-2014, is an interesting period containing the great recession and the sovereign debt crisis, both of which had tremendous impact on market volatility. Focusing on the behavior of the quadratic variation within a single trading day avoids the problem of the time gap between one trading day and the next. On any day, the market is open at most 6.5 hours. When it closes, it remains closed for at least 17.5 hours (longer over a weekend). Because we analyze volatility within a trading day, there is no gap between the intervals we are considering. Splitting a single trading day into 234 100-second intervals yield a number of observations similar to the number of daily quadratic variations in a year (252 per year on average for our sample). Furthermore, I can pool days by assuming that the parameters of the Heston model are invariant over the days contained in a pool, provided I do not link the the final quadratic variation of one day to the initial quadratic variation of the next. In a five-day pool, there are 1,710 100-second quadratic variations, comparable to five years of daily quadratic variation. This pooling technique is very useful in improving the standard errors of the parameter estimates and diminishing the influence of the outliers in the data.

The rest of the chapter is structured as follows: Section 1.2 introduces the Heston model of intraday stochastic volatility and the economic intuition behind the model. Section 1.3 introduces the estimation framework. Section 1.4 presents the empirical results. Section 1.5 provides additional evidence for our model. Section 1.6 compares our intraday model with a variation of the model estimated using daily RV. Section 1.7 concludes the chapter.

1.2 The Heston model of intraday volatility

Let $X_t = \log(S_t)$ denote the log of the stock price S_t at time t. Assume that $W = (W_t)_{t\geq 0}$ is a standard Wiener process. A process $(X_t)_{t\geq 0}$ follows a *geometric Brownian motion* if

$$X_t = X_0 + bt + \sqrt{c}\, W_t \qquad (t \geq 0)$$

where b (the *drift*) and c (the *volatility*) are constants.[2]

The Heston (1993) model replaces the constants b and c by stochastic processes $b = (b_t)_{t\geq 0}$ and $c = (c_t)_{t\geq 0}$. The log-price process becomes

$$X_t = X_0 + \int_0^t b_s ds + \int_0^t \sqrt{c_s}\, dW_s \quad (t \geq 0) \tag{1.1}$$

and the volatility process $c = (c_t)_{t\geq 0}$ is the solution of the stochastic differential equation (SDE)

$$dc_t = \kappa(\bar{c} - c_t)dt + \gamma\sqrt{c_t}\, dB_t \quad (t \in [0,1]) \tag{1.2}$$

where $B = (B_t)_{t\geq 0}$ is a standard Wiener process, possibly correlated with the Wiener process W. The processes b and c are assumed to be adapted to the filtration generated by (B, W). The parameter $\bar{c}$ is the asymptotic mean of the process c, κ is the rate of reversion to the mean and γ^2 is the volatility of volatility.[3] All three parameters are assumed to be strictly positive and to obey the Feller condition $2\kappa\bar{c} > \gamma^2$, which insures that, with probability one,

[2] In the literature, $\sqrt{c}$ is often called the volatility.

[3] In the literature, γ is often called the volatility of volatility.

c_t remains strictly positive for all t.

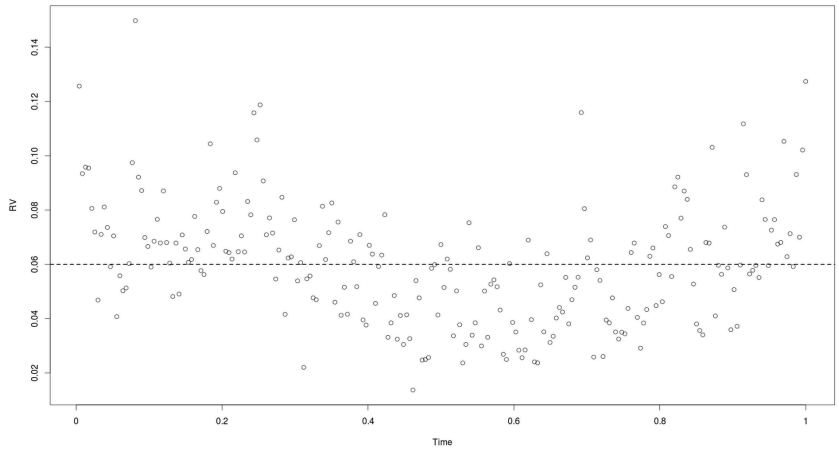

Figure 1.2: RV, 1/6/2011

Figure 1.2 plots the sequence of realized volatilities for SPY, an exchange-traded fund that tracks the $S\&P$ 500 index for a typical trading day, January 6, 2011. I use "Time" to indicate the fraction of the trading day expired since the market open. The stochastic differential equation of the Heston model characterizes the evolvement of the spot volatility c_t throughout the entire trading day. The quadratic variation for a 100-second interval is the integral of c_t over the interval. The GMM estimate of the asymptotic mean $\widehat{\bar{c}} = 0.060$ (indicated by the horizontal line) is an annual rate: i.e, the annual log return of a geometric Brownian motion with this volatility would have a standard deviation of $\sqrt{0.060} = 0.245$ (24.5%). The estimated speed of mean reversion for this trading day implies that on average 21% of the gap between c_t and $\bar{c}$ is eliminated within one hundred seconds. In Figure 1.2 the process has fallen well below the asymptotic mean by the seventh block, 700 seconds after the market opens.

The Heston model applied to intraday volatility has a nice economic interpretation. The value of c_t is the variance of instantaneous log return dX_t at time t. Our empirical results

suggest that the volatility of asset prices typically starts way above the asymptotic mean of the trading day. With a fast mean reversion, it quickly settles to a dynamic balance between the inflow of additional market uncertainty and reduction of uncertainty by market participants. They have a strong incentive to resolve uncertainty when c_t is above $\bar{c}$ which drives c_t downward, but have less incentive to do so when c_t is below $\bar{c}$, allowing c_t to move up.

The parameters of the Heston model are fixed for each day, but they are allowed to vary across different days or different pools. The time series for the asymptotic mean $\bar{c}$ and volatility of volatility γ^2 move smoothly overall in our 2007-2014 sample period but spike to a huge level at times of financial crisis. These parameters of the Heston model are natural candidates for state variables in modeling the long run behavior of stock prices.

1.3 The GMM estimation framework

I begin this section by introducing the definition of quadratic variation and realized volatility over a time interval, which I will refer to as a block. After that, I present the conditional moments of RV derived from the stochastic differential equation of the Heston model that are used to estimate the parameters of the model.

A trading day is represented by the interval $[t_0, t_N]$ where t_0 the market open and t_N the market close. The trading day is partitioned into one-second intervals with the set of times

$$\Pi^N = \{t_0, t_1, ..., t_N\} \qquad (t_0 < t_1 < ... < t_N)$$

where $N = 23{,}400$ is the number of one-second intervals in a 6.5-hour trading day. The trading day is also divided into 100-second intervals (*blocks*) using the set of times $\Pi^M \subset \Pi^N$,

$$\Pi^M = \{t_0, t_1, ..., t_M\} \qquad (t_0 < t_1 < ... < t_M)$$

where $M = 234$ is the number of 100-second intervals in a 6.5-hour trading day.

The *quadratic variation* $C_{t,t+h}$ *of the Heston model over the block* $[t, t+h]$ is given by

$$C_{t,t+h} = \frac{1}{h}\int_t^{t+h} c_s ds \tag{1.3}$$

I choose the time unit to be a year. Consequently, h here is equal to the length of a 100-second block relative to a calendar year of 365.25 days: $h = 100/(3600 \times 24 \times 365.25) = 1/315576$.

Let

$$\widehat{C}_{0,t} = \sum_{t_i \le t} (\Delta X_{t_i})^2 \quad (t \in [t_0, t_N], t_i \in \Pi^N)$$

represent the cumulative sum of squared log returns over the interval $[t_0, t] \subset [t_0, t_N]$. The *realized variation* $\widehat{C}_{t,t+h}$ *over the block* $[t, t+h]$, scaled to a rate per trading day, is given by

$$\widehat{C}^N_{t,t+h} := \frac{1}{h}(\widehat{C}^N_{0,t+h} - \widehat{C}^N_{0,t})$$

For the Heston model, the quadratic variations associated with any pair of adjacent blocks $[t, t+h]$ and $[t+h, t+2h]$ satisfies the following moment condition[4].

$$\mathbb{E}[C_{t+h,t+2h} - (1-\beta)C_{t,t+h} - \beta\bar{c} \mid \mathcal{F}_t] = 0 \tag{1.4}$$

where $\beta = 1 - e^{-\kappa h} \in (0,1)$ and $\mathcal{F}_t$ is the σ-algebra at time t belonging to the filtration of sigma-algebras generated by the Wiener processes in the price process and the volatility process of the Heston model. This equation establishes an autoregression model for the sequence of quadratic variations for the blocks of a trading day.

Equation (1.4), which is equation (1.20) in Sun (2016) corresponds to equation (4) in Bollerslev and Zhou (2002). Because they sample prices only once every five minutes, Bollerslev and Zhou (2002) assume that the quadratic variation can be replaced by realized volatilities. In contrast, we assume QV is measured by RV with an error and introduce an assumption that allows us to replace QVs with RVs without affecting the coefficients of the moment condition. Let $\widehat{C}_{t,t+h} = C_{t,t+h} + \nu_{t,t+h}$ for each time block $[t, t+h]$, where $\nu_{t,t+h}$

[4]The detailed proof can be found in Sun (2016)

is the measurement error.

Assumption 1.

$$\mathbb{E}[\nu_{t,t+h} \mid \mathcal{F}_s] = 0 \qquad for \quad all \quad s \leq t$$

The interpretation of the assumption is straightforward: the gap between the RV of the observed price process and the QV implied by the Heston model is mean zero and uncorrelated with what happens before the beginning of the block.

After replacing the QVs in equation (1.4) by the corresponding RVs of the observed price process, Assumption 1 implies that

$$\mathbb{E}[\widehat{C}_{t+h,t+2h} - (1-\beta)\widehat{C}_{t,t+h} - \beta\bar{c} \mid \mathcal{F}_t] = 0 \tag{1.5}$$

Because $\alpha = 1 - \beta$, equation 1.5 can be rewritten as

$$\mathbb{E}[\widehat{C}_{t+h,t+2h} - \widehat{C}_{t,t+h} \mid \mathcal{F}_t] = \beta(\bar{c} - \mathbb{E}[\widehat{C}_{t,t+h} \mid \mathcal{F}_t])$$

In other words, conditioned on $\mathcal{F}_t$, β is the average fraction of the gap between the conditional expectation of $\widehat{C}_{t,t+h}$ and the asymptotic mean $\bar{c}$ eliminated over the interval $[t+h, t+2h]$. Although in the GMM, I estimate β directly because of its natural interpretation of the speed of mean reversion, I can always recover κ as $\kappa = -\frac{1}{h}log(1-\beta)$.

Replacing quadratic variations by realized volatilities makes $\widehat{C}_{t,t+h}$ necessarily endogenous. To generate a consistent estimator with GMM, I use instrumental variables. Instrumental variables should be both valid and relevant: orthogonal to the error term and correlated with $\widehat{C}_{t,t+h}$. The lagged RV and its powers satisfy both conditions: they are independent of the error term according to assumption 1 and equation 1.4, and realized volatility is serially correlated. The number of instrumental variables should be no less than the number of parameters. I use the lagged RV, its square root and its fourth root as the

instruments, generating the following moment conditions for GMM:

$$\begin{aligned}
\mathbb{E}[\widehat{C}_{t+h,t+2h} - (1-\beta)\widehat{C}_{t,t+h} - \beta\bar{c}] &= 0 \\
\mathbb{E}[(\widehat{C}_{t+h,t+2h} - (1-\beta)\widehat{C}_{t,t+h} - \beta\bar{c})\widehat{C}_{t-h,t}] &= 0 \\
\mathbb{E}[(\widehat{C}_{t+h,t+2h} - (1-\beta)\widehat{C}_{t,t+h} - \beta\bar{c})\widehat{C}^{1/2}_{t-h,t}] &= 0 \\
\mathbb{E}[(\widehat{C}_{t+h,t+2h} - (1-\beta)\widehat{C}_{t,t+h} - \beta\bar{c})\widehat{C}^{1/4}_{t-h,t}] &= 0
\end{aligned} \tag{1.6}$$

These moment conditions provide the basis for estimating the parameters κ (or β) and $\bar{c}$ of the Heston model. The volatility of volatility parameter γ^2 is estimated using moment conditions based on the asymptotic autocovariances of the sequence of quadratic variations. The formulas for these asymptotic autocovariances, which depend only on the mean reversion parameter β, are given as[5]:

$$\begin{aligned}
V_0 &= (\frac{\gamma}{\kappa h})^2(h - \frac{\beta}{\kappa})\bar{c} \\
V_1 &= (\frac{\gamma}{\kappa h})^2\frac{\beta^2}{2\kappa}\bar{c} \\
V_j &= (1-\beta)V_{j-1} \quad (j \geq 2)
\end{aligned}$$

Let $V_j := \lim_{t\to\infty} \mathbb{E}[(C_{t,t+h} - \bar{c})(C_{t+jh,t+(j+1)h} - \bar{c})]$, V_0 is the asymptotic variance, V_1 is one-period lagged asymptotic covariance and V_j is the asymptotic autocovariance of lag $j \geq 2$. To obtain moment conditions for the autocovariances of RVs, we need another assumption on the measurement error.

Assumption 2. *The errors $\nu_{t,t+h}$ are i.i.d., and independent of the volatility process c with mean 0 and finite positive variance.*

Let $\widehat{V}_j := lim_{t\to\infty}\mathbb{E}[(\widehat{C}_{t,t+h} - \bar{c})(\widehat{C}_{t+h,t+2h} - \bar{c})]$, assumption 2 implies that $\widehat{V}_0 = V_0 + \nu^2$ and $\widehat{V}_j = V_j$ for $j \geq 1$[6]. In other words, the asymptotic variance V_0 is not robust to

[5]See Proposition 2.2 in Sun (2016) for a detail proof

[6]See proposition 2.6 of Sun (2016) for the proof.

measurement error but the asymptotic autocovariances V_j are. I will use V_1 and V_2 to estimate the volatility-of-volatility parameter γ^2. Specifically, the following moment conditions are established.

$$\begin{aligned}\mathbb{E}[(\widehat{C}_{t,t+h}-\bar{c})(\widehat{C}_{t+h,t+2h}-\bar{c})-(\frac{\beta^2\bar{c}}{2\kappa^3h^2})\gamma^2]=0\\ \mathbb{E}[(\widehat{C}_{t,t+h}-\bar{c})(\widehat{C}_{t+2h,t+3h}-\bar{c})-(\frac{(1-\beta)\beta^2\bar{c}}{2\kappa^3h^2})\gamma^2]=0\end{aligned} \tag{1.7}$$

In contrast to Sun(2016), I conduct non-linear joint estimation of β, $\bar{c}$ and γ^2. I rescale the moment conditions to make them have the same order of magnitude. Because the error terms are serially correlated, I use a heteroskedasticity and autocorrelation consistent (HAC) covariance matrix estimator with a Bartlett kernel (Newey and West (1987)). The model was estimated using the R gmm package (see Chausse (2010)).

The second-moment condition used in Bollerslev and Zhou (2002) is different from this thesis. Using our notation, their second-order moment condition is:

$$\mathbb{E}[C^2_{t+h,t+2h}-HC^2_{t,t+h}-IC_{t,t+h}-J]=0 \tag{1.8}$$

where H, I and J are constants depend only on the parameters h, κ, $\bar{c}$ and γ[7]. They replace the daily quadratic variations with daily realized variations. Because the measurement error for the second order moments does not disappear when prices are sampled infrequently, they introduce a "nuisance parameter" in an effort to deal with that issue. They use the moment conditions (1.4) and (1.8) with QVs replaced by RVs as the basic conditions for estimation. As in this thesis they use functions of RVs lagged one period as instruments, obtaining a total of six moment conditions.

[7]Please see the formal derivation in Appendix A.2 of BZ

1.4 Empirical results

1.4.1 The data sample

The high frequency data for this research comes from the NYSE Trade and Quote (TAQ) database provided by Wharton Research Data Services (WRDS). The sample includes price, number of shares and time of each transaction (to the nearest second). I include trades from 9:30 AM to 4:00 PM, coinciding with the market open and close. Trades that were canceled or illegitimate are removed using the TAQ condition codes[8].

Table 1.1: Trades per second and inactive time stamps for SPY

Year	2007	2008	2009	2010	2011	2012	2013	2014
Trades/second	13.4	12.1	14.1	12.9	13.4	13.5	13.5	15.0
Inactive (%)	34.4	17.0	18.1	20.2	17.6	25.1	26.7	22.6

Although SPY is heavily traded, many time stamps have no trade. As reported in Table 1.1, the average number of trades per second for each of the eight years of our study ranges from 12.1 to 15.0. Nevertheless, the percentage of time stamps with no trade ("inactive" time stamps) is large, ranging from a high of 34.4% in 2007 to a low of 17.0% in 2011. If the arrival of trades were Poisson with an arrival rate of 12 trades per second , then the probability a given second has no trade would be $e^{-12} = 6.1 \times 10^{-6}$. Instead roughly one in five time stamps is inactive. Clearly the counting process that counts the arrival of trades is not Poisson.

For time stamps with more than one trade, I use the *median share-price*, the median of the distribution of price per share for the time stamp, regarding each share traded as one single observation. For time stamps with no trade, I used the median share-price from the most recent time stamp which had a trade. This yields the series of prices for each second of the trading day that I use to calculate the sample quadratic variation for each

[8]The TAQ "condition codes" imply trades that were canceled or flagged as illegitimate

[8]'*', '**' and '***' indicate the z-score is larger than 1.645, 1.96 and 2.33

100-second block. Interestingly, this will not be much of an issue in the future as starting from 2015, the time stamps of the TAQ files are measured in milliseconds instead of seconds. At this resolution, it is very likely that most active seconds for SPY would have at most one trade, and the realized volatility for each 100-second block could be calculated as the sum of squared millisecond returns over the block.

The only other filtering of the data other than the TAQ condition codes is elimination of bouncebacks, which are defined in Aït-Sahalia and Jacod (2014)[9] as:

> bouncebacks are price observations that are either higher or lower than the sequence of prices that both immediately precede and follow them. Such prices generate a log-return from one transaction to the next that is large in magnitude and is followed immediately by a log-return of the same magnitude but of the opposite sign, so that the price returns to its starting level before that particular transactions

An influence statistic is used to detect and eliminate the bouncebacks. Eliminating boucebacks causes little reduction in the number of active time stamps because usually the bouceback is replaced by the median share-price of the remaining trades with the same time stamp[10].

1.4.2 Contrasting daily and pooling estimation of the Heston model

This section discusses the daily and pooled estimation results for the 2,014 trading days from 2007 to 2014. I estimate the parameters of the Heston model for both individual trading days and for five-day pools. The Heston model requires all of the three parameters: β, $\bar{c}$ and γ to be positive. A parameter estimate is called "good" if the ratio of the estimate to its standard error (its z score) is large enough to reject at a 5% significance level the null hypothesis that it is zero in favor of an alternative that it is positive. I refer to a J-statistic

[9] Aït-Sahalia and Jacod (2014), p.74

[10] See Whang(2012) for more details about the construction of the data set.

as "good" if the model is not rejected at a 10% significance level. We declare the estimation of a trading day or pool to be good if the parameter estimates for β, $\bar{c}$ are good, the estimate of γ^2 is strictly positive and the J-statistic is good as well. Recall that the Feller condition is defined as $\gamma^2 < 2\kappa\bar{c}$, which guarantees that the volatility process c remains strictly positive with probability 1. The Feller conditions are satisfied for every good day and every good pool.

Table 1.2: Overall performance: 2007–2014

Classification	days (%)	pools(%)
Good days/pools	923 (45.8%)	286 (70.9%)
Bad days/pools	1091 (54.2%)	117 (29.1%)
Good $\widehat{\beta}$	967 (48.0%)	304 (75.4%)
Good $\widehat{\bar{c}}$	1495 (74.2%)	352 (87.3%)
Good $\widehat{\gamma^2}$	527 (26.2%)	252 (62.5%)
Good J-statistic	1899 (94.3%)	360 (89.3%)

Table 1.2 displays measures of overall performance of the estimation for individual trading days and for 5-day pools. Pooling increases the success rate of estimating the Heston model dramatically from 45.8% of trading days to 70.9% of 5-day pools. The percentage of good parameter estimates is improved for all three parameters. In particular for γ^2, the percentage of good estimates more than doubled from daily to pooling estimation. The percentage of good J-statistics declined by 5%, which is probably due to the restriction of parameters being the same for all 5 days of the pool.

Table 1.3 describes parameter estimates for the good days and good pools. Pooling has little impact on the estimates of the asymptotic mean $\bar{c}$, where the mean, median, lower and upper quartile are almost the same, except that the standard errors and z score are considerably improved. The median estimate of $\bar{c}$ is 0.085 for good pools, equivalent to a standard deviation $\sqrt{0.081} = 0.29(29\%)$ of annualized log returns with a volatility of volatility $\sqrt{1.11 \times 10^3} = 33.3$.[11] The lower and upper quartiles for pools, 0.053 and 0.15,

[11] According to Cochrane (2005), the annual standard deviation of postwar U.S. stock returns was 16%.

Table 1.3: Estimates of β, $\bar{c}$ and γ^2

	good days			good pools		
	$\widehat{\beta}$	$\widehat{\bar{c}}$	$\widehat{\gamma^2}(\times 10^3)$	$\widehat{\beta}$	$\widehat{\bar{c}}$	$\widehat{\gamma^2}(\times 10^3)$
median	0.19	0.081	1.89	0.10	0.081	1.11
lower quartile	0.14	0.051	0.97	0.07	0.053	0.64
upper quartile	0.27	0.14	3.82	0.13	0.15	2.31
median standard error	0.07	0.007	1.11	0.031	0.006	0.52
mean	0.22	0.14	4.07	0.11	0.14	1.97
median z-score	2.62	11.72	1.68	3.16	15.11	2.33

correspond to 23% and 37% yearly standard deviations respectively. The impact of pooling on the estimates of β and γ^2 is much larger. The median speed of mean-reversion β decreases almost by half from 0.19 to 0.10, and the interquartile range (the spread between the upper and lower quartiles) falls from 0.13 to 0.06. The median estimate of γ^2 falls from 1.89×10^3 to 1.11×10^3 and the interquartile range from 2.85×10^3 to 1.67×10^3. Standard errors and z statistic for both parameters improved substantially. The median z score indicates that $\bar{c}$ is much more precisely estimated than β or γ^2. The median as well as the lower and upper quartiles of the estimates for γ^2 have a much larger magnitude than the corresponding statistic for $\bar{c}$, suggesting that the volatility of volatility exercises a dominant influence on the asymptotic variance $\gamma^2\bar{c}/2\kappa$ of c_t. However, because the estimates of γ^2 also have much higher standard errors than the estimates of $\bar{c}$, this conclusion must be considered with caution.

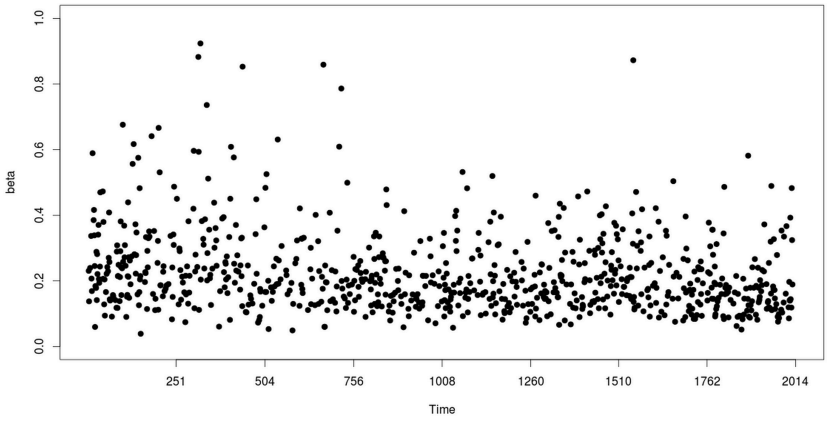

Figure 1.3: Time series for $\widehat{\beta}$ (good days)

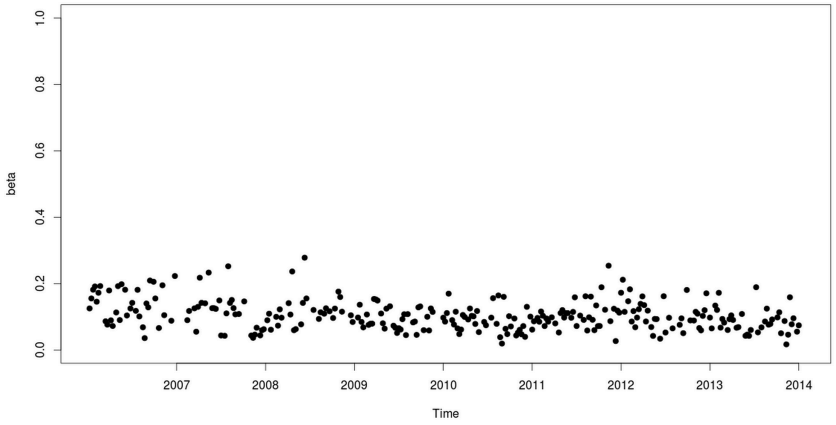

Figure 1.4: Time series for $\widehat{\beta}$ (good weeks)

The time series of $\widehat{\beta}$ provides a clearer portrayal of the impact of pooling on the estimation. Figure 1.3 and 1.4 plots the estimates for good days and good pools respectively.

Neither plots shows any evidence of a trend over time but the daily estimates vary a lot with many estimates over 0.5. The pooled estimates are tightly clustered in a plausible range of speed of mean reversion below 0.25, consistent with a constant beta subject to sampling error.

Table 1.4: Estimates of mean reversion (good pools)

	median	lower quartile	upper quartile
$\widehat{\beta}$: 100 seconds	0.10	0.07	0.13
$\widehat{\beta}$: 5 minutes	0.27	0.20	0.34
$\widehat{\beta}$: 10 minutes	0.47	0.35	0.57
$\widehat{\beta}$: 30 minutes	0.85	0.73	0.92
$\widehat{\kappa}$ (rate per year)	3.32×10^4	2.29×10^4	4.39×10^4

Table 1.4 shows alternative measures of the speed of mean reversion using 5-day pool estimates of β. The top row of each table gives the estimates of β for good pools from Table 1.3. Inverting $\beta = 1 - e^{-\kappa h}$ gives $\kappa = -\log(1-\beta)/h$, the parameter that measures the speed of mean reversion in the Heston model. Using the estimate of β for 100-second blocks gives an estimate of κ, reported in the final row of Table 1.4. These estimates of κ help us to compute β_h for any length h using the formula $\beta_h = 1 - e^{-\kappa h}$. The top panels display estimates of β_h for various lengths h. The 5-day pool median estimates indicate that 10% of the gap between volatility and its asymptotic mean is eliminated in 100 seconds, 27% in 5 minutes, 47% in 10 minutes and 85% within a half hour. Even the lower quartile estimates suggest mean reversion is rapid.

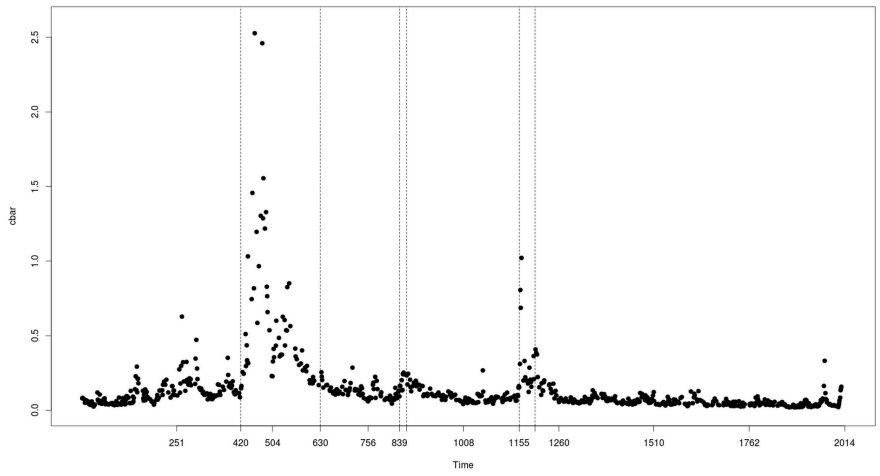

Figure 1.5: Time series for $\widehat{\bar{c}}$ (good days)

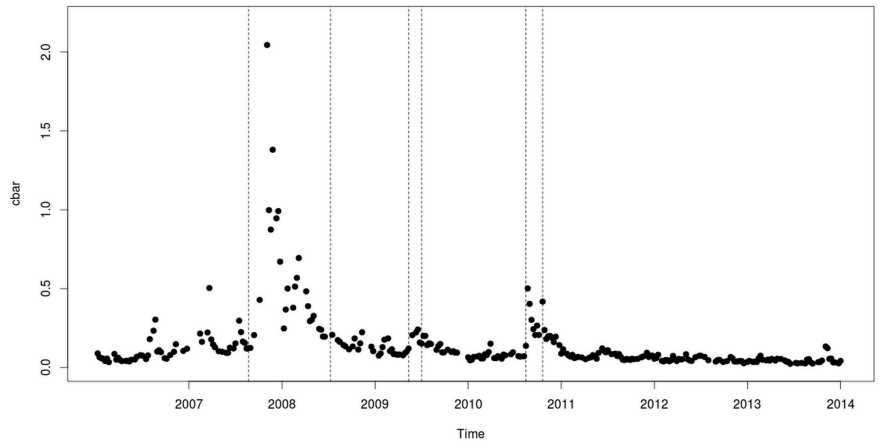

Figure 1.6: Time series for $\widehat{\bar{c}}$ (good pools)

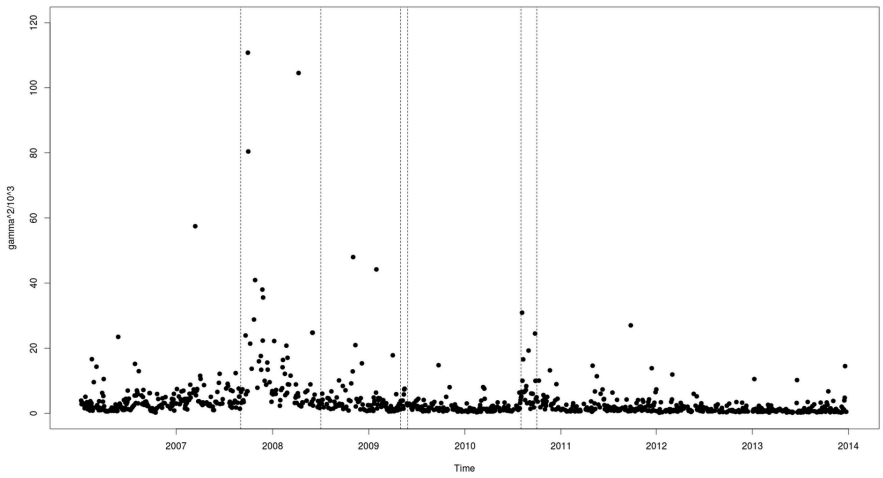

Figure 1.7: Time series for $\widehat{\gamma^2}$ (good days)

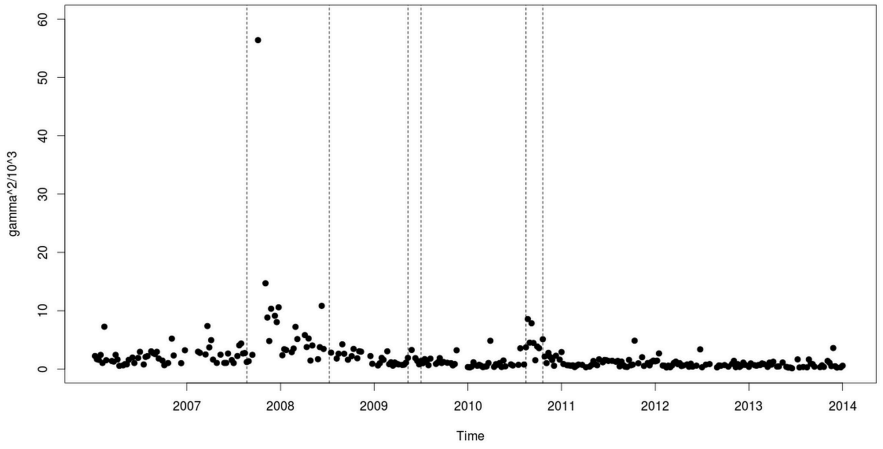

Figure 1.8: Time series for $\widehat{\gamma^2}$ (good pools)

Table 1.5 tabulates the number of gaps between good days by duration: of the 472 gaps,

Table 1.5: Length of gap between good days

Length of gap	1	2	3	4	5	6	7	8	9	10	11	12
Number of gaps	199	117	69	36	28	11	3	5	2	1	0	1

Table 1.6: Length of gap between good pools

Length of gap	1	2	3	4	5	6
Number of gaps	61	13	5	1	1	1

316 (67.0%) are of 1 or 2 day duration and 4 are of 9 to 12-day duration. Table 1.6 tabulates the number of gaps between good pools by duration. Most of the gaps (74 out of 82) are of 1 or 2 pool duration and there are three long gaps of 4, 5 and 6 pool lengths each, roughly a month time. They happen at the end of year 2007 and the end of year 2008. The long gaps between good days and good pools will be revisited in chapter 3 when I discuss the model outliers.

In contrast to the time series for β estimates, we see very clear evidence of variation over time in the asymptotic mean and the volatility of volatility, especially during the financial crisis that began late in 2008. Figures 1.5 and 1.6 plot the time series of daily and pool estimates for $\bar{c}$. The peaks in the two time series show up simultaneously. As a visual guide, six vertical lines have been added to these figures to mark off periods of interest.The vertical lines at day 420 and day 630 highlight the mortgage-financing crisis. Day 420 is 9/2/2008, shortly before Fannie Mae and Freddie Mac declared bankruptcy. Day 630 corresponds to 7/2/2009, when our estimate of $\bar{c}$ has returned to roughly the level it had before the crisis. The two vertical lines at days 839 (5/3/2010) and 858 (5/28/2010) mark another surge in volatility associated with the sovereign debt crisis in the Eurozone. The Flash Crash occurred near the beginning of this period and day 858 is the date of the Deepwater Horizon explosion. The final two vertical lines at days 1155 and and 1197 mark off a third period of high volatility stretching from the first day of August to the end of September. Standard

and Poor lowered the credit rating of the U.S. Government shortly before the start of this period.

Figure 1.7 and 1.8 display the daily and 5-day pool estimates of γ^2 estimates. There is some noisiness in the graphs but the three periods of high market volatility still stand out. Comparing Figure 1.8 with Figure 1.6, γ^2 follows a similar pattern to $\bar{c}$. We observe high volatility of volatility during the crisis periods identified in Figure 1.6. The difference is that γ^2 is much larger than the magnitude of $\bar{c}$ which provide more evidence that volatility of volatility dominates the asymptotic mean in determining the variation of stock price volatility. At the peak of the financial crisis both parameters exceeded their medians by an order of magnitude, astonishing testimony to the severity of the crisis.

1.5 Additional evidence for the model

Several aspects of the estimation procedure for the Heston model are examined in this section. I first show the importance of rescaling by examining sample autocovariances of RVs. This is then followed by a detailed comparison between sample first and second order moments and model predicted ones. Furthermore, I compare the time series of $\widehat{\bar{c}}$ to that of VIX.

1.5.1 The effect of scaling RV

Using unscaled RV for very short intervals such as 100 seconds can cause serious computational issues, such as weak instruments and singularity. The squared 1-second log return of a stock unscaled is usually less than 10^{-10}, which implies a 100-second RV of 10^{-8}. Therefore the absolute value of the autocovariance of the RV process is usually less than 10^{-16}. This is likely to cause a computational error when computing standard errors of the parameter estimates. However, appropriate scaling of RV can avoid this problem. The daily sample 1-lag autocovariances of RVs is $\frac{1}{M}\sum_{i=2}^{M}\widehat{C}_{t-h,t}\widehat{C}_{t,t+h}$, where M is the number of blocks, which is 232 for daily estimation and 1170 for 5-day pools. For a good day, the daily average 1-lag autocovaraince of RVs has a mean of 0.081 and a minimum of 0.0056. For a good pool, it has a mean of 0.084 and minimum of 0.007. It is quite an improvement from 10^{-16} to avoid

computational errors.

1.5.2 First order moments: model versus predicted

In this section I would like to check whether model predicted mean is close to the sample mean of RV. Figure 1.9 and 1.10 compares my estimates of $\bar{c}$ for good days and good pools with the median and mean of the realized variation for all blocks in the same pool, together with the 45 degree lines. My GMM estimates are very close to both the median and mean for a great majority of pools. My estimates are occasionally significantly larger than the median and are rarely smaller, while estimates are sometimes significantly smaller than the mean and are rarely larger. Estimates in good pools lie closer to the 45 degree line than good day estimates.

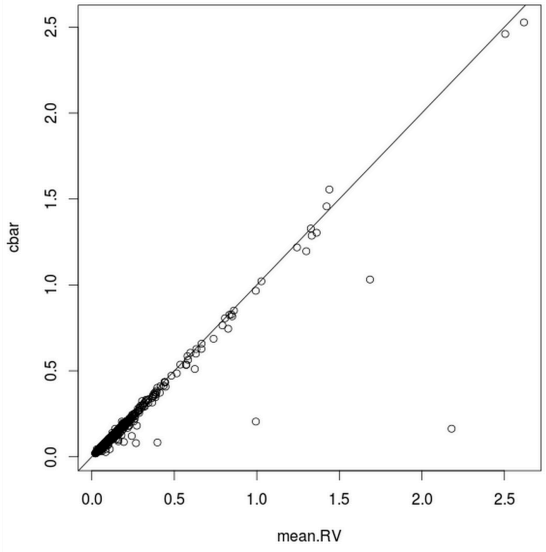

Figure 1.9: $\widehat{\bar{c}}$ versus mean of RV (good day)

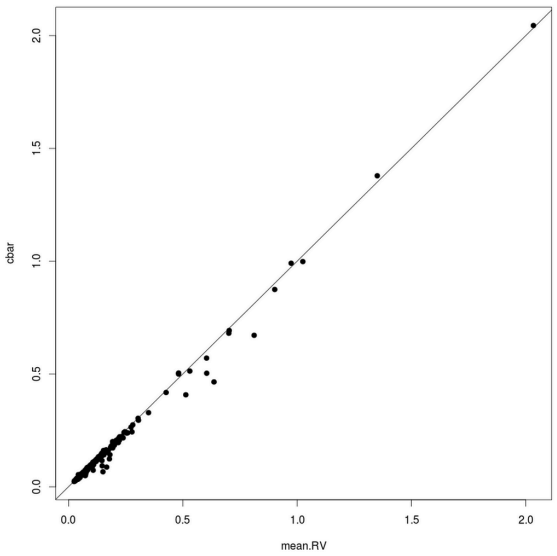

Figure 1.10: $\widehat{\widehat{c}}$ versus mean of RV (good pool)

1.5.3 Second order moments: model versus predicted

The next task is to use the sample autocorrelations for good days and good pools to test our claim that asymptotic autocovariances of all lags $j \geq 1$ are robust to measurement error but asymptotic variances are not. We use the following result from Sun(2016): The autocorrelations $R_j := V_j/V_0$ of $C_{t,t+h}$ for lags $j \geq 0$ are given by

$$R_0 = 1$$

$$R_1 = \frac{\beta^2}{2(\log(1-\beta)+\beta)}$$

$$R_j = (1-\beta)R_{j-1}, \qquad j \geq 2$$

Asymptotic autocorrelations of $\widehat{C}_{t,t+h}$ depend only on the parameter β, which gives us a simple way to test the robustness our second order moments to measurement error. For

example, if $\beta = 0.10$ (the sample median of good pool estimates), then $R_1 = 0.93$, $R_2/R_1 = 1 - \beta = 0.90$ and $R_3/R_1 = (1-\beta)^2 = 0.81$. Figures 1.11 and 1.12 display box plots of the sample autocorrelation $\widehat{R_1}$ and the ratios $\widehat{R_2}/\widehat{R_1}$ and $\widehat{R_3}/\widehat{R_1}$. The horizontal line within the box of each box plot corresponds to the median and the upper and lower sides of the box indicate the upper and lower quartiles of the distribution. The isolated points above the "whiskers" indicate the position of outliers. In these figures, the median of the box plot for $\widehat{R_1}$ (the boxplot on the left) are 0.54 and 0.57, far below the median predicted by the formula for R_1 (0.96 and 0.93 for good days and good pools respectively). This finding conforms with the expectation based on our analysis of measurement error because the autocorrelation R_1 has the variance in the denominator. Measurement error increases the variance but not the autocovariance for lag 1, which lowers the sample autocorrelation below the prediction of the formula. On the other hand, the ratios $\widehat{R_2}/\widehat{R_1}$ and $\widehat{R_3}/\widehat{R_1}$ are not affected by measurement error because variances cancel out.

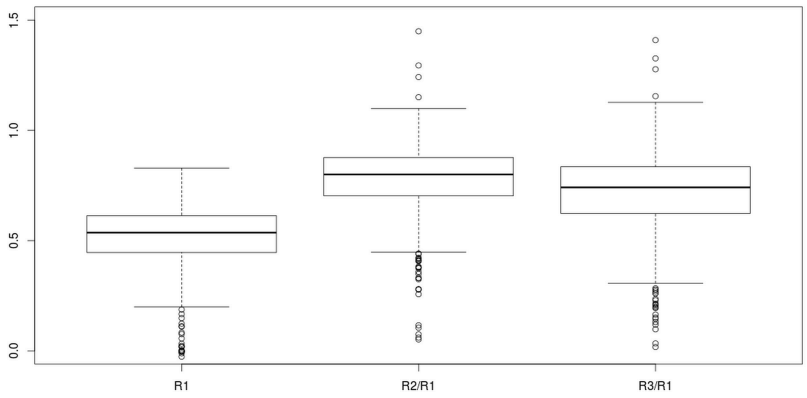

Figure 1.11: Box plot of asymptotic autocorrelations (good days)

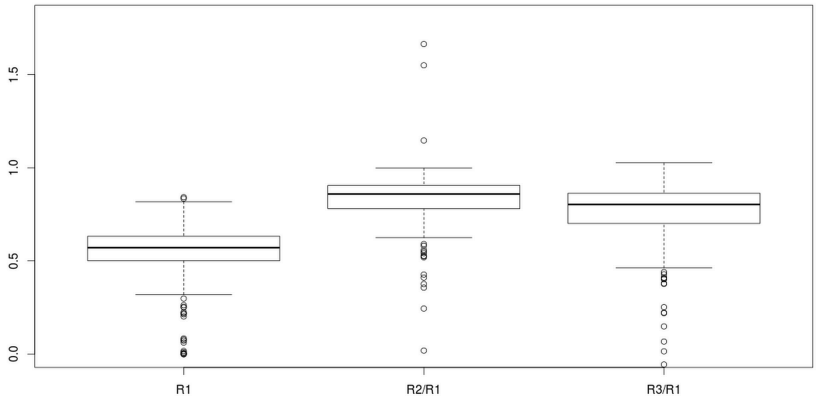

Figure 1.12: Box plot of asymptotic autocorrelations (good pools)

The medians of the box plots for good days are 0.81 and 0.72, close to the predicted 0.81 and 0.66. The medians of their box plots for good pools are 0.87 and 0.80, also close to the prediction (0.90 and 0.81 as mentioned above). These are consistent with our conclusion that autocovariances of lag $j \geq 1$ are unaffected by measurement error.

Moment conditions 1.7 match the sample autocovariances of lag 1 and lag 2 to the formulas we derived for the asymptotic covariances V_1 and V_2 respectively, formulas that depend on solely on h and the parameters β, $\bar{c}$ and γ^2 of the Heston model. Figure 1.13 to 1.14 plot the sample variances versus the estimated asymptotic variances predicted by the parameter estimates for each good day and good pool, along with the 45^o line. The two graphs both indicate that the asymptotic variances are not robust to measurement error. Figure 1.15 to 1.18 plot sample autocovariances versus the estimated asymptotic autovariances predicted by the parameter estimates for each good day and good pool. Although there are a few outliers, most of the 923 good days and 306 good pools are clustered along the 45^o line.

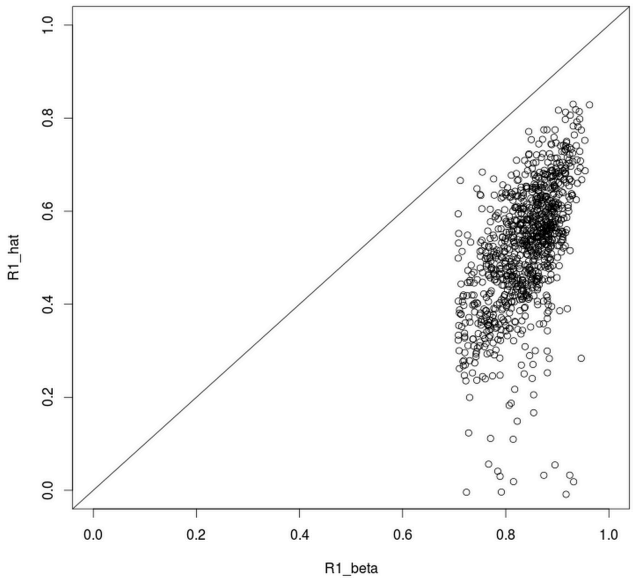

Figure 1.13: Asymptotic variance: real versus model (good days)

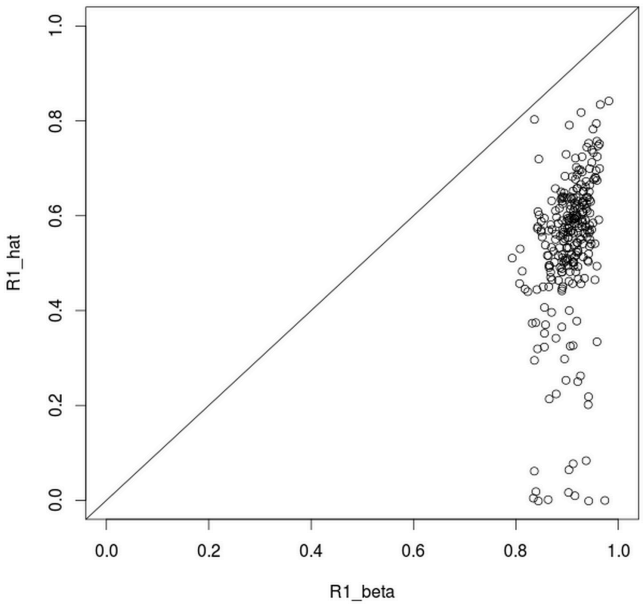

Figure 1.14: Asymptotic variance: real versus model (good pools)

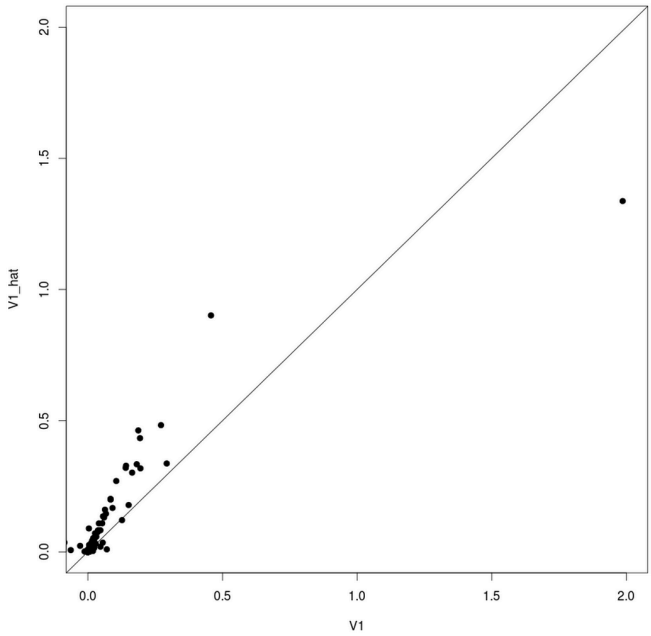

Figure 1.15: $\widehat{V_1}$ versus V_1 (good days)

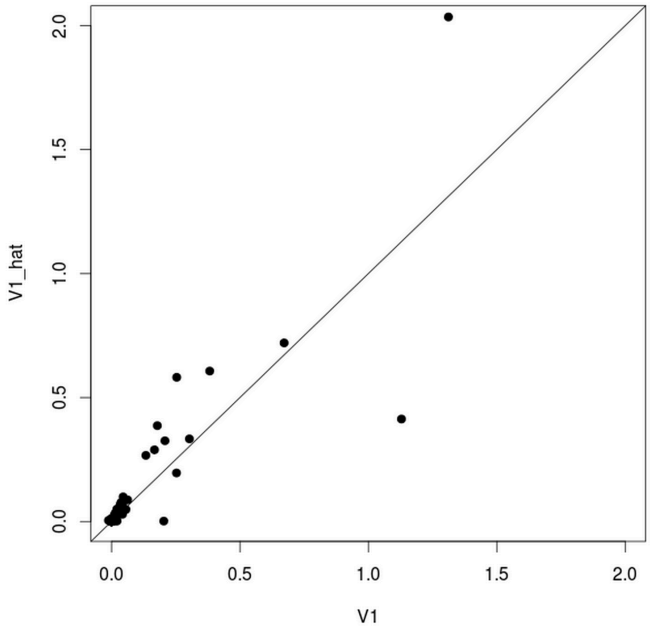

Figure 1.16: $\widehat{V_1}$ versus V_1 (good pools)

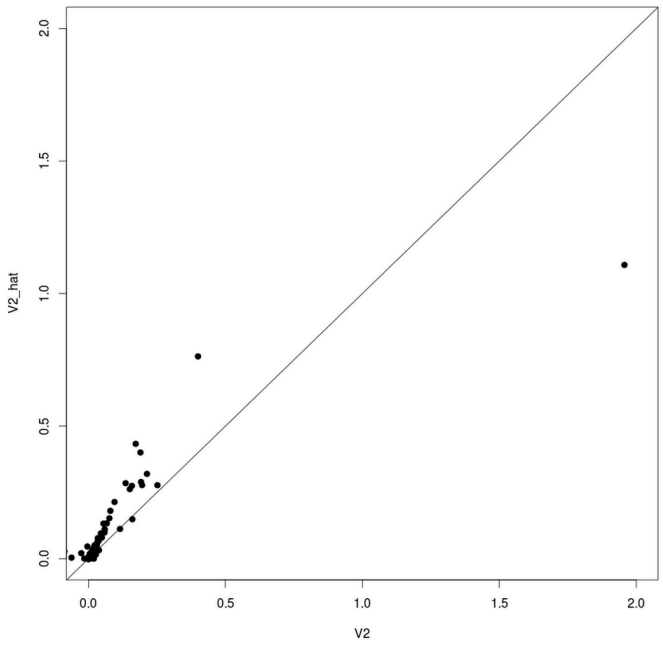

Figure 1.17: $\widehat{V_2}$ versus V_2 (good days)

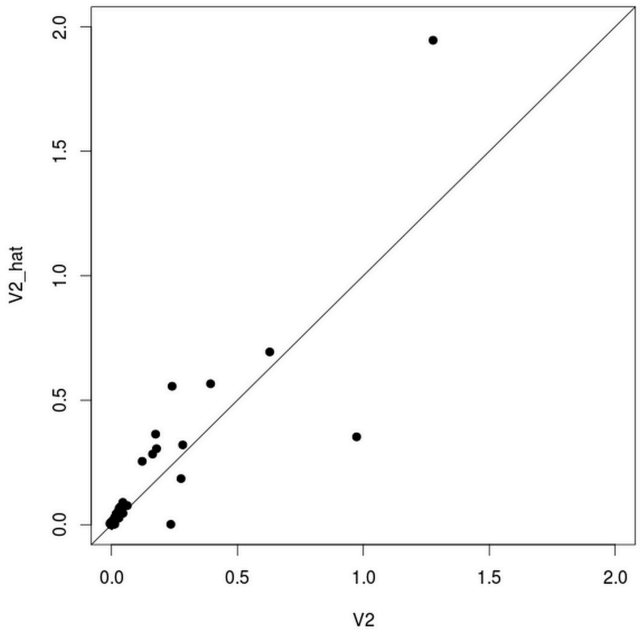

Figure 1.18: $\widehat{V_2}$ versus V_2 (good pools)

1.5.4 Comparison to the VIX

Figure 1.19 plots the VIX index week by week over our 8-year sample period. The VIX is the implied volatility of S&P 500 index options. The 3 pairs of vertical lines in the VIX graph correspond to the vertical lines in our plot of the time series for $\widehat{\widehat{c}}$. We see that the largest peak for the VIX lies inside the first pair of lines, and $\widehat{\widehat{c}}$ follows a trajectory similar to that of the VIX over this period. VIX is near its mean at both the beginning and the end of the period. It takes 40 days for VIX to climb up to the top in the week of 10/22/2008. Similar to the plot for $\widehat{\widehat{c}}$, the VIX exhibits higher volatility in the period leading up to the great eruption, and there are two peaks in 2010 and 2011 lying in the regions identified by the second and third periods of vertical lines. The VIX is relatively quiet in the last three years, just like our plot of the estimates of $\widehat{\widehat{c}}$.

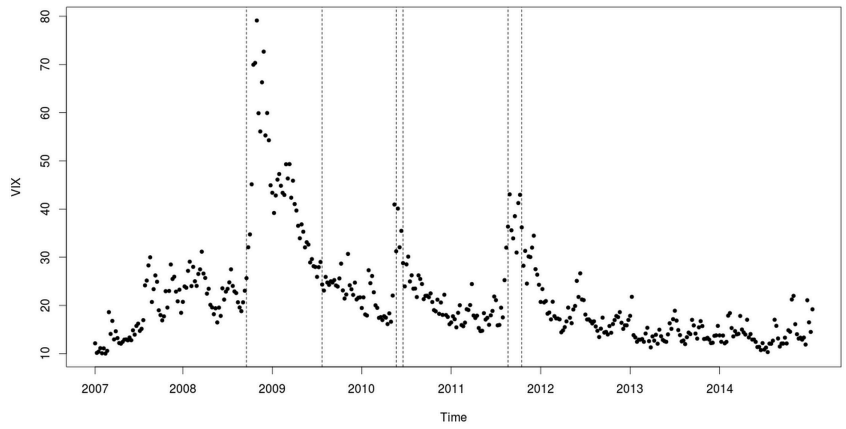

Figure 1.19: Volatility Index of S&P 500, 2007-2014

1.6 Comparison with the interday model

In this final part of the chapter, I would like to use our moment conditions to estimate the Heston model using daily realized volatilities, with prices sampled either once every five minutes (the usual procedure in the literature) or every second. We apply the moment conditions (1.6) and (1.7) of our model to the sequence of daily quadratic variations implied by the Heston model. Because there are gaps between the quadratic variations from two different trading days, the derivation from the Heston model no longer makes much sense. Nevertheless, I estimate the model for the entire eight-year sequence of 2014 trading days from 2007-2014, a sample roughly equal in size to two five-day pools with realized volatility computed over 100-second blocks. I adjust h to match the length of a 6.5 hour day relative to a year: $h = 6.5/(24 * 365.25) = 1/1348.6$.

Table 1.7: Heston model using daily RV

	5-minute sampling		1-second sampling	
parameter	estimate	z score	estimate	z score
$\widehat{\beta}$	0.04	2.25	0.002	0.48
$\widehat{\bar{c}}$	0.13	3.87	0.12	0.78
$\widehat{\gamma^2}$	36.6	1.35	13.6	0.96

Table 1.7 reports the results of the estimation, giving the parameter estimates and their z scores. When prices are sampled every 5-minutes, the estimates of β and $\bar{c}$ are significantly different from 0 at the 2.5% level, the estimate of γ^2 is significantly different from 0 at the 10% level, the J-statistic does not reject the specification and the parameter estimates satisfy the Feller condition. The estimate $\widehat{\bar{c}} = 0.13$ is close to the mean estimates reported in Table 1.3 for good days or good pools (0.14). However, the estimate of the parameter γ^2 is about 1.8% of the mean estimate for good pools in Table 1.3. The parameter β in the interday estimation scenario now measures mean reversion relative a 6.5-hour day: 4% of the gap between instantaneous volatility and the asymptotic mean is eliminated on average in the course of a 6.5-hour trading day. This is much slower mean reversion compared to

our model. The implied estimate of $\kappa = \log(1-\beta)/h = 689$ is about 2% of the median estimate of $\kappa = 3.32 \times 10^4$ reported in Table 1.3 for good pools[12]. The current literature advocates sampling prices no more often than once every five minutes. The estimation results in Table 1.7 is consistent with this opinion: When prices are sampled once a second, the estimation using daily realized volatilities breaks down: z scores are all less than one.

1.7 Conclusion

This chapter demonstrates that the path of quadratic variation during a trading day can be described by a Heston model of stochastic volatility. I estimate all parameters of the Heston model using GMM with six moment conditions of the realized volatilities over 100-second blocks. The estimation shows the three parameters of the Heston model can be used to describe the characteristics of market uncertainty not only within a trading day, but across different days as well. Enlarging the sample size by pooling realized volatilities over five consecutive days leads to a dramatic increase in our model performance. Model outliers will be examined in detail in chapter 3.

This chapter also demonstrates the importance of using appropriate units for time when modeling realized volatility over very short intervals. Choosing the calendar year as the unit of time rather than 100 seconds improved estimates considerably.

The chapter also compares intraday estimation of the Heston model using 100 second RVs with the interday estimation using daily RVs. The results provide a clear interpretation of the difference: The intraday model finds much higher volatility of volatility balanced with much more rapid mean reversion.

[12]Bergantini (2013) estimated the Bollerslev and Zhou (2002) for the period 8/1/1987 to 6/20/2011 using the S&P 500 index sampled at 5 minute frequency. The estimation she obtained was $\widehat{c} = 0.0103$, $\widehat{\kappa} = 0.01135$, $\widehat{\gamma^2} = 0.0840$, with standard errors equal to 0.0011, 0.0353 and 0.0104 respectively. The Feller condition in her exercise was not satisfied.

CHAPTER 2

Estimating Intraday Stochastic Volatility: Seven Case Studies

SPY is one of the most heavily traded assets on the U.S. stock market. A natural question is whether our estimation procedure will meet with as much success for assets less liquid than SPY.

In this chapter I estimate the Heston model for seven assets: IWM (which tracks the Russell 2000 index), EEM (which tracks the MSCI emerging markets index), and five components of the Dow Jones Industrial Average: BAC (Bank of America), CVX (Chevron), IBM, INTC (Intel) and MSFT (Microsoft).

I begin by demonstrating that the one-dimensional Heston model is consistent with a model in which both the price and volatility process are driven by D-dimensional Wiener processes, which allows the volatility process for different assets to be sensitive to different dimensions of risk. The rest of the chapter follows the outline of the discussion for the empirical results on SPY in chapter 1. I begin by examining the overall empirical performance of estimation day by day and with 5-day pools. I also examine the influence of the volume of trade on empirical performance. I then describe in detail the parameter estimates for each of the seven assets for good pools and plot the time series of the estimates over the 8-year sample period, comparing and contrasting with those of SPY. I also compute the sample moments of RVs with the population moments used in GMM estimation and compare the intraday model with estimates of an interday model. Our basic conclusion is that GMM estimation of the Heston model works well for these seven assets despite lower trade volume and higher fraction of inactive seconds.

The rest of the chapter is organized as follows: Section 2.1 describes how the Heston model can incorporate multidimensional risks. Section 2.2 introduces the seven stocks and ETFs and discusses the frequency of trades and the fraction of missing time stamps for each. Section 2.3 presents estimation results for the seven assets and compares them with those of SPY. Section 2.4 extends the discussion of the preceding section, comparing and contrasting the seven assets with each other. Section 2.5 concludes the chapter.

2.1 Heston model as a general model

The Heston model can be formulated within the setting of multi-dimensional risks. In particular a Heston model driven by a D-dimensional Wiener process can be reduced to a one-dimensional Heston model, provided that the price process depends on the same D-dimensional Wiener process. Let

$$X_t = X_0 + \int_0^t b_s \, ds + \sum_{d=1}^{D} \int_0^t \sigma_s^d \, dW_s^d \qquad (t \geq 0) \tag{2.1}$$

where $(W^1, W^2, \ldots, W^D)$ is a standard D-dimensional Wiener process and $c_t := \sum_{d=1}^{D} (\sigma_t^d)^2$ for all $t \geq 0$, which is never zero. Also assume that the stochastic process c is the solution to the stochastic differential equation

$$dc_t = \kappa(\bar{c} - c_t) \, dt + \sqrt{c_t} \sum_{d=1}^{D} \gamma^d \, dW_t^d \qquad (t \geq 0) \tag{2.2}$$

where the parameters γ^d are constant and $\gamma^2 := \sum_{d=1}^{D} (\gamma^d)^2$ is never zero.

We claim that equations (2.1) and (2.2) imply equations (1.1) and (1.2), the usual representation of the Heston model. If we define

$$W_t = \sum_{d=1}^{D} \int_0^t \frac{\sigma_s^d}{\sqrt{c_s}} \, dW_s^d \qquad (t \geq 0) \tag{2.3}$$

and

$$B_t = \sum_{d=1}^{D} \int_0^t \frac{\gamma^d}{\gamma} \, dW_s^d \qquad (t \geq 0) \tag{2.4}$$

then W and B are standard 1-dimensional Wiener processes, possibly correlated.[1] Equation (2.3) implies $\sqrt{c_t} \, dW_t = \sum_{d=1}^{D} \sigma_t^d \, dW_t^d$ for all $t \geq 0$. Substituting into the differential version of equation (2.1) yields $dX_t = b_t \, dt + \sqrt{c_t} \, dW_t$, which is the differential version of equation (1.1). Equation (2.4) shows $\gamma \, dB_t = \sum_{d=1}^{D} \gamma^d \, dW_t^d$, which when substituted into equation (2.2) leads to equation (1.2).

Therefore, we can always reduce the D-dimensional Heston model represented by equation (2.1) and (2.2) to the one-dimensional Heston model given by equations (1.1) and (1.2). As a result, there is no reason to distinguish between one-dimensional and multi-dimensional versions of the Heston model as in Bollerslev and Zhou (2002). It is important to believe that our estimation technique is consistent with a multi-dimensional world of risk.

2.2 Introduction to the assets

Table 2.1 lists all the stocks and exchange-traded funds used in this study. All of the stocks are "high cap" stocks, listed as components of the Dow Jones Industrial Average in the sample period 2007-2014. The first and second columns of Table 2.1 give the ticker symbol and the name of the asset respectively. SPDR is an abbreviation for *Standard and Poor's Depositary Receipts*. All SPDF ETFs including SPY are managed by State Street Global Advisors (SSGA). *Russell* refers to the *FTSE Russell indexes*. The *FTSE Russell 2000* index tracks 2000 U.S. small-cap stocks. *iShare* is a family of ETFs managed by Black Rock Inc. MSCI Emerging is the component of the MSCI World index that tracks emerging markets. It is maintained by Morgan Stanley Capital International. I will often use the ticker symbol to identify points in graphs associated with a particular asset. Column 3 of Table 2.1 gives

[1] See Shreve (2004), p. 226. The quadratic variation of W is the same as that of a standard Wiener process, which implies by Lévy's Theorem that W is a standard Wiener process. The same argument applies to the process B. The instantaneous correlation of the processes W and B at time t equals the differential of the quadratic covariation $[W, B]$ at time t, $d[W, B]_t = \left(\sum_{d=1}^{D} \sigma_t^d \gamma^d \right) / \sqrt{c_t} \, \gamma$.

the percentage of time stamps over the 8-year period that were "inactive", i.e., there is no trade associated with an inactive time stamp. The fourth column gives the average number of trades per second over the 8-year period.

As Table 2.1 shows, SPY averaged 17.2 trades per second over the 8-year sample period, and 23% of the time stamps were inactive. Although not as high as SPY, the number of trades per second for the other assets is also very high, ranging from a low of 1.5 for IBM to a high of 8.9 for BAC, with an average of 6 trades per second. However, the percentage of inactive seconds is much higher than it is for SPY, varying from a low of 45% for BAC to a high of 70% for CVX, with an average of 52%[2].

Table 2.1: Stocks and ETFs

Ticker	Name	Percent Inactive Time Stamps	Trades per second
SPY	SPDR S&P 500	23	17.2
IWM	iShares Russell 2000	52	6.4
EEM	iShares MSCI Emerging	59	5.1
BAC	Bank of America	45	8.9
CVX	Chevron Corporation	70	2.2
IBM	IBM Corporation	64	1.5
INTC	Intel Corporation	53	3.2
MSFT	Microsoft Corporation	51	3.5

[2]The average trade per second for the 30 DJIA component stocks is 3 and the average percent of inactive time stamps is 58%

Table 2.2: Market Capitalization and Daily Volume, Stocks and ETFs

Ticker	Name	Market Cap(b)	Daily Vol(m)
SPY	SPDR S&P 500	188.51	130.05
IWM	iShares Russell 2000	25.77	38.13
EEM	iShares MSCI Emerging	25.80	69.72
BAC	Bank of America	143.09	105.54
CVX	Chevron Corporation	13	25.94
IBM	IBM Corporation	143.48	4.56
INTC	Intel Corporation	143.5	22.96
MSFT	Microsoft Corporation	407.41	29.98

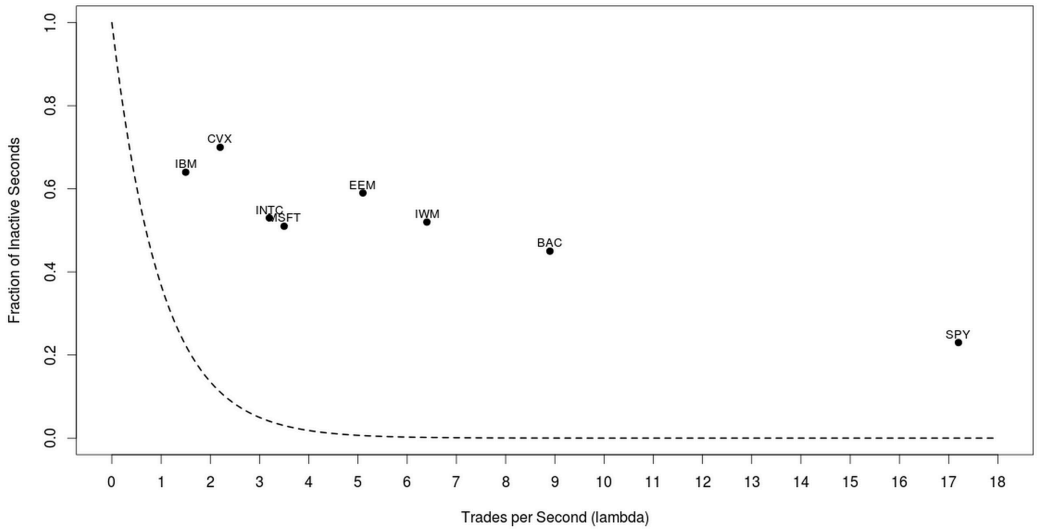

Figure 2.1: Inactive seconds versus trades per second

The high percentage of time stamps with no trade is surprising. To put this into perspective, suppose that the arrival of trades follows a Poisson process with intensity λ, where λ is the arrival rate of trades per second. In that case, the probability there are exactly k arrivals in an interval of length h is[3]

$$\mathbb{P}(N_{t+h} - N_t = k) = \frac{(\lambda h)^k}{k!} e^{-\lambda h} \tag{2.5}$$

If $k = 0$ and $h = 1$, this simplifies to

$$\mathbb{P}(N_{t+1} - N_t = 0) = e^{-\lambda} \tag{2.6}$$

Take the number of arrivals per second reported in column 4 of Tables 2.1 as the estimate of λ for each stock or ETF, and take the left-hand side of equation (2.6) as the predicted probability that a given time stamp has no trade. The dashed declining exponential curve in Figure 2.1 plots equation 2.6 for all the 8 assets. The dots labeled with ticker symbols plot the data given in column 3 (percentage inactive divided by 100, to convert the percentage to a fraction) and column 4 (trades per second) for all the 8 assets. As Figure 2.1 illustrates, all of the assets lie well above the percentage of inactive seconds that would be expected if the arrival of trades were a Poisson process. For the lowest trading volume stocks (IBM and CVX), the fraction of inactive seconds is relatively close to the fraction expected if arrivals were Poisson. The gap widens as trades per second increases. For example, the fraction of time stamps with no trades is 0.45 for Bank of America, but the Poisson equation predicts the fraction should be $e^{-8.9} = 1.4 \times 10^{-4}$.

2.3 Overall performance of selected stocks

In the previous section we showed the trade arrival process is far from Poisson and assets except SPY have significantly fewer trades. Nevertheless, I find the Heston model works well

[3]Here we are indexing time by the interval $[0, T]$ rather than $[0, 1]$, where $T = 23{,}000$ is the number of seconds in a trading day.

even for assets with a high percentage of inactive time stamps. Table 2.3 and 2.4 present the performance ratings for the daily and pooled estimates respectively, comparable to Table 1.2. To save space, the table gives only percentages and not the counts. For all 7 assets, there are 2014 trading days and 403 five-day pools during the sample period 2007-2014, formed exactly as the pools used in the analysis for SPY.

Table 2.3: Overall performance: 2007–2014, daily estimation

Classification	IWM	EEM	BAC	CVX	IBM	INTC	MSFT
Good overall	47.9%	35.2%	39.1%	56.8%	52.8%	40.0%	29.7%
Bad overall	52.1%	64.9%	60.9%	43.2%	47.2%	60.0%	70.3%
Good $\widehat{\beta}$	50.6%	37.5%	42.2%	59.6%	55.6%	38.9%	32.3%
Good $\widehat{\bar{c}}$	78.4%	64.9%	65.9%	78.8%	73.1%	64.7%	57.1%
Good $\widehat{\gamma^2}$	25.2%	19.1%	24.3%	18.5%	15.6%	20.9%	17.2%
Good J-statistic	94.2%	92.2%	91.6%	93.5%	90.1%	93.2%	90.6%

Table 2.4: Overall performance: 2007–2014, 5-day pool estimation

Classification	IWM	EEM	BAC	CVX	IBM	INTC	MSFT
Good overall	65.9%	53.0%	59.7%	61.7%	65.9%	52.5%	54.2%
Bad overall	34.1%	47.0%	40.3%	38.3%	34.1%	47.5%	45.8%
Good $\widehat{\beta}$	79.1%	57.0%	66.4%	78.4%	80.3%	57.5%	60.2%
Good $\widehat{\bar{c}}$	90.8%	79.4%	80.1%	86.3%	87.1%	78.1%	83.3%
Good $\widehat{\gamma^2}$	67.9%	41.1%	56.0%	50.7%	50.5%	44.8%	44.5%
Good J-statistic	84.3%	90.3%	86.1%	72.1%	77.1%	84.1%	85.3%

The percentage of good daily estimates varies from a low of 29.7% to a high of 56.8% for CVX, with IWM and IBM as well as CVX exceeding the daily performance of SPY. Pooling increases performance across the board. The percentage of good pools ranges from a low of 52.5% for Intel to a high of 65.9% for IWM and IBM, somewhat short of SPY (70.9%). As in the case of SPY, the percentage of good parameter estimates increased for all three parameters from daily to pool estimation for these assets. Especially for $\widehat{\gamma^2}$, the percentage

of good estimates more than doubled from daily to pooling estimation for each asset. The percentage of good J-statistics all worsened somewhat similar to that of SPY.

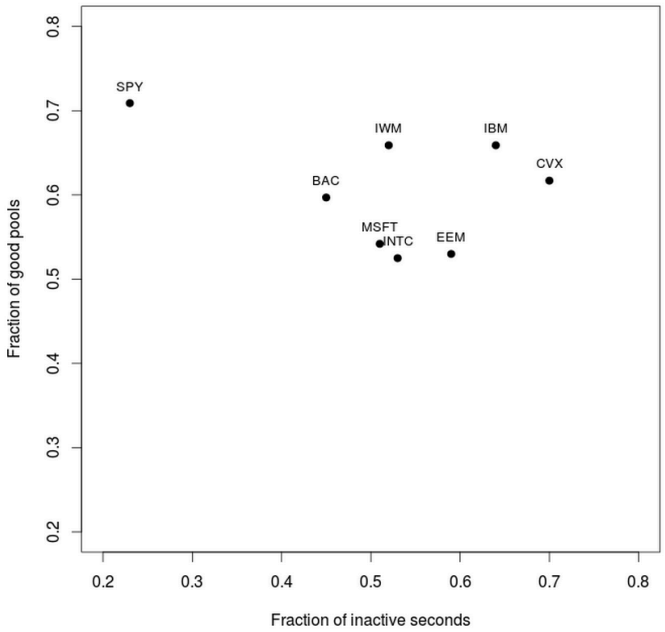

Figure 2.2: Model performance and fraction of inactive seconds

Figure 2.2 plots the fraction of inactive time stamps versus percentage of good pools in the estimation. SPY distinguishes itself from other assets because of better estimation performance and low fraction of inactive seconds. However, for the seven other assets, the decrease of the fraction of inactive seconds is not associated with a clear improvement in the fraction of good pools. For IBM and CVX, 60% of their time stamps have no trade, but around 60% of their pools are good. These two stocks do have a significant number of failures of the Feller inequality, 119 and 51 cases respectively. The Feller inequality is satisfied for almost all of the pools for the other 5 assets, as will be discussed in the next section.

2.4 Empirical analysis of different stocks

This section discusses the estimation results for each of the seven assets. In each subsection devoted to all of the assets, there is a table paralleling Table 1.3 that describes the parameter estimates for each asset followed by the time series graphs of $\widehat{\beta}$, $\widehat{\bar{c}}$ and $\widehat{\gamma^2}$ for good pools in the sample period 2007-2014. I also display graphically the feller conditions for each good pool and compare the sample first and second order moments with the values predicted by the model. These exercises provide evidence for the general applicability of the Heston model to different assets.

2.4.1 IWM

Table 2.5 describes the parameter estimates for good days and good pools for IWM. Similar to SPY, pooling substantially improves the standard errors and z scores for estimates of all three parameters. Pooling has little impact on the estimates of $\bar{c}$ (the mean, median and interquartile range are almost the same), but pooling affects the estimates of β and γ^2 greatly. The median $\widehat{\beta}$ fell from 0.17 to 0.09 and the interquartile range shrunk from 0.12 to 0.05. The median estimate of γ^2 fell from 4.85×10^3 to 3.23×10^3 and the interquartile range fell from 6.7×10^3 to 4.0×10^3. The median estimate of $\bar{c}$ is 0.17 for good pools, equivalent to a standard deviation $\sqrt{0.17} = 0.41(41\%)$ of annualized log returns with a volatility of volatility $\sqrt{3.23 \times 10^3} = 56.83$.

Figure 2.3 plots $\widehat{\beta}$ for good pools over the 8 year sample period for IWM. The estimates are tightly clustered with no evidence of a trend over time.

Figure 2.4 and 2.5 plot $\widehat{\bar{c}}$ and $\widehat{\gamma^2}$ for good pools of IWM. Three pairs of vertical lines are added to these figures in the same locations as those in Figure 1.6 and 1.8 for SPY. Three pairs of lines indicate three periods where we observe a surge in volatility in SPY associated with specific economic events: the financial crisis, the sovereign debt crisis and the credit crisis. We see these events impact the volatility of IWM as well. The asymptotic mean estimates rise in these three periods, reaching a peak higher than SPY. The γ^2 estimates have a larger scale and are noisier than SPY. This result is not surprising because IWM is

Table 2.5: Estimates of β, $\bar{c}$ and γ^2, IWM

	good days			good pools		
	$\widehat{\beta}$	$\widehat{\bar{c}}$	$\widehat{\gamma^2}(\times 10^3)$	$\widehat{\beta}$	$\widehat{\bar{c}}$	$\widehat{\gamma^2}(\times 10^3)$
median	0.17	0.15	4.85	0.09	0.17	3.23
lower quartile	0.12	0.09	2.65	0.07	0.10	2.03
upper quartile	0.24	0.25	9.35	0.12	0.29	6.03
median standard error	0.06	0.02	2.98	0.03	0.014	1.34
mean	0.20	0.24	9.70	0.10	0.27	16.45
median z-score	2.67	8.59	1.62	3.11	11.15	2.31

the exchange traded fund tracking small cap stocks. Figure 2.6 checks the Feller condition for good pool estimates. I plot γ^2 on the vertical axis and $2\kappa\bar{c}$ on the horizontal axis using the parameter estimates for good pools, along with the 45^o line. Points above the 45^o line violates the Feller condition$\gamma^2 \leq 2\kappa\bar{c}$. We see all the Feller conditions are strictly satisfied. Figure 2.7 parallels Figure 1.10 for SPY, plotting for each good pool the mean RV for the pool versus the estimate of the asymptotic mean $\bar{c}$. All of the estimates of the asymptotic mean match closely with the mean realized volatility. Figure 2.8 and 2.9 provide evidence that the sample autocovariances of lag 1 and lag 2 match the asymptotic autocovariances predicted by the model, (compare Figure 1.16 and 1.18 for SPY). Except for a few outliers, most of the 265 good pools are clustered along the 45^o line.

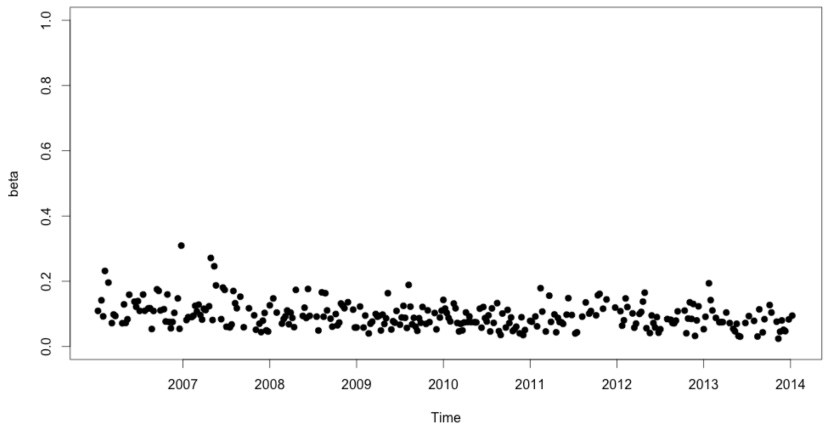

Figure 2.3: Time series for $\widehat{\beta}$ (good pools), IWM

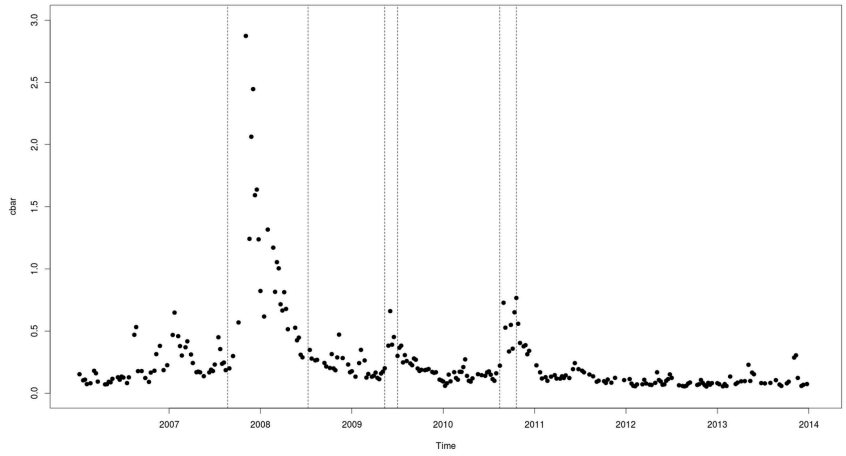

Figure 2.4: Time series for $\widehat{\bar{c}}$ (good pools), IWM

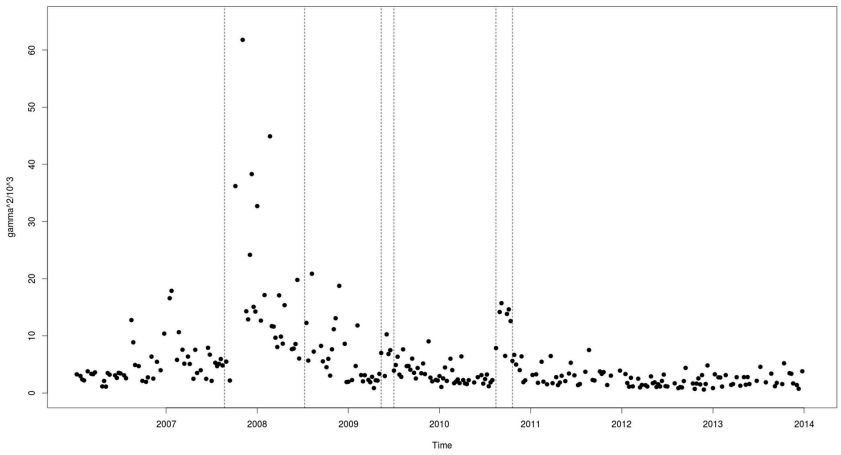

Figure 2.5: Time series for $\widehat{\gamma^2}$ (good pools),IWM

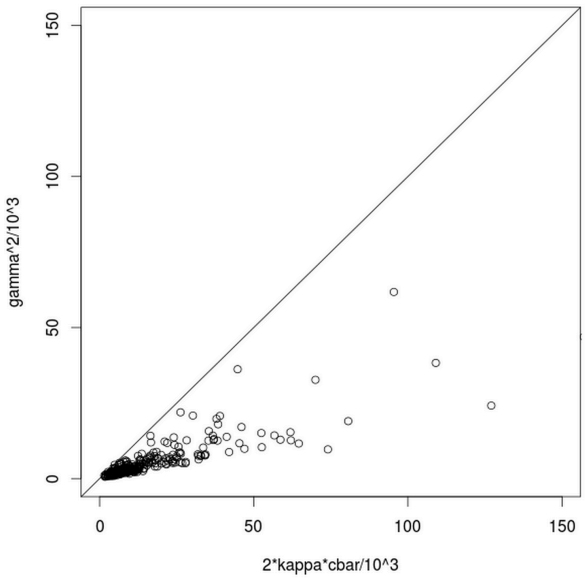

Figure 2.6: Feller condition (good pools), IWM

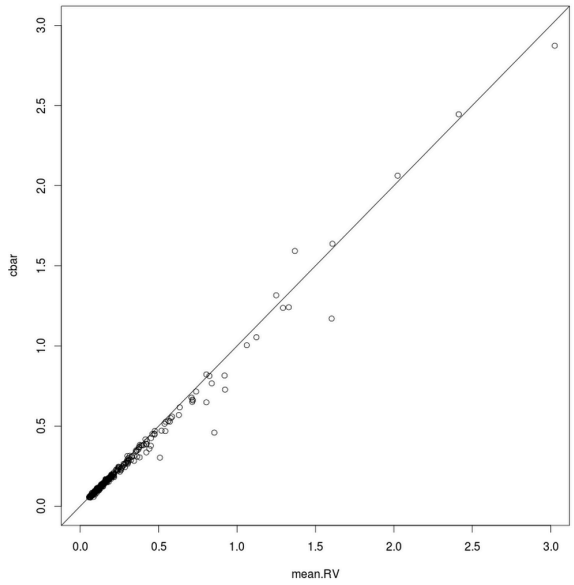

Figure 2.7: $\widehat{\bar{c}}$ versus mean of RV (good pools), IWM

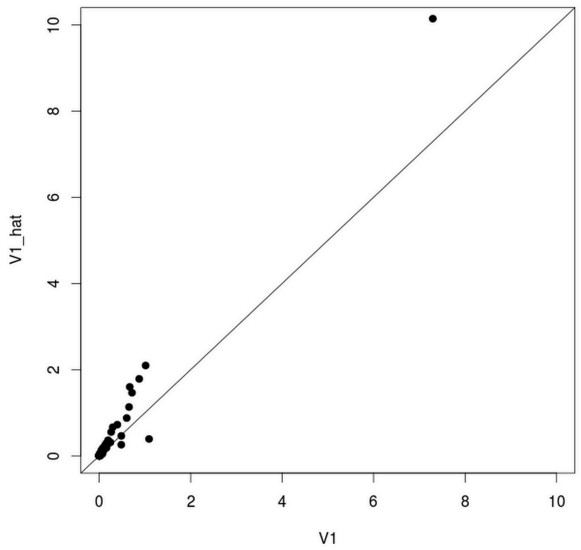

Figure 2.8: V_1 versus $\widehat{V_1}$ (good pools), IWM

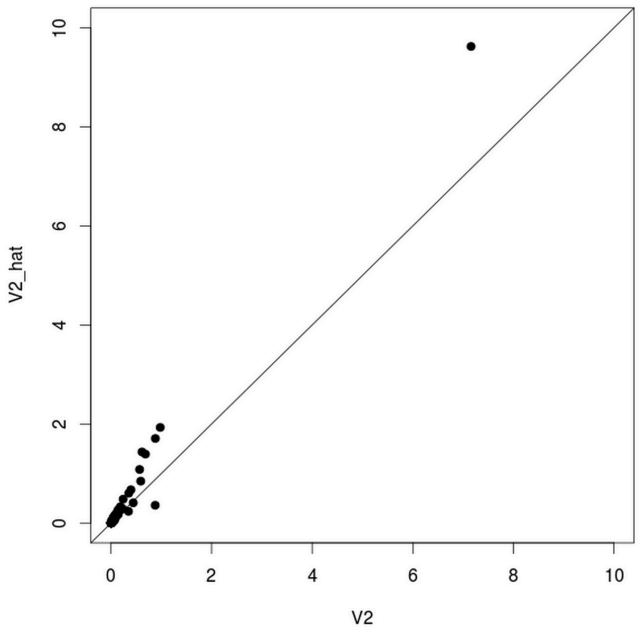

Figure 2.9: V_2 versus $\widehat{V_2}$ (good pools), IWM

2.4.2 EEM

Because of the similarity in the estimation results across assets, I will describe tables and graphs for other assets more briefly. Table 2.6 indicates similar impact of pooling on the estimation: better standard errors and z score, smaller range of estimates for β and γ^2 and little effect on the distribution of estimates for $\bar{c}$.

Figures 2.10, 2.11 and 2.12 show time series of the estimates for the three parameters over the 8 year sample period for EEM. The mean reversion rate β shows no evidence of a trend over time but $\bar{c}$ and γ^2 estimates vary. The same three pairs of dashed lines are added in these two graphs. The magnitude of $\widehat{\bar{c}}$ is more than 2 times larger than that of SPY. The impact of the financial crisis on $\bar{c}$ and γ^2 is clear but there is little evidence of surge in volatility in the other two periods. Because EEM tracks emerging market indexes, it is not surprising that EEM is less impacted by the Eurozone crisis and the lowering of credit rating for the U.S. government. In contrast to SPY and the other assets, the volatility of volatility is very noisy in 2007.

There are 11 cases that fail the Feller inequality, illustrated by Figure 2.13. However, most of the good pools have γ^2 smaller than $2\kappa\bar{c}$. The sample first and second order moments, except for a few outliers, cluster along the 45^o line.

Table 2.6: Estimates of β, $\bar{c}$ and γ^2, EEM

	good days			good pools		
	$\widehat{\beta}$	$\widehat{\bar{c}}$	$\widehat{\gamma^2}(\times 10^3)$	$\widehat{\beta}$	$\widehat{\bar{c}}$	$\widehat{\gamma^2}(\times 10^3)$
median	0.22	0.20	6.73	0.11	0.20	3.11
lower quartile	0.15	0.14	4.09	0.08	0.15	2.28
upper quartile	0.32	0.31	12.30	0.14	0.30	6.10
median standard error	0.08	0.02	4.05	0.04	0.02	1.42
mean	0.26	0.36	21.92	0.12	0.34	8.02
median z-score	2.60	10.23	1.61	2.65	13.04	2.00

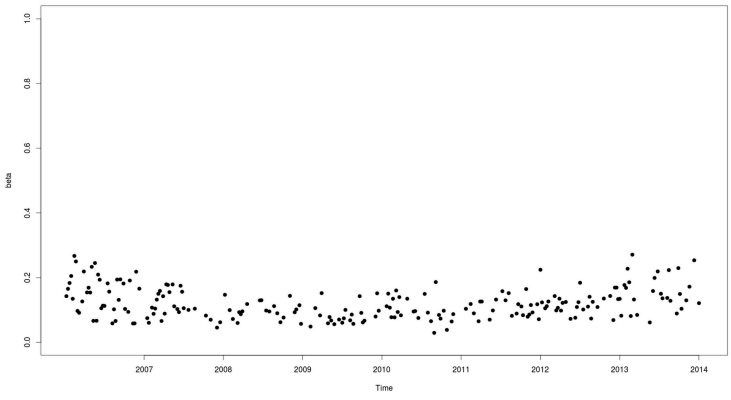

Figure 2.10: Time series for $\widehat{\beta}$ (good pools), EEM

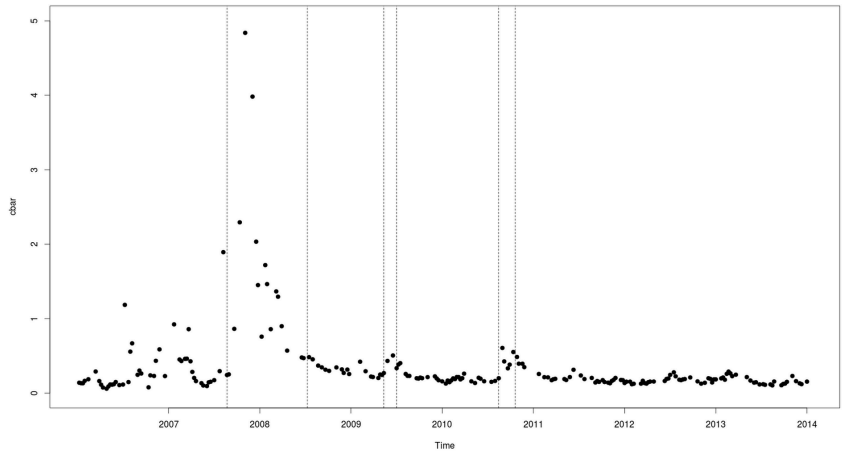

Figure 2.11: Time series for $\widehat{\widehat{c}}$ (good pools), EEM

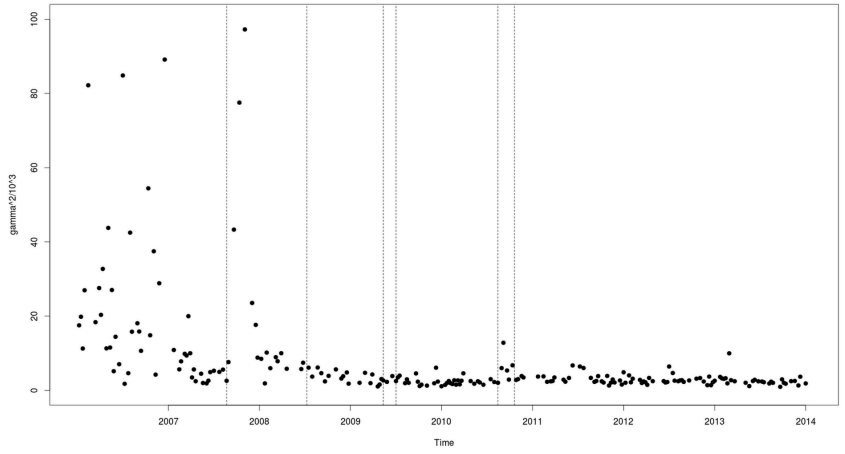

Figure 2.12: Time series for $\widehat{\gamma^2}$ (good pools),EEM

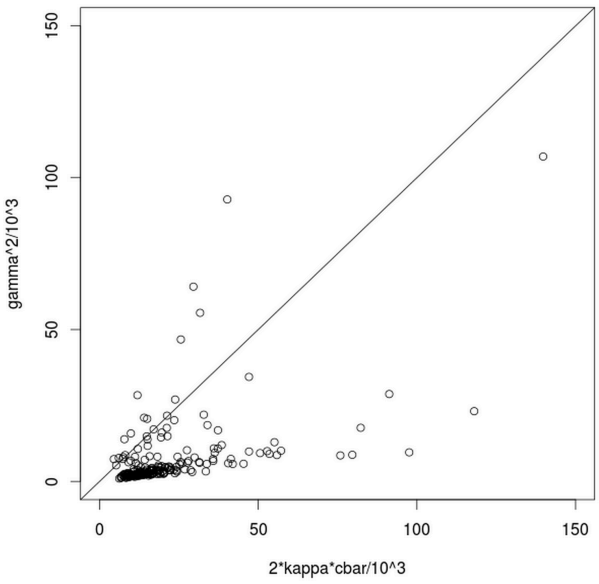

Figure 2.13: Feller condition (good pools), EEM

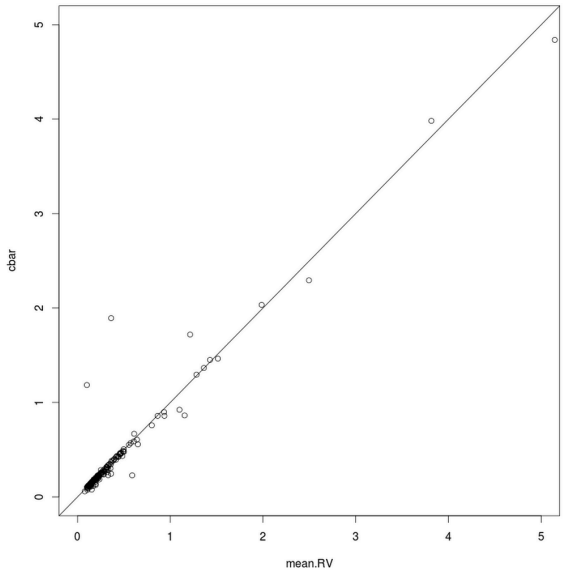

Figure 2.14: $\widehat{\overline{c}}$ versus mean of RV (good pools), EEM

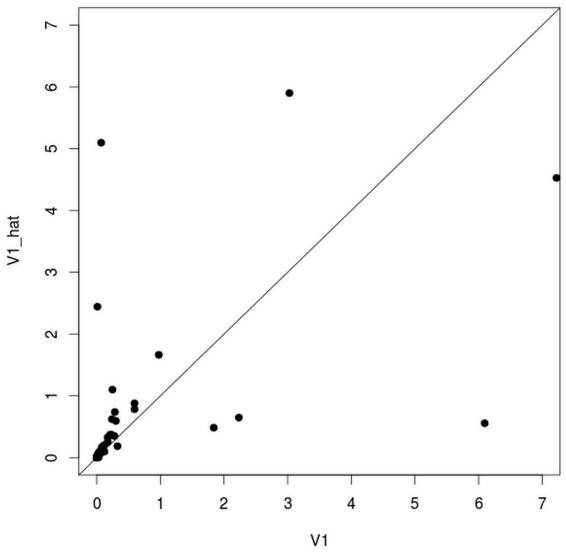

Figure 2.15: V_1 versus $\widehat{V_1}$ (good pools), EEM

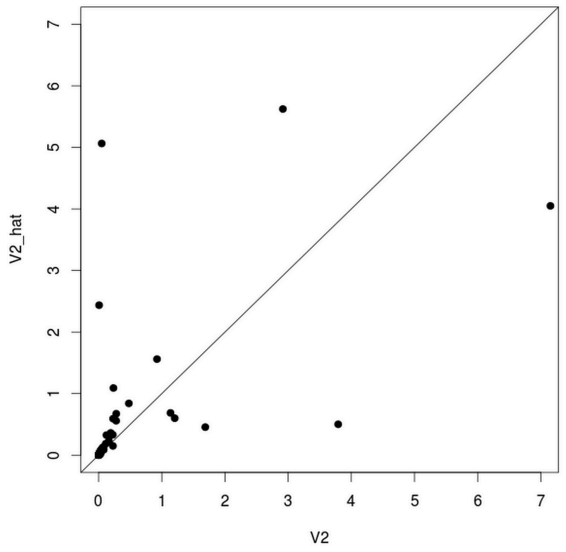

Figure 2.16: V_2 versus $\widehat{V_2}$ (good pools), EEM

2.4.3 BAC

Table 2.7 indicates that pooling helps to generate better standard errors and z scores for all the parameter estimates. Pool estimation also provides smaller mean, median and interquartile range for estimates of β and γ^2 but has little effect on the distribution of $\bar{c}$ estimates.

The time series graphs demonstrate the rate of mean reversion has no evidence of a trend over time but $\bar{c}$ and γ^2 estimates varies tremendously. The scale of $\widehat{\bar{c}}$ for BAC is more than 20 times larger than the scale of SPY, showing a profound impact of the financial crisis on the banking sector. On the other hand, the eurozone crisis (indicated by the middle pair of vertical lines) had little impact on BAC. The credit crisis however, seems to have had a more lasting effect than SPY, taking more than two years to settle down. It provides evidence of the multi-dimensional nature of market risks.

There are no cases in which the Feller inequality fails, illustrated by Figure 2.20. Despite a few outliers, Figure 2.21 to 2.23 show the sample first and second order moments in RVs for BAC match the predicted moments fairly closely for most good pools.

Table 2.7: Estimates of β, $\bar{c}$ and γ^2, BAC

	good days			good pools		
	$\widehat{\beta}$	$\widehat{\bar{c}}$	$\widehat{\gamma^2}(\times 10^3)$	$\widehat{\beta}$	$\widehat{\bar{c}}$	$\widehat{\gamma^2}(\times 10^3)$
median	0.23	2.87	31.04	0.12	3.10	19.14
lower quartile	0.16	1.44	15.89	0.09	1.60	11.87
upper quartile	0.32	5.35	73.95	0.15	6.25	42.65
median standard error	0.07	0.15	17.27	0.04	0.12	8.32
mean	0.27	4.87	63.88	0.13	4.69	42.23
median z-score	2.91	17.74	1.71	3.04	23.86	2.22

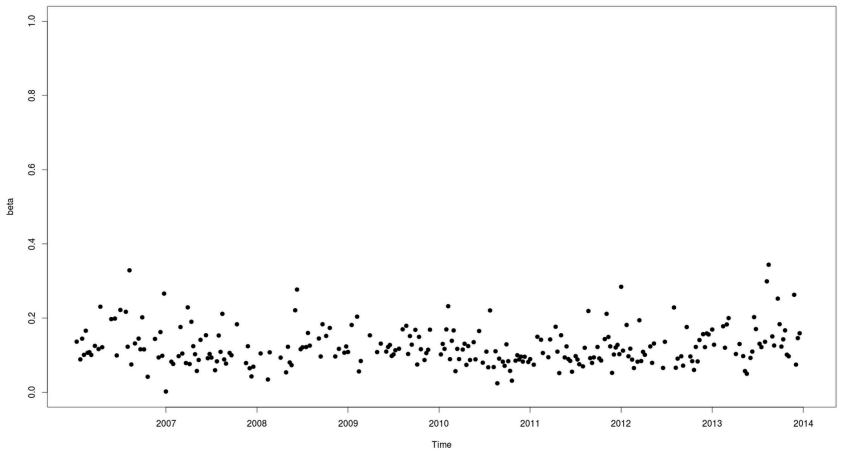

Figure 2.17: Time series for $\widehat{\beta}$ (good pools), BAC

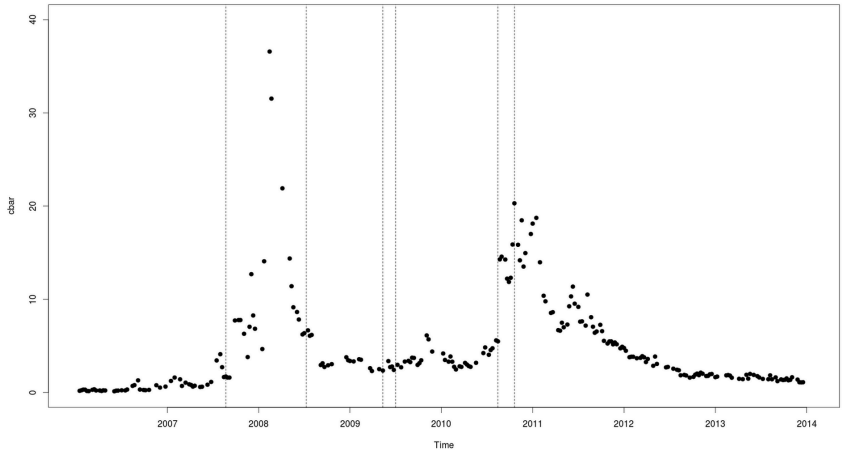

Figure 2.18: Time series for $\widehat{\bar{c}}$ (good pools), BAC

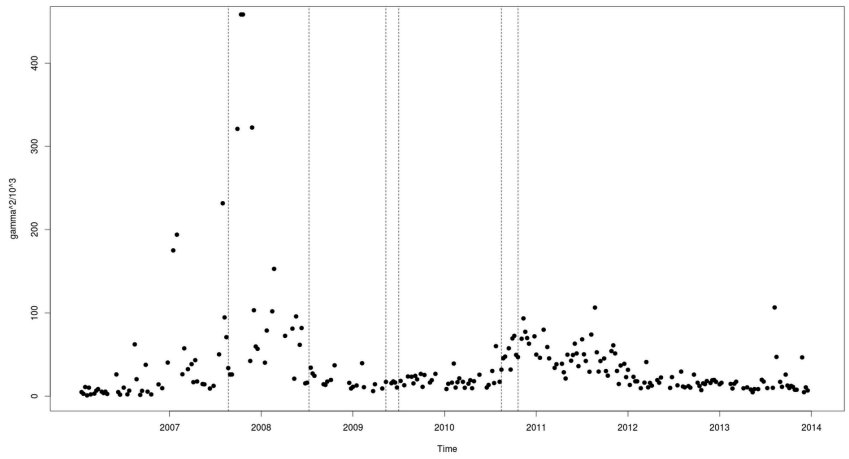

Figure 2.19: Time series for $\widehat{\gamma^2}$ (good pools),BAC

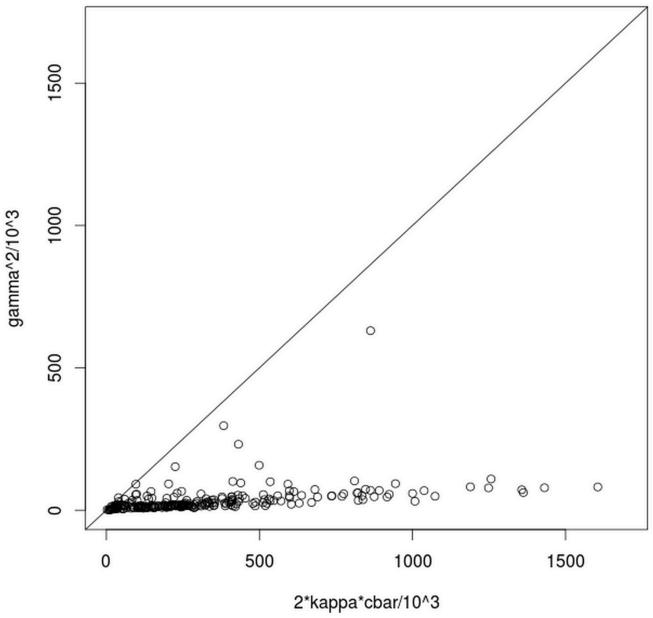

Figure 2.20: Feller condition, BAC

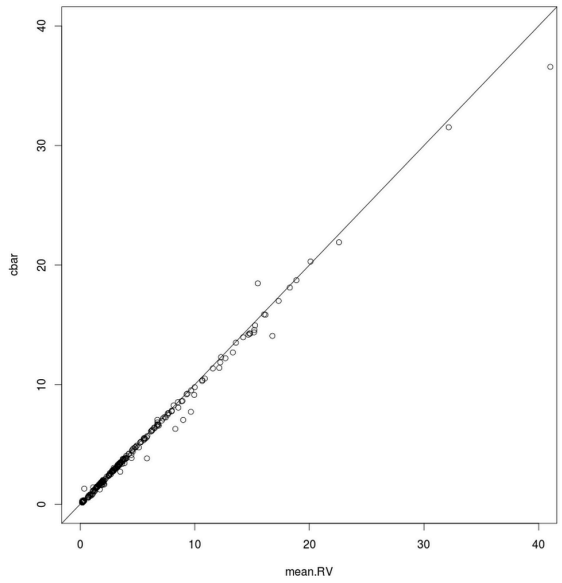

Figure 2.21: $\widehat{\bar{c}}$ versus mean of RV (good pools), BAC

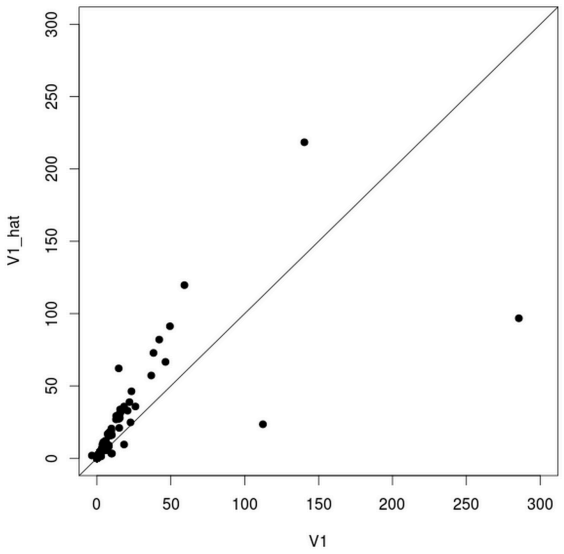

Figure 2.22: V_1 versus $\widehat{V_1}$ (good pools), BAC

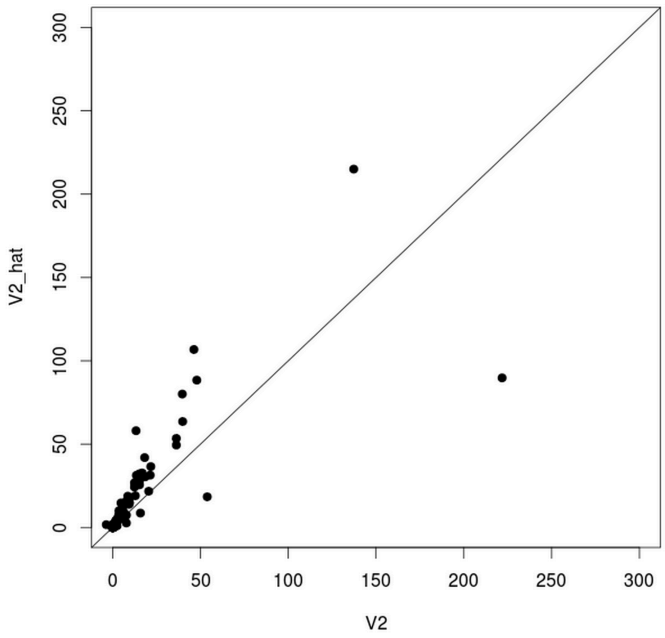

Figure 2.23: V_2 versus $\widehat{V_2}$ (good pools), BAC

2.4.4 CVX

Pooling has a similar impact on the estimation for CVX, as shown by Table 2.8. The time series graphs for the mean reversion rate evolves in the same fashion as that of SPY. In Figure 2.25, the scale is three times than the $\widehat{\bar{c}}$ graph of SPY, showing a profound impact of the financial crisis. However, there is little sign that sovereign debt crisis laid an impact on CVX. Moreover, the credit crisis did cause a surge of volatility. The same is true of the estimates of γ^2 in Figure 2.26. There are 51 good pools fail the Feller inequality, as illustrated in Figure 2.27. Most of the pools that violate the Feller condition lie reasonably close to the 45^o line. Despite a few outliers, Figure 2.28 to 2.30 show the sample first and second order moments in RVs for CVX are, except from a few outliers, close to the 45^o line.

Table 2.8: Estimates of β, $\bar{c}$ and γ^2, CVX

	good days			good pools		
	$\widehat{\beta}$	$\widehat{\bar{c}}$	$\widehat{\gamma^2}(\times 10^3)$	$\widehat{\beta}$	$\widehat{\bar{c}}$	$\widehat{\gamma^2}(\times 10^3)$
median	0.17	0.16	7.04	0.11	0.17	7.67
lower quartile	0.12	0.09	3.52	0.08	0.10	4.22
upper quartile	0.27	0.29	14.90	0.15	0.31	13.77
median standard error	0.05	0.02	6.38	0.03	0.02	3.85
mean	0.21	0.29	17.17	0.12	0.31	27.39
median z-score	3.36	7.53	1.29	3.75	10.06	1.87

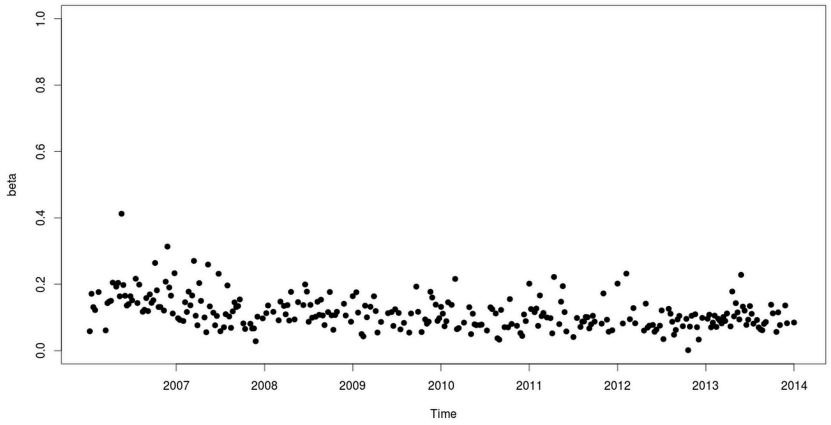

Figure 2.24: Time series for $\widehat{\beta}$ (good pools), CVX

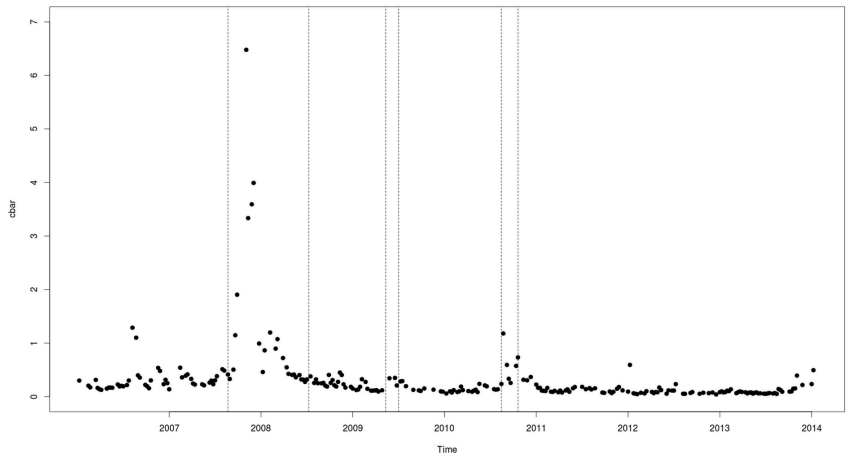

Figure 2.25: Time series for $\widehat{\overline{c}}$ (good pools), CVX

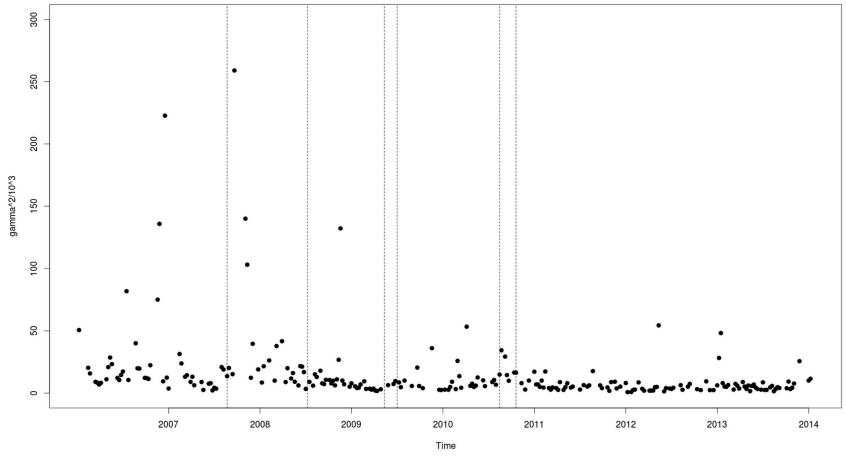

Figure 2.26: Time series for $\widehat{\gamma^2}$ (good pools),CVX

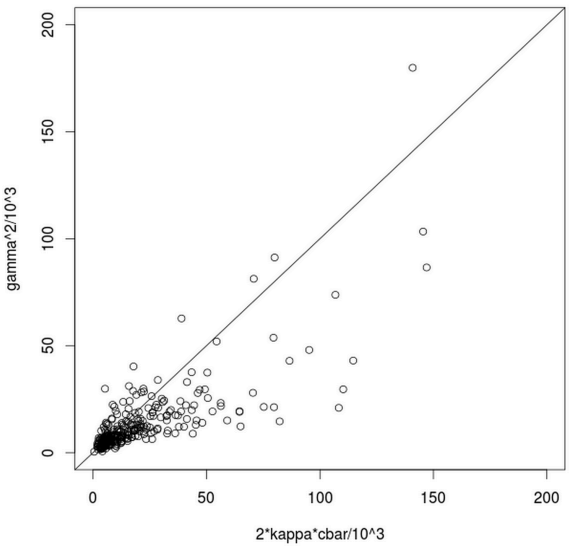

Figure 2.27: Feller condition (good pools), CVX

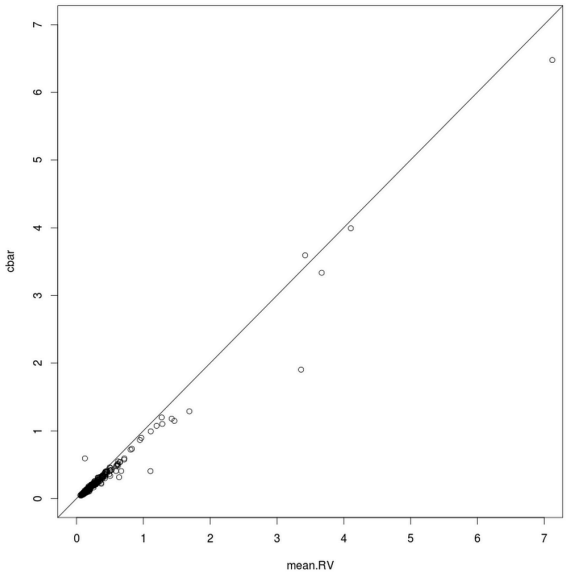

Figure 2.28: $\widehat{\bar{c}}$ versus mean of RV (good pools), CVX

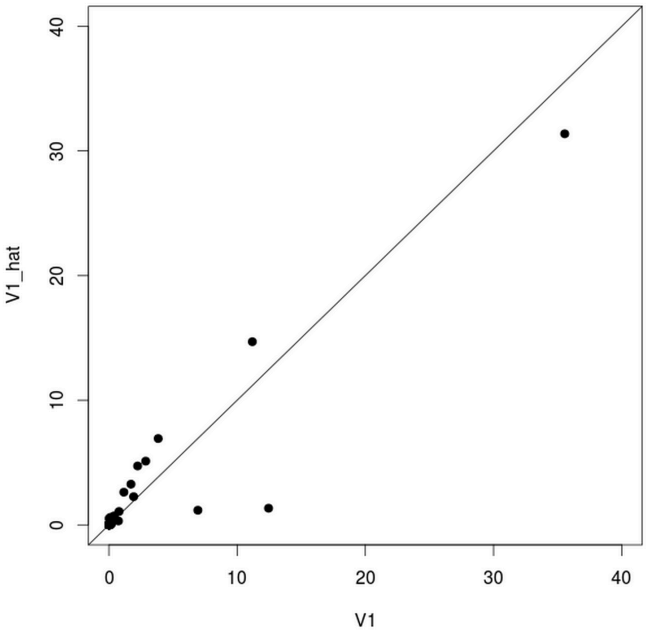

Figure 2.29: V_1 versus $\widehat{V_1}$ (good pools), CVX

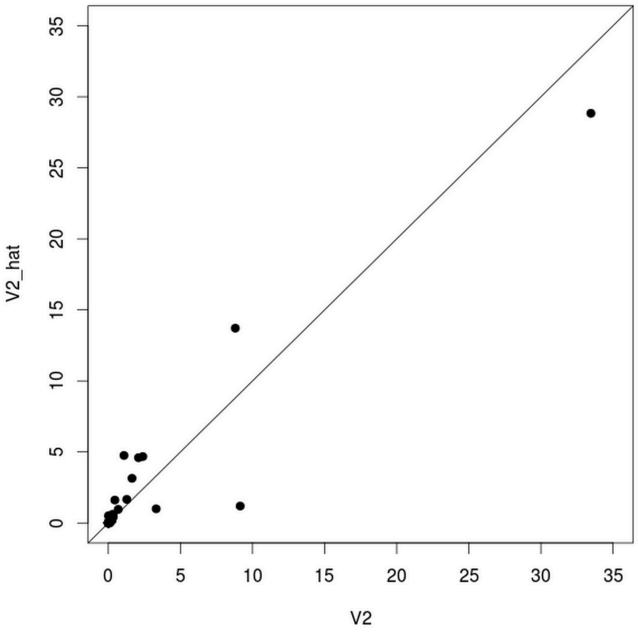

Figure 2.30: V_2 versus $\widehat{V_2}$ (good pools), CVX

2.4.5 IBM

Pooling has the by now familiar impact on the estimation for IBM, as shown in Table 2.9. The time series graphs of $\widehat{\bar{c}}$ and $\widehat{\gamma^2}$ for IBM are almost identical to the ETFs but the magnitude of the peaks is much larger. There are 119 cases that fail the Feller inequality, the largest number of differences of all the 8 assets including SPY. Fortunately, most of the pools that violate the Feller condition still lie reasonably close to the 45^o line, illustrated by Figure 2.34. We conjecture that sampling prices every millisecond would alleviate this problem, because the number of trades per active time stamp is quite high. Despite a few outliers, Figure 2.35, 2.36 and 2.37 show that the moment conditions have relatively small errors.

Table 2.9: Estimates of β, $\bar{c}$ and γ^2, IBM

	good days			good pools		
	$\widehat{\beta}$	$\widehat{\bar{c}}$	$\widehat{\gamma^2}(\times 10^3)$	$\widehat{\beta}$	$\widehat{\bar{c}}$	$\widehat{\gamma^2}(\times 10^3)$
median	0.18	0.13	9.60	0.12	0.12	10.30
lower quartile	0.13	0.08	5.35	0.09	0.09	6.40
upper quartile	0.26	0.23	20.38	0.15	0.22	17.09
median standard error	0.05	0.02	8.34	0.03	0.02	5.15
mean	0.22	0.26	24.75	0.12	0.24	24.00
median z-score	3.45	6.71	1.26	3.92	8.93	1.90

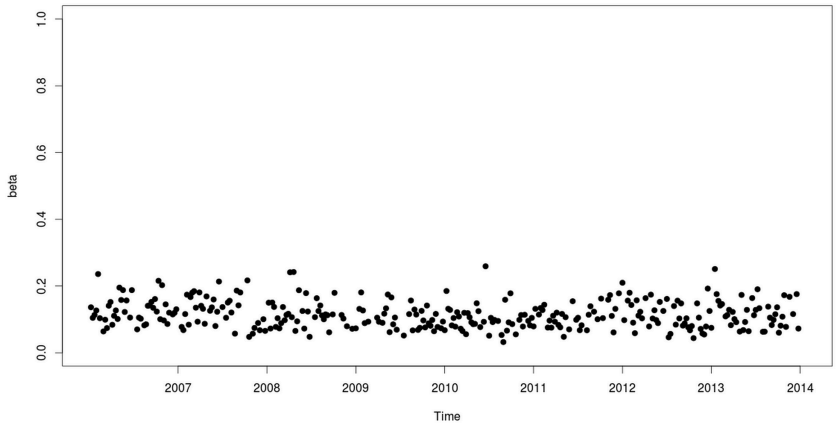

Figure 2.31: Time series for $\widehat{\beta}$ (good pools), IBM

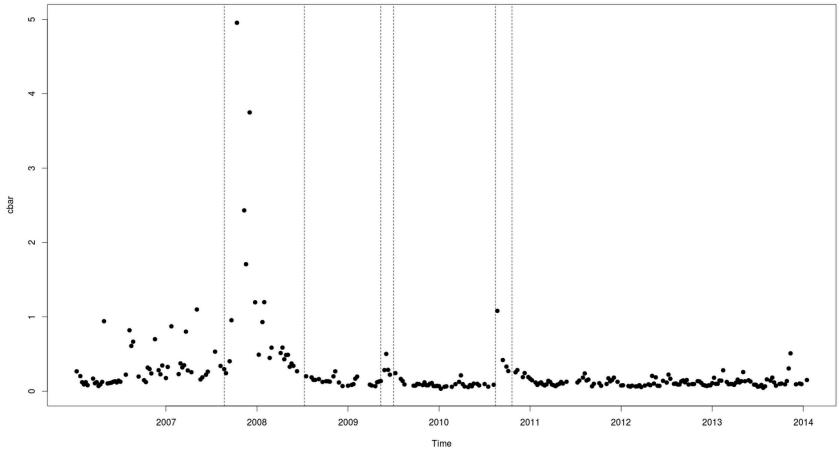

Figure 2.32: Time series for $\widehat{c}$ (good pools), IBM

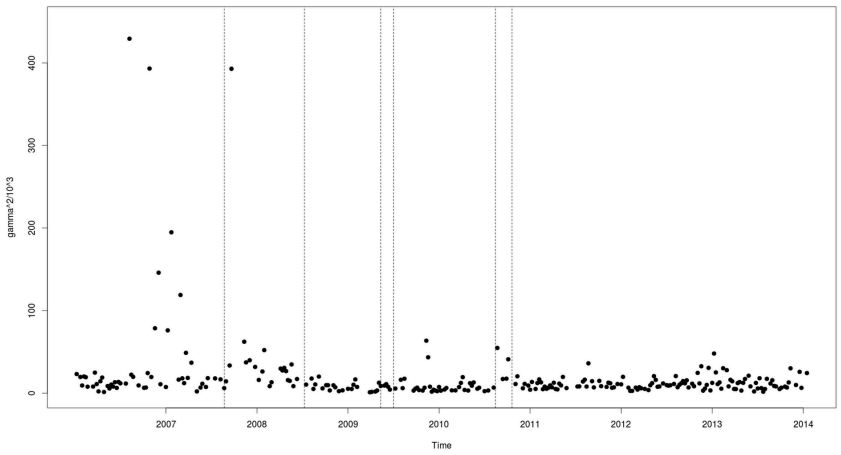

Figure 2.33: Time series for $\widehat{\gamma^2}$ (good pools), IBM

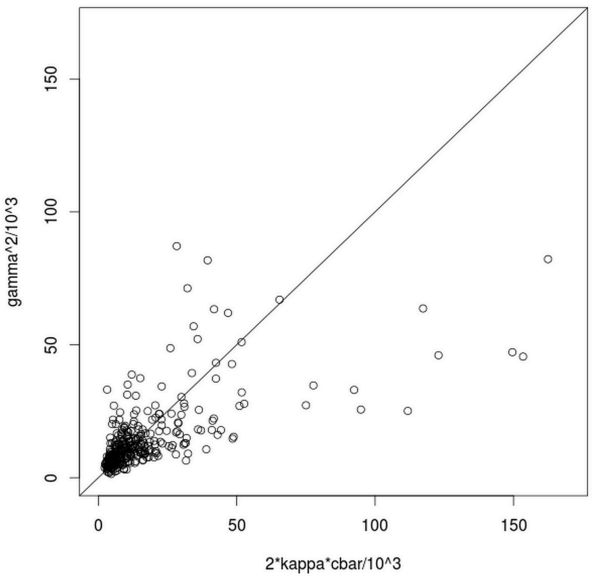

Figure 2.34: Feller condition (good pools), IBM

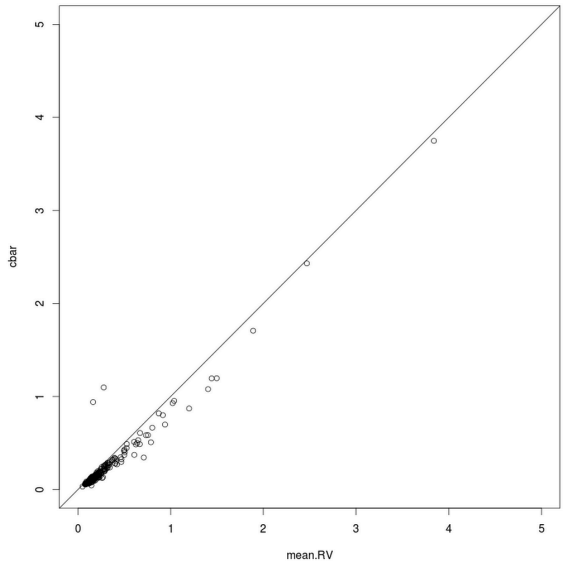

Figure 2.35: $\widehat{\bar{c}}$ versus mean of RV (good pools), IBM

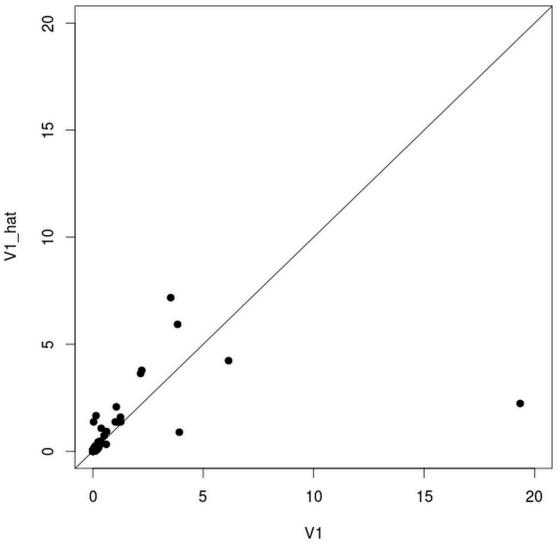

Figure 2.36: V_1 versus $\widehat{V_1}$ (good pools), IBM

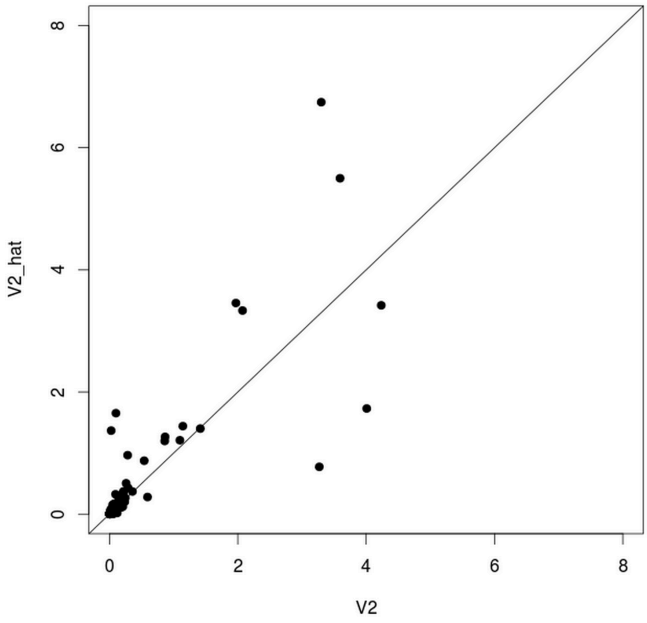

Figure 2.37: V_2 versus $\widehat{V_2}$ (good pools), IBM

2.4.6 INTC

The impact of pooling on the estimation for INTC fits the usual pattern, illustrated by Table 2.10. The time series graph for $\bar{c}$ estimates for INTC shows a different pattern than Figure 1.6 for SPY. After the financial crisis, $\bar{c}$ returns to a level slightly higher than that before the crisis and gradually declines until the end of the sample period. This is not surprising as the volatility of a technology stock like INTC may hardly be impacted by the sovereign debt crisis or the credit downgrade of U.S. government. All good pools for INTC satisfy the Feller condition strictly, illustrated by Figure 2.41. Despite a few outliers, the points in Figure 2.42 to 2.44 lie close to the 45^o line.

Table 2.10: Estimates of β, $\bar{c}$ and γ^2, INTC

	good days			good pools		
	$\widehat{\beta}$	$\widehat{\bar{c}}$	$\widehat{\gamma^2}(\times 10^3)$	$\widehat{\beta}$	$\widehat{\bar{c}}$	$\widehat{\gamma^2}(\times 10^3)$
median	0.21	0.90	15.29	0.11	0.95	8.74
lower quartile	0.15	0.58	9.05	0.08	0.64	5.33
upper quartile	0.29	1.24	25.44	0.14	1.27	15.24
median standard error	0.06	0.06	9.05	0.04	0.05	4.11
mean	0.24	1.05	31.71	0.12	1.06	16.98
median z-score	2.79	13.70	1.66	2.83	17.22	2.05

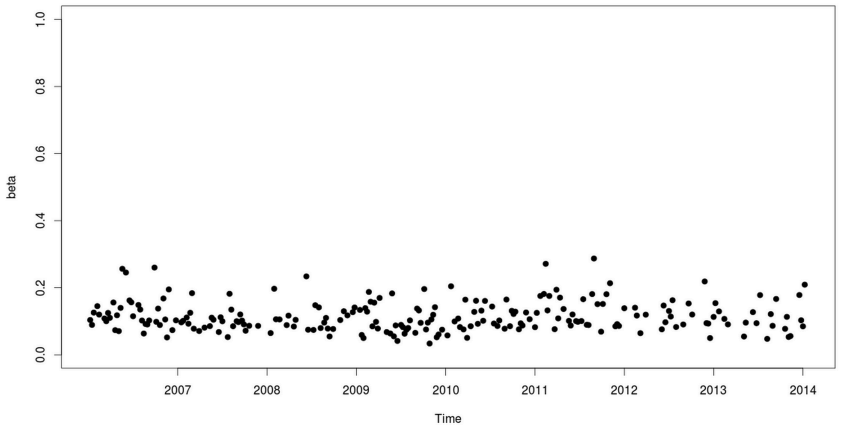

Figure 2.38: Time series for $\widehat{\beta}$ (good pools), INTC

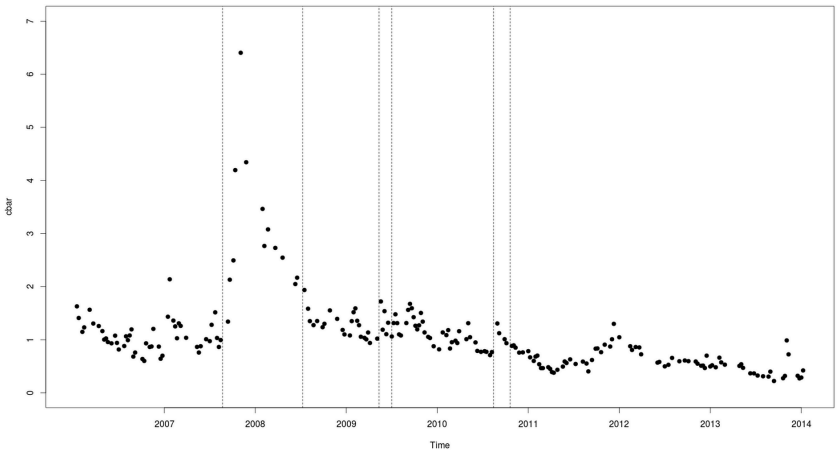

Figure 2.39: Time series for $\widehat{\widehat{c}}$ (good pools), INTC

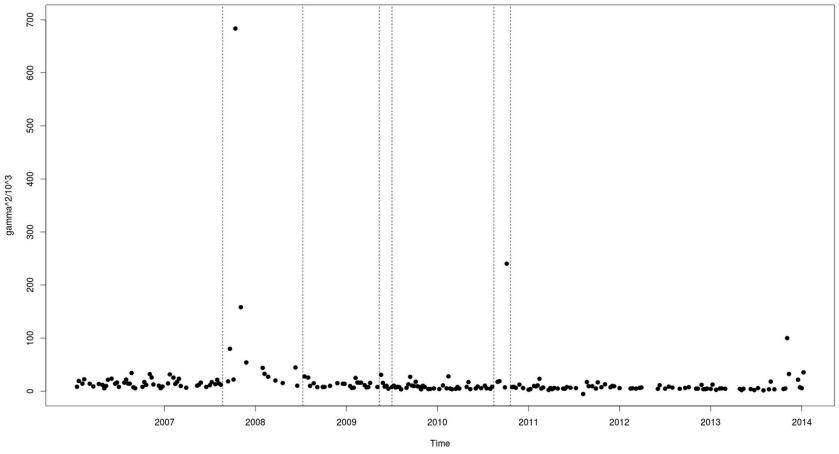

Figure 2.40: Time series for $\widehat{\gamma^2}$ (good pools), INTC

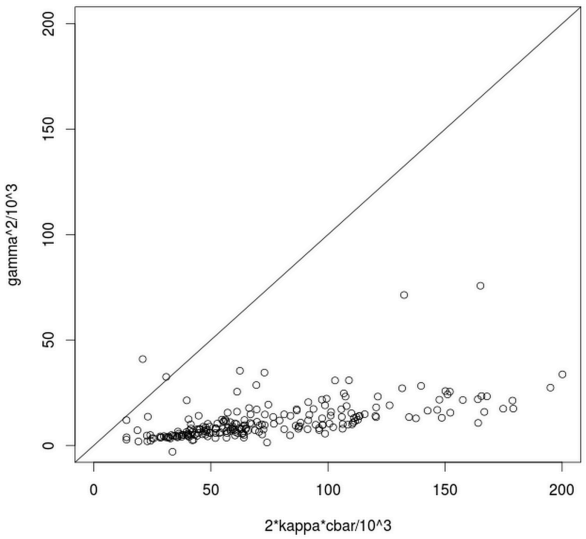

Figure 2.41: Feller condition, INTC

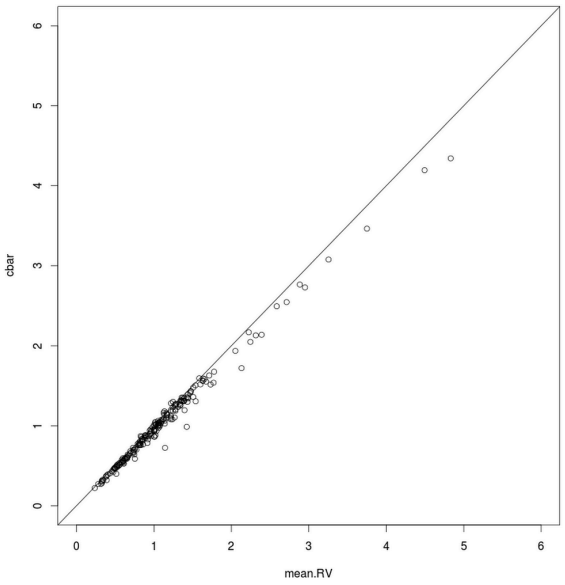

Figure 2.42: $\widehat{\widehat{c}}$ versus mean of RV (good pools), INTC

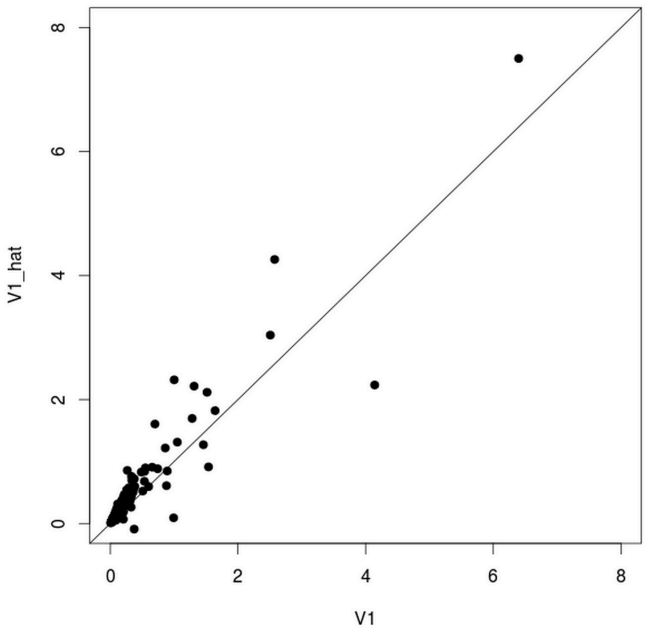

Figure 2.43: V_1 versus $\widehat{V_1}$ (good pools), INTC

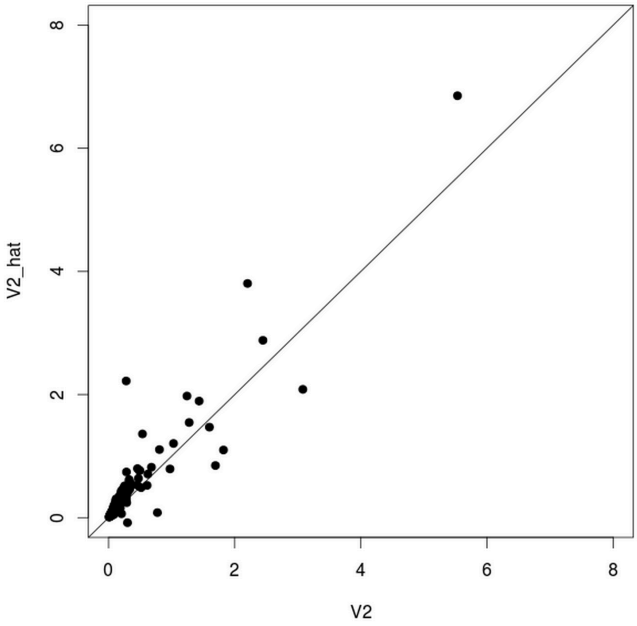

Figure 2.44: V_2 versus $\widehat{V_2}$ (good pools), INTC

2.4.7 MSFT

The impact of pooling on the estimation for MSFT fits the regular pattern, illustrated by Table 2.11. The time series graph of parameter estimates for MSFT are similar to those of INTC, not surprising since they belong to the technology sector. The volatility of volatility estimates are smooth over time except for one huge outlier in the financial crisis that is 33 times its mean. There are no failures for the Feller condition. Despite a few outliers, the sample first and second order moments in RVs for MSFT are close to the 45^o line.

Table 2.11: Estimates of β, $\bar{c}$ and γ^2, MSFT

	good days			good pools		
	$\widehat{\beta}$	$\widehat{\bar{c}}$	$\widehat{\gamma^2}(\times 10^3)$	$\widehat{\beta}$	$\widehat{\bar{c}}$	$\widehat{\gamma^2}(\times 10^3)$
median	0.21	0.58	11.91	0.12	0.57	6.71
lower quartile	0.15	0.40	6.79	0.09	0.40	4.26
upper quartile	0.31	0.80	21.02	0.15	0.74	10.25
median standard error	0.07	0.04	7.45	0.04	0.03	3.03
mean	0.25	0.75	28.90	0.13	0.66	10.21
median z-score	2.88	12.92	1.60	2.85	17.61	1.98

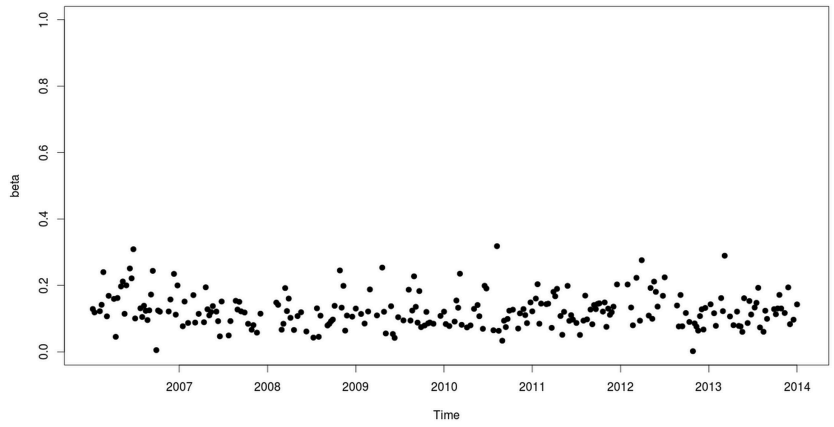

Figure 2.45: Time series for $\widehat{\beta}$ (good pools), MSFT

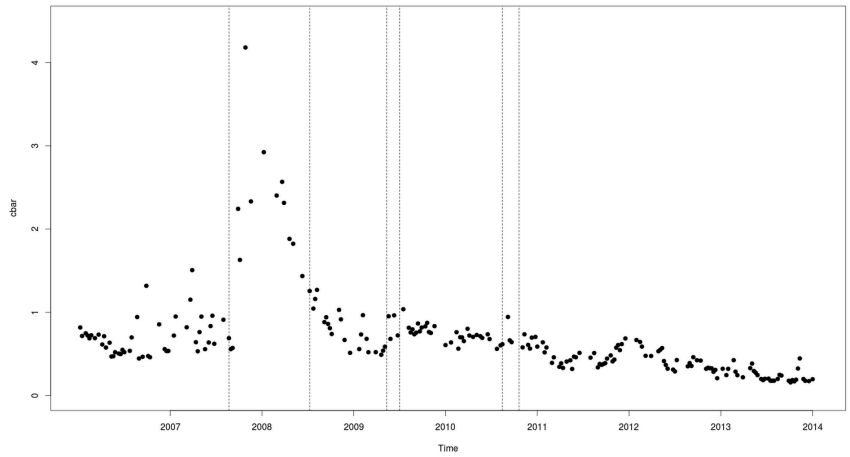

Figure 2.46: Time series for $\widehat{\bar{c}}$ (good pools), MSFT

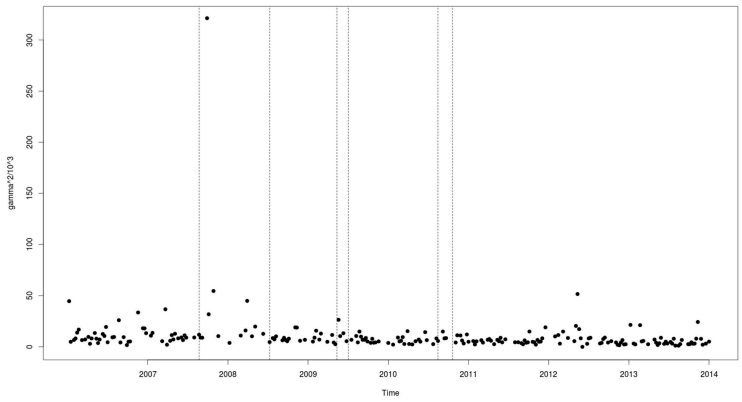

Figure 2.47: Time series for $\widehat{\gamma^2}$ (good pools), MSFT

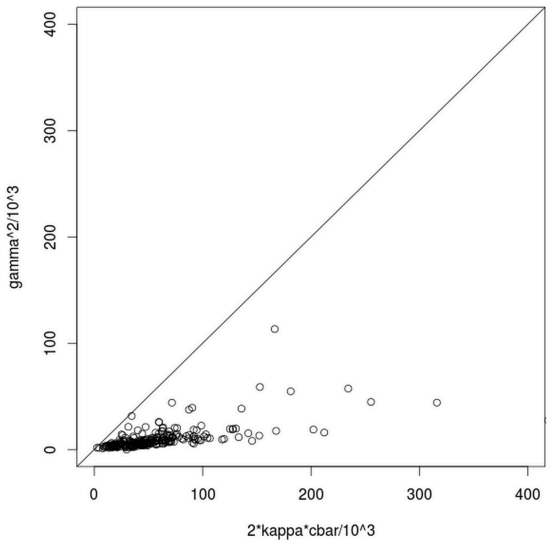

Figure 2.48: Feller condition (good pools), MSFT

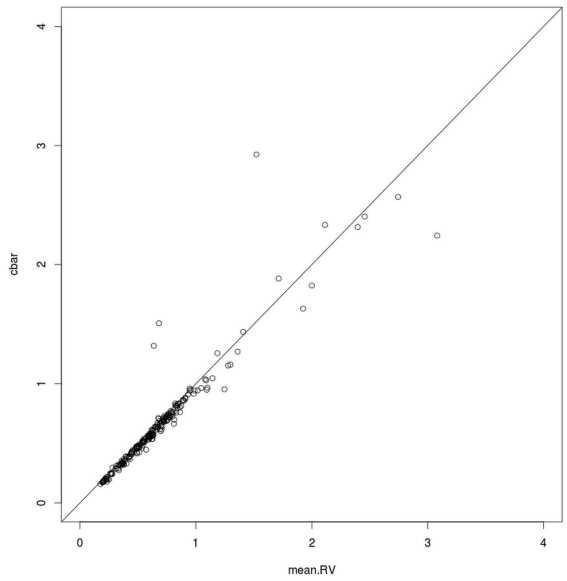

Figure 2.49: $\widehat{\overline{c}}$ versus mean of RV (good pools), MSFT

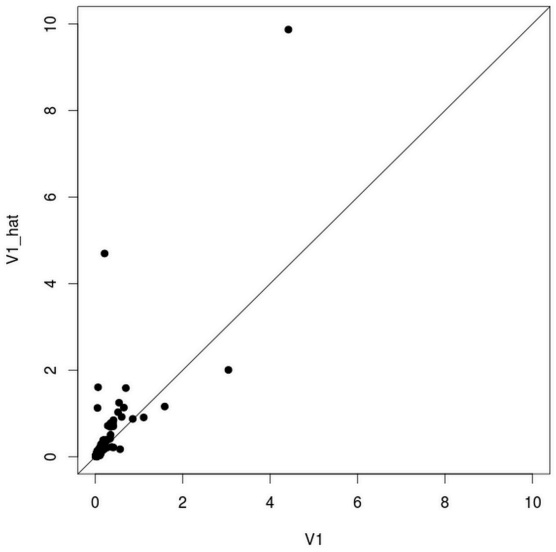

Figure 2.50: V_1 versus $\widehat{V}_1$ (good pools), MSFT

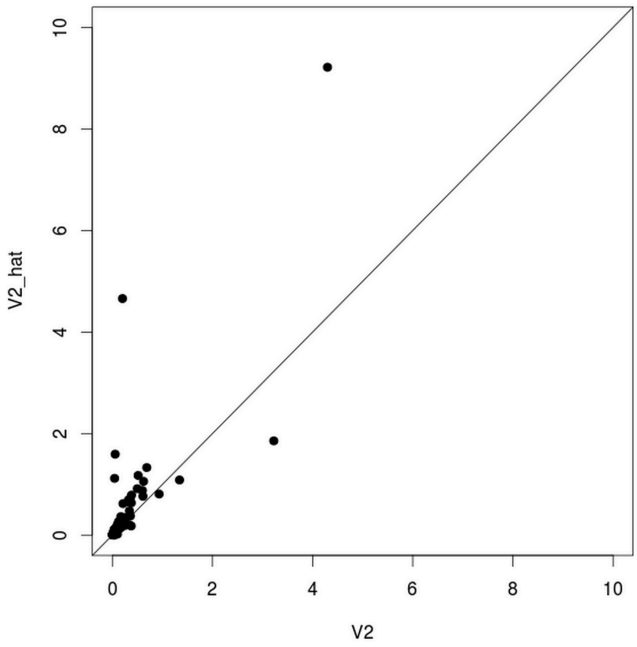

Figure 2.51: V_2 versus $\widehat{V}_2$ (good pools), MSFT

2.5 Common patterns and differences among assets

This section considers the parameter estimates for all 8 assets as a whole. We show some common patterns for the three parameters and point to some notable differences in parameter estimates across assets.

The first three rows of Table 2.12 present the median and interquartile range of the estimates for β, and the median estimate of κ. The interquartile range for the mean reversion rate is tight and almost identical for all assets. The median estimates for of mean reversion rate is similar to that of SPY for all assets as well, which is an astonishing impact of pooling.

Table 2.12: Summary of parameter estimates (good pools)

	IWM	EEM	BAC	CVX	IBM	INTC	MSFT
median $\widehat{\beta}$	0.09	0.11	0.11	0.11	0.11	0.11	0.12
IQ range $\widehat{\beta}$	0.05	0.07	0.06	0.06	0.06	0.05	0.06
median $\widehat{\kappa}(\times 10^3)$	3.0	3.7	3.7	3.7	3.7	3.7	4.0
median $\widehat{c}$	0.17	0.20	3.1	0.18	0.13	0.99	0.58
IQ range $\widehat{c}$	0.19	0.15	4.65	0.21	0.13	0.63	0.34
mean $\widehat{c}$	0.27	0.33	4.5	0.32	0.27	1.1	0.73
median $\widehat{\gamma^2}(\times 10^3)$	3.3	3.6	17.6	9.0	10.8	9.4	6.8
IQ range $\widehat{\gamma^2}(\times 10^3)$	4.00	3.82	30.78	9.55	10.69	5.91	5.99
(max/mean) $\widehat{c}$	11.11	14.71	9.10	20.97	20.83	6.13	6.44
(max/mean) $\widehat{\gamma^2}$	3.77	12.47	10.63	9.50	18.75	40.64	32.81

Figure 2.52 displays the box plot of β estimates for good pools of all assets. The top and bottom of the box give 75% and 25% quartiles of the distribution. The horizontal line inside the box is the median. The two horizontal lines lie outside of the box are called the whiskers. Estimates outside the whiskers (the outliers) are plotted as individual points. The top and bottom whisker for a distribution is calculated by

$$W_T = \min(\max(\widehat{\beta}), Q_3 + 1.5IQR)$$

and

$$W_B = \max(\min(\widehat{\beta}), Q_1 - 1.5IQR)$$

where Q_1 and Q_3 are the 25% and 75% quartiles of the distribution and IQR is the interquartile range, $Q_3 - Q_1$. In Figure 2.52, $W_B = 0.003$ and $W_T = 0.236$, so 99% of the

estimates are within the range of about 0.23. There are no observations below W_B but there are 57 outliers above W_T.

The estimates for $\bar{c}$ and γ^2, on the other hand, vary considerably across stocks. The forth to sixth row of Table 2.12 display the median, IQ range and mean of the estimates for $\bar{c}$. Not surprisingly the banking stock BAC registered the highest level median and mean of $\bar{c}$ over this eight-year period. The interquartile range of $\widehat{\bar{c}}$ for BAC is also largest among all assets, more than 7 times of the second largest (INTC). The seventh and eighth row of Table 2.12 show the median and interquartile range of estimates for γ^2. The interquartile range of stocks are clearly larger than that of ETFs. Figure 2.53 displays box plots of γ^2 estimates of good pools for all assets.

Figure 2.54 compares estimates of $\bar{c}$ with the mean of RVs for all blocks in good pools for all 8 assets. The GMM estimates of $\bar{c}$ are very close to the 45^o line with only two exceptions.

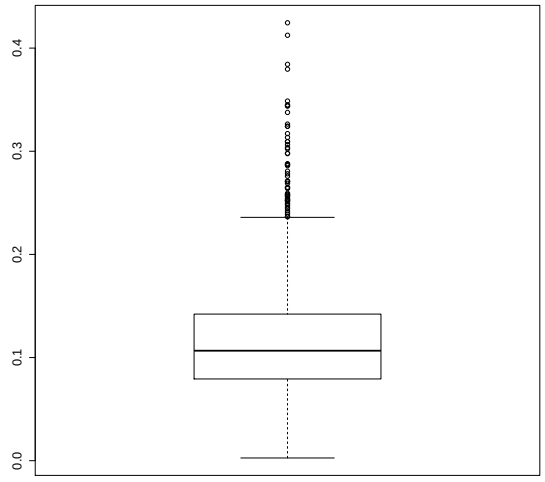

Figure 2.52: Box plots of $\widehat{\beta}$ (good pools), all assets

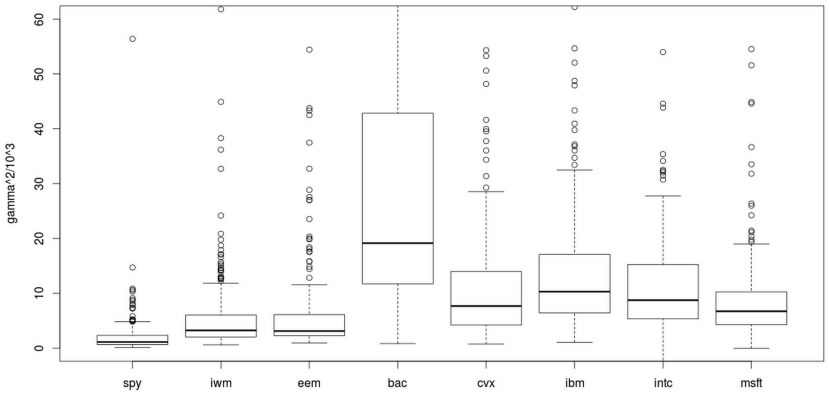

Figure 2.53: Box plots of $\widehat{\gamma^2}$ (good pools), all assets

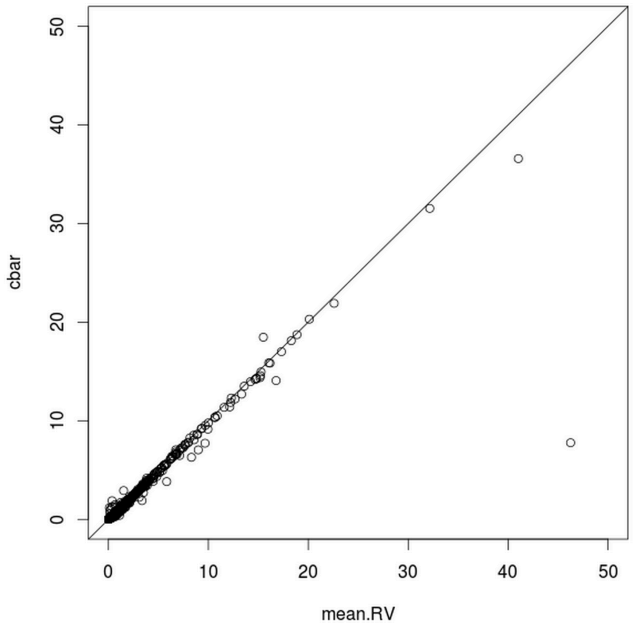

Figure 2.54: $\widehat{\overline{c}}$ versus mean of RVs (good pools), all assets

We also estimated the Heston model for these assets using daily RV sampled every five

minutes and once every second. Results are demonstrated in Table 2.13. The results are similar to the case of SPY: when prices are sampled every five minutes, the estimates of $\bar{c}$ are usually roughly similar to the mean of intraday estimates. However, estimates of κ and γ^2 are two orders of magnitude smaller than the mean of intraday estimates. In the intraday setting, volatility is very volatile but quickly reverts toward its mean. In the interday model, volatility is much less volatile and reverts much smaller to its mean.

2.6 Conclusion

This chapter provides additional evidence for the Heston intraday stochastic volatility model, testing the model for two additional ETFs and five stocks. While these other assets are traded less frequently than SPY, the fraction of active time stamps does not fall as quickly as their frequency of trades. Lower trade volume and a high fraction of inactive time stamps have little impact on the model performance.

For estimates in good pools, I find strong evidence that the rate of mean reversion is roughly constant across the entire sample. The estimates of $\bar{c}$ and γ^2 for the seven assets vary a lot over time similar to SPY, but with very different scales. For example, the times series of $\widehat{\bar{c}}$ and $\widehat{\gamma^2}$ for the financial stocks have a much higher peak than the other stocks. The interquartile range of $\widehat{\bar{c}}$ and $\widehat{\gamma^2}$ for stocks are obviously larger than ETFs. I also compare our model with the model using daily realized volatility and parameters held constant over the entire sample period. The results are very different. The speed of mean reversion is much more rapid in our model and the volatility-of-volatility is much higher.

Table 2.13: Heston model using daily RV with different sampling frequency

		Interday		Intraday	
Ticker	parameter	estimate	zscore	mean estimate	median z score
IWM	$\widehat{\kappa}$	83	2.99	3.32×10^4	3.11
	$\widehat{\bar{c}}$	0.26	4.80	0.27	11.15
	$\widehat{\gamma^2}$	64.94	2.28	16.45	2.31
EEM	$\widehat{\kappa}$	55	2.35	3.85×10^4	2.65
	$\widehat{\bar{c}}$	0.19	4.16	0.34	13.04
	$\widehat{\gamma^2}$	63.06	1.41	8.02	2.00
BAC	$\widehat{\kappa}$	55	2.44	4.39×10^4	3.04
	$\widehat{\bar{c}}$	0.87	3.63	4.69	23.86
	$\widehat{\gamma^2}$	519.61	1.62	42.23	2.22
CVX	$\widehat{\kappa}$	69	3.48	3.85×10^4	3.75
	$\widehat{\bar{c}}$	0.27	5.33	0.31	10.06
	$\widehat{\gamma^2}$	76.41	1.17	27.39	1.87
IBM	$\widehat{\kappa}$	55	2.16	3.85×10^4	3.92
	$\widehat{\bar{c}}$	0.21	4.29	0.24	8.93
	$\widehat{\gamma^2}$	32.40	1.37	24.00	1.90
INTC	$\widehat{\kappa}$	83	3.32	3.85×10^4	2.83
	$\widehat{\bar{c}}$	0.31	7.98	1.06	17.22
	$\widehat{\gamma^2}$	38.54	2.03	16.98	2.05
MSFT	$\widehat{\kappa}$	83	2.88	4.39×10^4	2.85
	$\widehat{\bar{c}}$	0.28	6.99	0.66	17.61
	$\widehat{\gamma^2}$	72.93	2.28	10.21	1.98

CHAPTER 3

The Evidence for Jumps in Intraday Stochastic Volatility

3.1 Introduction

In Chapters 1 and 2 I estimated the Heston model using SPY and other 7 assets. I demonstrate the continuous path of quadratic variation during a trading day can be described by the Heston model. However, the Heston model is not the whole story, as jumps could happen when volatility is volatile. Thus an attractive extension of the model is to allow for jumps in the price process or the volatility process. This chapter examines the evidence for the presence of jumps.

The study focuses on the realized volatilities on each trading day during 2007-2014 for SPY, the asset we have investigated the most in the previous chapters. I examine trading days pool by pool. Because the average RV varies substantially from pool to pool, we can not rely on the absolute magnitude of RVs to look for jumps. Therefore, I construct a measure of relative realized volatility (RRV) to overcome this difficulty.

After identifying pools with large jumps using the distribution of RRVs, I investigate the path behavior of these pools. I begin with good pools, which occupy 71% of the sample for SPY. In these pools, I find large RVs are relatively rare. They tend to occur together and are likely to trigger a cascade of volatility jumps. The remaining RVs stay quiet most of the time but are often higher at the beginning of a trading day. With the presence of volatility jumps, the pool estimate of $\bar{c}$ is likely to be higher than the median RV.

For the bad pools, I find large RVs happen considerably more often. As in the case for

good pools, large RVs for bad pools are tend to occur together and are likely to trigger a series of volatility jumps. Moreover, I provide evidence that most of the data in a pool are explained by the Heston model if we take out the jumps. The discussion paves the way for future modeling of jumps in the Heston model.

The rest of chapter is organized as follows: Section 3.2 provides our classification of jumps based on the empirical distribution of realized volatilities over 100 second time blocks. Section 3.3 and 3.4 investigate the path behavior of RV processes in good and bad pools respectively when jump are present. Section 3.5 concludes the chapter.

3.2 Classifying realized volatilities

We have relied on realized volatilities over 100 second intervals to estimate the Heston model. In this chapter, we would like to develop an empirical definition of jumps independent of any models but simply depend on the 100-second RVs. In other words, we would like to start with the empirical distribution of RVs for SPY over the entire 8 year sample period and identify outliers. We conclude the price or volatility process contain a jump when RV some threshold. This strategy is complicated by the fact that the average volatility changes greatly over the sample period. For example, the largest average RV over a trading day is 17.42 in the financial crisis while the average RV of the entire sample is only 0.087.

The relative realized volatility(RRV) measure solves this difficulty by looking at the ratio of RV divided by the median RV of the pool. RRV judges what constitutes an outlier by a relative standard that uses the median RV as a reference point. In other words, a large deviation from the median is not supposed to be captured by mean reversion or stochastic volatility, and hence likely to be a jump. We use median RV instead of $\bar{c}$ because median RV is model free. The median is a measure of central tendency that is less sensitive to the presence of outliers than the mean.

Table 3.1: Order statistics of RRV

	Q_1	Q_3	median	W_U	max
good pools	0.72	1.41	1.00	2.45	1368.9
bad pools	0.71	1.42	1.00	2.48	7308.5
RRV in $[0, 2.5)$ (good pools)	0.70	1.33	0.97	2.28	2.50
RRV in $[0, 2.5)$ (bad pools)	0.70	1.33	0.97	2.28	2.50

Table 3.1 presents the order statistics for RRV. There are $234 \times 2014 = 471{,}276$ blocks in the sample, of which $234 \times 286 \times 5 = 334{,}620$ are blocks for good pools, and 136,656 blocks from bad pools[1]. The lower and upper quartile of the distribution of RRVs are indicated by Q_1 and Q_3 correspondingly. W_U is the upper whisker and calculated as $W_U = min[max(RRVs), Q_3 + 1.5IQR]$, where IQR is the interquartile range. W_U is not an order statistic but a reasonable threshold for outliers.

To make use of W_U in identifying jumps, I separate the RRVs into good pools and bad pools, presented in Table 3.1. The two distributions have the same median and almost same interquartile range[2]. Their W_U are also very close. Moreover, the distribution of RRVs below W_U is not much affected by the outliers larger than the W_U, shown by the third and fourth columns of Table 3.1. The order statistics of distribution of RRVs below W_U is identical for good and bad pools.

[1]Because there are 2,014 days, the final pool has only 4 days

[2]The lower bound, W_L, is left out of the table. W_L is 0 because RV =0 when there is no trading activity in the afternoon of some public holiday

Table 3.2: Distribution of RRV

RRV	Good pools	Bad pools	Total
$[1000, +\infty)$	1	44	45
$[100, 1000)$	11	186	197
$[10, 100)$	353	352	705
$[5, 10)$	1291	659	1950
$[2.5, 5)$	13875	5649	19524
$[0, 2.5)$	319,089	129,766	448,855
Total	334,620	136,656	471,276

Table 3.3: Right tail distribution of RRV(percentage)

RRV	Good pools	Bad pools	Total
$[1000, +\infty)$	0.0003%	0.03%	0.0095%
$[100, 1000)$	0.003%	0.14%	0.042%
$[10, 100)$	0.11%	0.26%	0.15%
$[5, 10)$	0.39%	0.48%	0.41%
$[2.5, 5)$	4.15%	4.13%	4.14%
$[0, 2.5)$	95.36%	94.36%	95.22%
Total	100%	100%	100%

Table 3.4: RRVs per pool

RRV	Good pools	Bad pools	Total
$[1000, +\infty)$	0.004	0.38	0.11
$[100, 1000)$	0.04	1.59	0.48
$[10, 100)$	1.23	3.01	1.75
$[5, 10)$	4.51	5.63	4.84
$[2.5, 5)$	48.51	48.28	48.45
$[0, 2.5)$	1115.7	1109.1	1113.8
Total	1170	1170	1170

There are in total 22,421 RRVs larger than 2.5, 13,875 of which are from good pools. Overall the number of RRVs over 2.5 occupies 4.78% of all the blocks in the 403 pools. Moreover, the max RRV of good and bad pools are 1369 and 7309, very different from the rest of the distribution. These facts inspire me further divide the distribution of RRVs above W_U to find a threshold for large outliers. I classify $[2.5, \infty)$ into 5 intervals: $[2.5, 5)$, $[5, 10)$, $[10, 100)$, $[100, 1000)$ and $[1000, \infty)$. I show the number of RRVs in each of these intervals in Table 3.2 for good and bad pools separately. I also show the number of RRVs in the range of $[0, 2.5)$ as a comparison. The percentage of blocks in each category is listed in Table 3.3.

The two tables tell us that bad pools are much more likely to have very large RRVs than good pools and large RRVs are relatively rare. The difference between bad and good pools shrinks rapidly as we decrease the threshold. The table starts from the most extreme case when RRVs exceed 1000, i.e., RVs are over 1000 times the median RV of the pool to which they belong. There is only 1 block in this scenario for good pools but there are 44 in bad pools. The number of RRVs in the range of $[10, 100)$ for good pools and bad pools are nearly equal. However, because we have more than twice the number of good pools than bad pools, the percentage of RRVs in this range for bad pools is still much larger. When we get to

$[2.5, 5)$, their percentage of RRVs are nearly the same.

Table 3.4 converts the counts of Table 3.3 to rates per pool by dividing the counts of good pools by the number of good pools and the counts of bad pools by the number of bad pools. We see the same pattern continues in this table: The incidence of tail events for the first four categories is greater for bad pools than good pools, but the difference decreases as the threshold decreases.

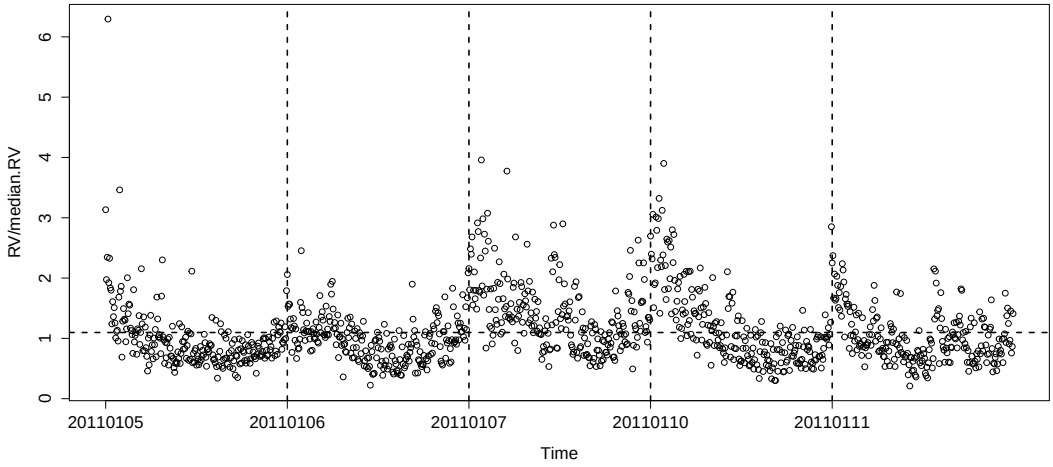

Figure 3.1: RRV by block, 1/5/2011 - 1/11/2011(WRFMT, pool 203)

Table 3.5: Parameter estimates of a typical pool[3]

Pool	$\widehat{\beta}$	$\widehat{\bar{c}}$	$\gamma^2 \times 10^3$	jpvalue
203	0.17***	0.067***	1.16***	0.31

Table 3.1 to 3.4 provide a good guidance for the path analysis of pools in the next section. Figure 3.1 provides an example. This is pool 203 which includes 1/6/2011, the good day portrayed in Figure 1.1 in chapter 1. Because this is a good pool, the estimates of $\bar{c}$ and

[3]'*', '**' and '***' indicate the z-score is larger than 1.645, 1.96 and 2.33

β are significant and the model specification is also good. Although not required for good pools, the γ^2 estimate is also statistically significant at the 1% level. Details of parameter estimates can be found in Table 3.5. The horizontal dashed line in Figure 3.1 is $\widehat{\bar{c}}$ divided by the median RV of the pool. The caption lists the sequence of weekdays included in the pool: pool 203 starts on Wednesday and ends with Tuesday, described as "WRFMT". Realized volatilities has a scalloped pattern each day: RRVs of the first few blocks of each day are often above 2.5. They fall below 1 in the middle of the day and usually tend to rise at the end of the day. In this pool, there are no bad blocks and all but one of the RRVs is below 5.

Now I focus on RRVs above 10 to select some other interesting pools for the analysis in the next section. RRVs in this range occupies only 0.15% (1.75 per pool) in the sample. I call RRVs in $[10, \infty)$ "bad blocks". I refer to RRVs in $[10, 100)$, $[100, 1000)$ and $[1000, \infty)$ as Category 1, 2 and 3 respectively. Table 3.6 provides a complete catalog of bad blocks for every good pool. Each row describes a profile of a good pool characterized by the number of bad blocks in the pool, the number of bad blocks in each category and the number of pools fitting the profile. There are 18 rows in the table, representing 18 distinctive profiles. For example, 155 good pools have no bad blocks. Only one pool has one bad block of category 3. For the 131 good pools that have bad blocks, most have 1 or 2 bad blocks. One pool have 25 bad blocks, all of category 1.

Table 3.6: Distribution of the number of bad blocks (good pools)

bad blocks per pool	Cat 1	Cat 2	Cat 3	pools
0	0	0	0	155
1	0	0	1	1
1	0	1	0	4
1	1	0	0	56
2	2	0	0	26
3	3	0	0	15
4	4	0	0	12
4	2	2	0	1
5	5	0	0	3
6	6	0	0	3
7	7	0	0	2
8	7	1	0	1
9	8	1	0	1
9	7	2	0	1
10	10	0	0	2
14	14	0	0	1
23	22	1	0	1
25	25	0	0	1

Table 3.7 catalogs the distribution of bad blocks for bad pools. There are 37 bad pools with no bad blocks, accounting for 32% of total bad pools. Bad pools with 0, 1, 2 bad blocks account for 69% of all bad pools. The bad pool with 184 bad blocks includes February 27, 2007, when the S&P 500 Index dropped 3.5% following a 9% sell-off in China's stock market overnight. The 44 Cat 3 bad blocks belong to 6 pools. The 186 Cat 2 bad blocks come from 30 bad pools. Thus bad blocks are clustered into a few bad pools.

Table 3.7: Distribution of the number of bad blocks (bad pools)

bad blocks per pool	Cat 1	Cat 2	Cat 3	pools
0	0	0	0	37
1	1	0	0	25
1	0	1	0	4
1	0	0	1	1
2	2	0	0	11
2	1	1	0	2
2	1	0	1	1
3	3	0	0	7
3	2	1	0	1
3	1	2	0	2
4	4	0	0	2
4	1	3	0	2
5	4	1	0	1
6	6	0	0	1
6	5	1	0	1
6	4	2	0	1
7	2	5	0	1
7	1	6	0	1
8	7	1	0	1
8	4	4	0	1
8	3	5	0	1
8	2	6	0	1
10	10	0	0	1
11	4	5	2	1
11	9	2	0	1
12	8	4	0	1
13	11	2	0	1
13	6	7	0	1
14	14	0	0	1
18	1	8	9	1
20	19	1	0	1
29	17	11	1	1
74	46	28	0	1
184	98	78	30	1

3.3 Examining RRV for good pools

The previous section sets up a framework for identifying jumps in RVs using relative realized volatilities. I will now use this classification to explore the path behavior of RRVs in pools containing bad blocks. The path analysis allows us to visualize how the Heston model reacts to jumps.

Table 3.8 lists the pools that will be discussed. Among the 35 pools, 23 are good pools and 12 are bad. Half of the pools come from 2007-2009 and the rest from the last 5 years of the sample. As we saw in chapter 1, RVs are more volatile in the first three years of our sample due to the financial crisis.

The first column of Table 3.8 indicates whether the pool is good (G) or (B). The second column gives the number of the pool. Pools are numbered from 1 to 403. The third column gives the beginning and end date of the pool. Columns 4 to 6 indicate the number of RRVs falling into each of the three categories of bad blocks. The last column attaches descriptive labels to some pools, e.g.,:

- Pool 11 is labeled "FOMC" because there was a FOMC announcement on one of the trading days.
- Pool 169 is labeled "Flash Crash" because the Flash Crash event happened in this pool.
- Pool 6 is labeled "Gang of Nine", the nine good pools having "Cat 2" bad blocks.
- "The Great Six" indicates the only six bad pools having "Cat 3" bad blocks.

Other labels indicate pools at the beginning and the end of the financial crisis, as well as its peak and bottom, and other market events of interests.

Table 3.8: Summary of pools in the path behavior analysis

G/B	pool	dates	Cat1	Cat 2	Cat 3	description
G	6	2/8/07-2/14/07	22	1	0	Gang of Nine
B	8	2/23/07-3/1/07	98	78	30	Worst pool
G	11	3/16/07-3/22/07	14	0	0	FOMC
B	26	7/3/07-7/10/07	14	0	0	Bernanke effect
G	42	10/25/07-11/2/07	8	1	0	FOMC
B	45	11/15/07-11/21/07	1	0	1	The Great Six
G	71	5/23/08-5/30/08	7	2	0	Gang of Nine
B	87	9/17/08-9/23/08	19	1	0	Beginning of the financial crisis
G	88	9/24/08-9/30/08	25	0	0	Largest dive of DJIA
G	92	10/22/08-10/28/08	1	0	0	Peak of the financial crisis
G	106	2/3/09-2/9/09	0	0	0	Bottom of the financial crisis
G	121	5/21/09-5/28/09	4	0	0	
B	128	7/13/09-7/17/09	0	0	1	End of the financial crisis
G	133	8/17/09-8/21/09	2	2	0	Gang of Nine
B	137	9/15/09-9/21/09	1	8	9	The Great Six
B	144	11/3/09-11/9/09	46	28	0	Job effect
G	159	2/23/10-3/1/10	0	0	0	
B	169	5/5/10-5/11/10	17	11	1	Flash Crash
G	184	8/20/10-8/26/10	3	0	0	
G	194	11/1/10-11/5/10	10	0	0	FOMC
G	203	1/5/11-1/11/11	0	0	0	Includes Figure 1.1
B	222	5/23/11-5/27/11	4	5	2	The Great Six
G	250	12/9/11-12/15/11	0	1	0	
B	262	3/8/12-3/14/12	0	0	0	
G	282	7/31/12-8/6/12	7	0	0	FOMC
G	289	9/19/12-9/25/12	10	0	0	Apple effect
G	297	11/16/12-11/23/12	0	0	1	Worst good pool
G	320	5/6/13-5/10/13	0	1	0	Gang of Nine
G	324	6/4/13-6/10/13	0	1	0	Gang of Nine
B	326	6/18/13-6/24/13	1	0	0	FOMC
G	351	12/13/13-12/19/13	7	1	0	FOMC
G	368	5/17/14-4/24/14	0	1	0	Gang of Nine
B	380	7/15/14-7/21/14	0	0	0	
G	389	9/17/14-9/23/14	5	0	0	FOMC
G	395	10/29/14-11/4/14	5	0	0	FOMC

3.3.1 Two good pools in the financial crisis

I begin with two well-behaved good pools in the financial crisis. These two pools are pool 92 and 106, labeled as "Peak of the financial crisis" and "Bottom of the financial crisis" in Table 3.8. Their labels tell the reasons they are selected: The average magnitude of RVs in the two pools represent the highest and lowest respectively among all good pools in the financial crisis.

Figure 3.2 plots the RRVs for pool 92, the peak of the financial crisis. The $\bar{c}$ estimate for this pool is 2.04, slightly higher than the median RV (1.59) of the pool and 15 times the mean estimate of $\bar{c}$ for the entire 8 years. The RRVs fall in the range $[0, 5)$ except for a few outliers in $[5, 12)$ at the end of the second and the beginning of the third day. Most of the RRVs above 2.5 appear at the beginning of the trading day.

Figure 3.3 plots RRVs for pool 106, which has the lowest $\widehat{\bar{c}}$ among good pools in the financial crisis and half the mean estimate of $\bar{c}$ for the entire sample. RRVs in this pool look similar to pool 92. Most stay below 5. We observe some mid-range jumps between $[2.5, 5)$, all of which appear at the beginning and end of each trading day. Table 3.9 gives details about the parameter estimates in the two pools.

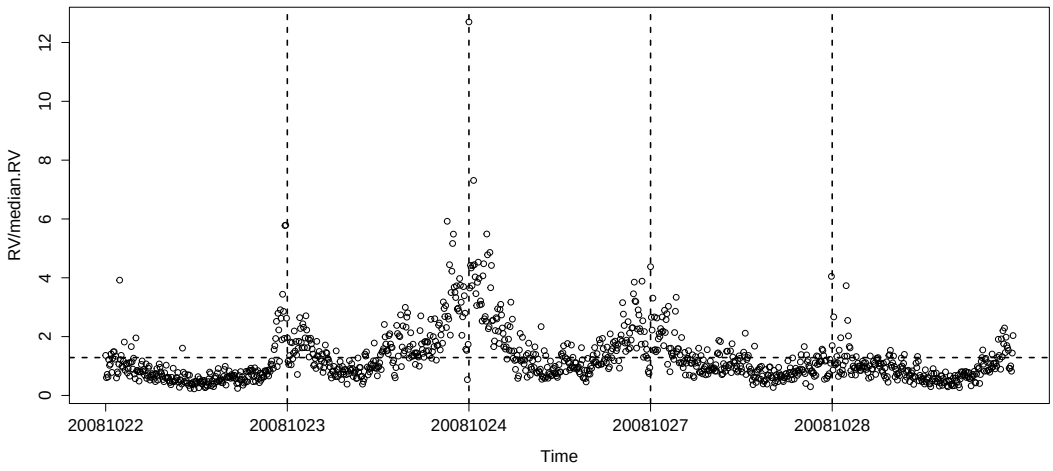

Figure 3.2: RRV by block, 10/22/2008 - 10/28/2008 (WRFMT, pool 92)

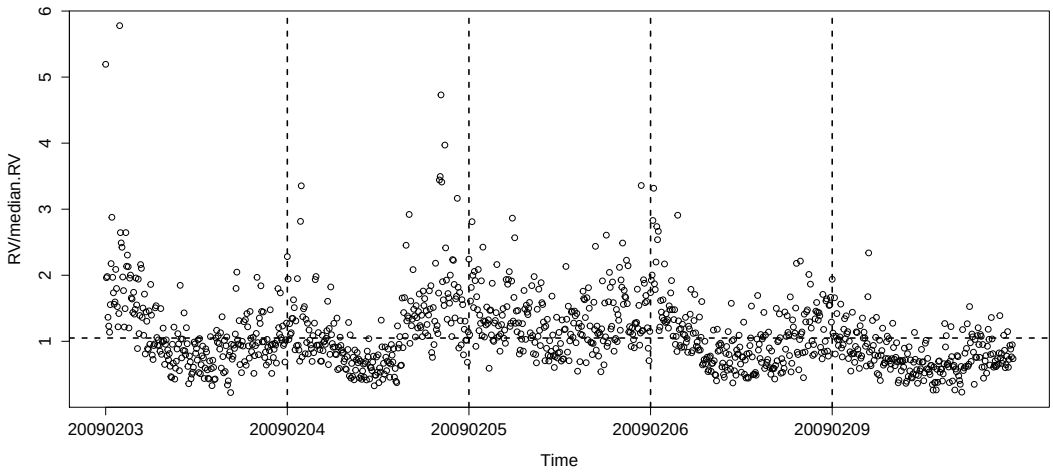

Figure 3.3: RRV by block, 2/3/2009 - 2/9/2009 (TWRFM,pool 106)

Table 3.9: Parameter estimates of two good pools

Pool	$\widehat{\beta}$	$\widehat{\bar{c}}$	$\gamma^2 \times 10^3$	jpvalue
92	0.04***	2.04***	14.7**	0.55
106	0.10***	0.38***	2.89***	0.19

3.3.2 Good pools with large jumps

I now turn to good pools having Cat 2 and Cat 3 bad blocks. The only good pool having a Cat 3 bad block is pool 297, listed in Table 3.8 as the "Worst good pool". All of the Cat 2 bad blocks for good pools are located in 9 pools, labeled as the "Gang of Nine" in Table 3.8. Table 3.10 gives an overview of the 10 pools with information extracted from Table 3.8.

Table 3.10: Ten good pools with large jumps

Pool	Time period	Cat 1	Cat 2	Cat 3
6	2/8/07-2/14/07	22	1	0
42	10/25/07-11/2/07	8	1	0
71	5/23/08-5/30/08	7	2	0
133	8/17/09-8/21/09	2	2	0
250	12/9/11-12/15/11	0	1	0
320	5/6/13-5/10/13	0	1	0
324	6/4/13-6/10/13	0	1	0
351	12/13/13-12/19/13	7	1	0
368	5/17/14-4/24/14	0	1	0
297	11/16/12-11/23/12	0	0	1

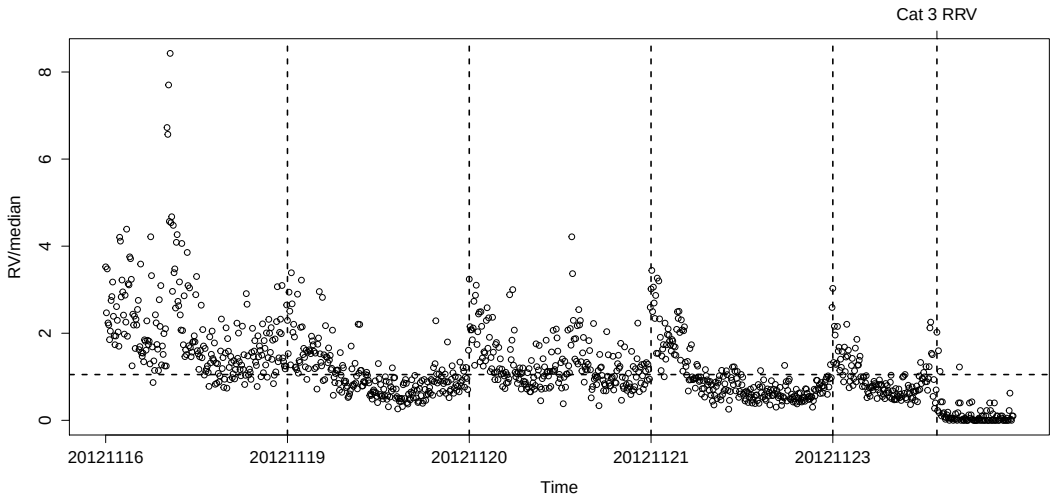

Figure 3.4: RRV by block, 11/16/2012 - 11/23/2012 (FMTWR, pool 297)

Figure 3.4 plots RRVs of pool 297 after removing the Cat 3 RRV equal to 1369. The

timing of this RRV is indicated at the top of the plot in the middle of 11/23/2012, the day before Thanksgiving. Trading activities almost cease at that time, with RVs quickly approaching 0. Thus the Cat 3 RRV is probably a data error. On the other days of the pool RRVs are below 5 except for a volatility cascade on 11/16/2012. On this day, the stock market experienced a sell-off attributed to investor worry about the negative impact of fiscal policy on the recovery of the U.S. economy.

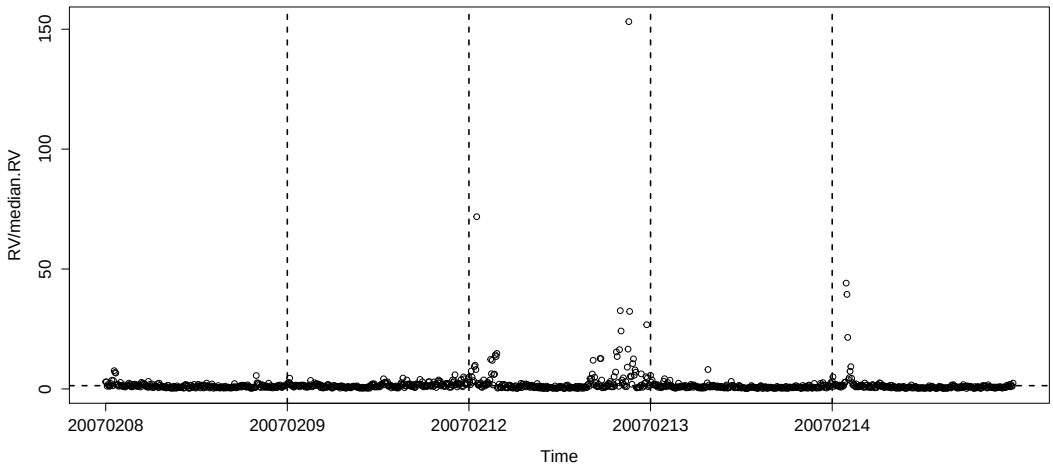

Figure 3.5: RRV by block, 2/8/2007 - 2/14/2007 (RFMTW, pool 6)

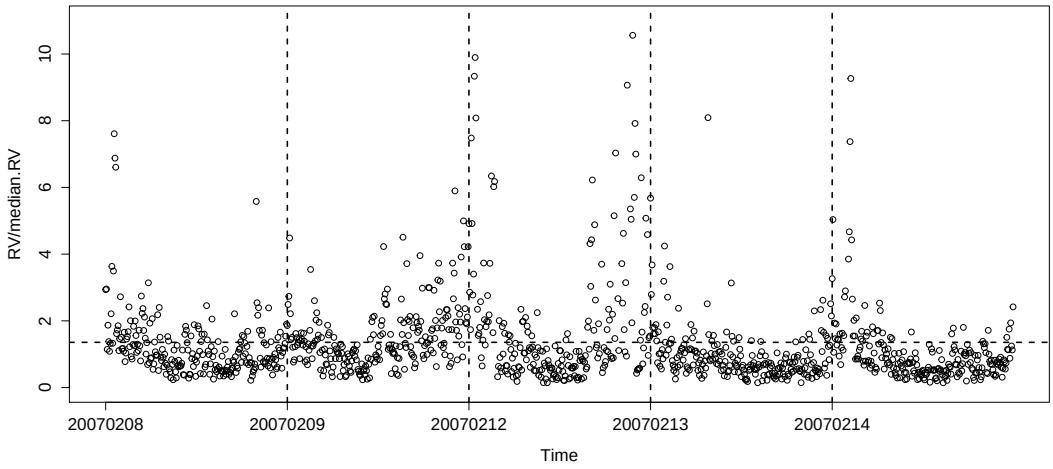

Figure 3.6: RRV by block, 2/8/2007 - 2/14/2007 (RFMTW, pool 6), truncated

Figure 3.5 and 3.6 display pool 6, a member of the "Gang of Nine". There are 23 bad blocks, one of them is a Cat 2 bad block. Figure 3.6 truncates the graph to show a clearer structure of RRVs at the bottom. We group these 23 bad blocks into three clusters: 7 bad blocks in the beginning of 2/12/2007, 13 bad blocks at the end of 2/12/2007 and 3 at the beginning of 2/14/2007. Each cluster of bad blocks is accompanied by many middle-sized volatility jumps in $[5, 10)$. The estimate of $\bar{c}$ of the pool is affected by these large RRVs, showing a value 1.5 times the median RV of the pool. The $\widehat{\beta}$ is higher than the upper quartile of all good pool estimates. On 2/12/2007, the stock market experienced a large slide after a 3.5% rapid drop of oil prices.

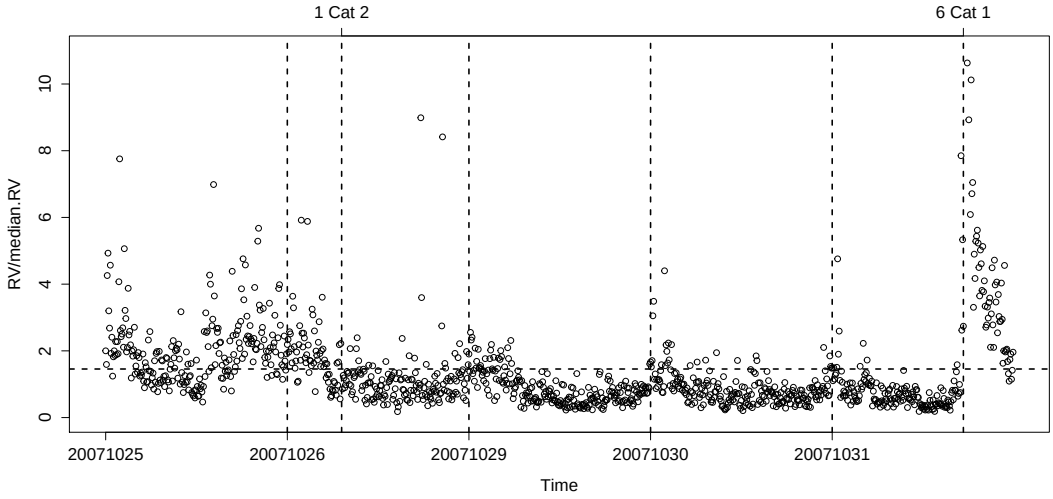

Figure 3.7: RRV by block, 10/25/2007 - 10/31/2007 (RFMTW, pool 42)

Figure 3.7 shows the second member of the "Gang of Nine", labeled in Table 3.8 as "FOMC". The pool has 9 bad blocks, among which 1 Cat 2 and 6 Cat 1 bad blocks lie outside the range of this plot. I include the timing of these bad blocks on top of the figure. I also use a vertical dashed line to mark the timing as well. The remaining 2 Cat 1 bad blocks are plotted in the figure on the last day. They happen at the same time as the other 6 Cat 1 bad blocks. At 2PM on the last day, the Fed released the FOMC announcement to cut the Federal funds rate. These Cat 1 bad blocks are followed by a volatility cascade until the end of the day. The other RRVs stay below 5 most of the time and we observe some large RRVs at beginning of these trading days. There was exceptional volatility on the first day as uncertainties in the housing market gathered before the subprime mortgage crisis. The estimate for $\bar{c}$ is much larger than the median RV, presumably a result of the volatility cascade.

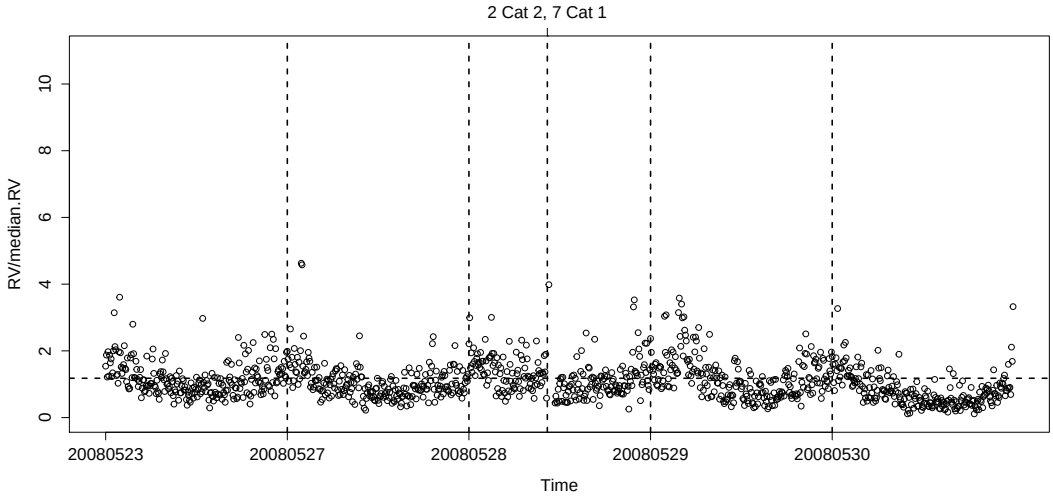

Figure 3.8: RRV by block, 5/23/2008 - 5/30/2008 (FMTWR, pool 71)

Figure 3.8 displays pool 71, the third member of the "Gang of Nine". There are 2 Cat 2 and 7 Cat 1 bad blocks happening around 12:20PM on the third day: the Cat 2 bad block, equaling 351, was immediately followed by a cascade of 7 Cat 1 bad blocks. The rest of the RRVs stay below 5 and only 27 RRVs are above 2.5, most happening at the beginning of a trading day.

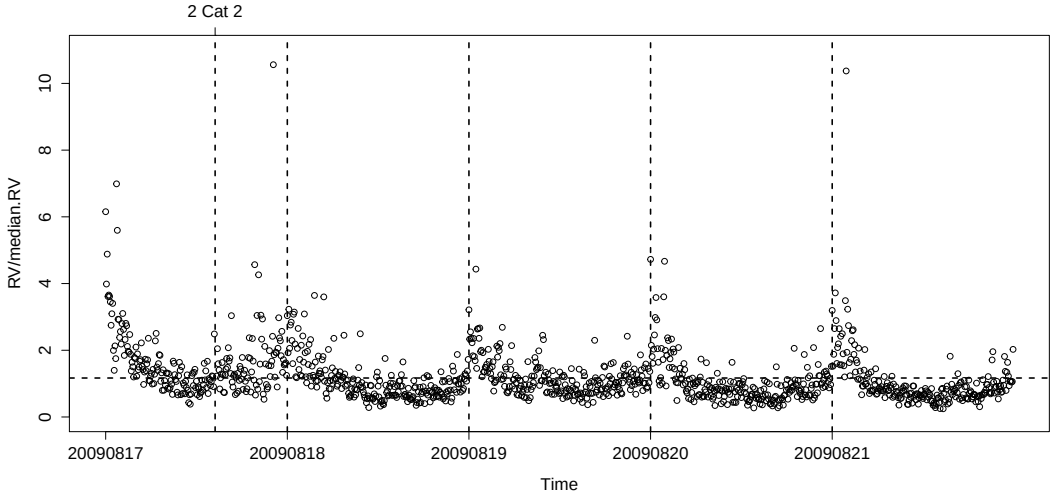

Figure 3.9: RRV by block, 8/17/2009 - 8/21/2009 (MTWRF, pool 133)

Figure 3.9 shows the RRVs of pool 133, another member of the "Gang of Nine". There are only 2 Cat 2 bad blocks in this pool, both occurring around 1:30PM of the first day as indicated in the figure. There is not much sign of a volatility cascade after the Cat 2 bad blocks. In addition, seven RRVs are above 5.

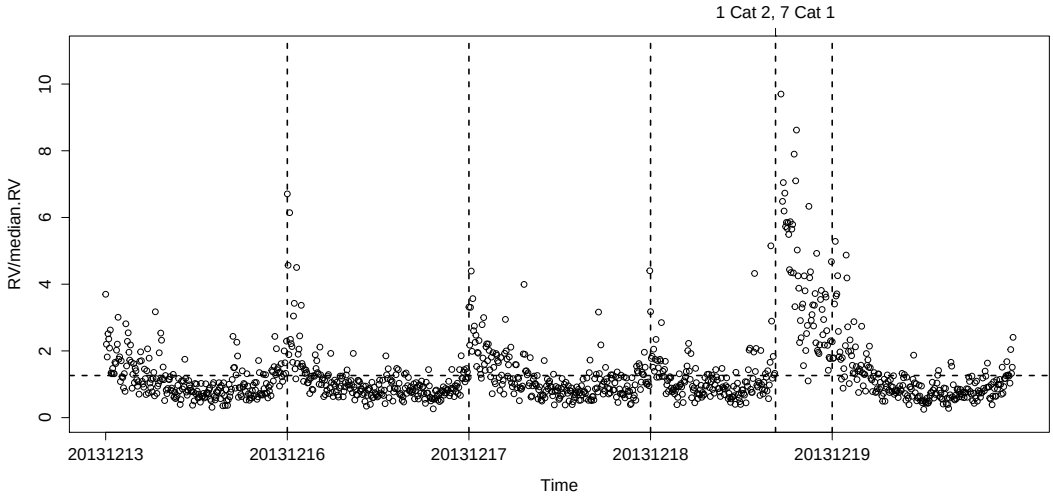

Figure 3.10: RRV by block, 12/13/2013 - 12/19/2013 (FMTWR, pool 351)

Figure 3.10 shows the plot of pool 351, the fifth member of the "Gang of Nine". It is also labeled "FOMC" in Table 3.8, and the volatility process is impacted by the Fed announcement on the fourth day of the pool. There are 1 Cat 2 and 7 Cat 1 bad blocks in this pool. All happened near 2PM, when the Federal government announced to taper back the QE3 plan. These bad blocks in turn triggered a series of middle-sized jumps in $[5, 10)$. Except for their reaction to the FOMC announcement, most RRVs stay below 2.5 except at beginning of each trading day. The estimate of $\bar{c}$ is roughly 1.5 times higher than the median RV.

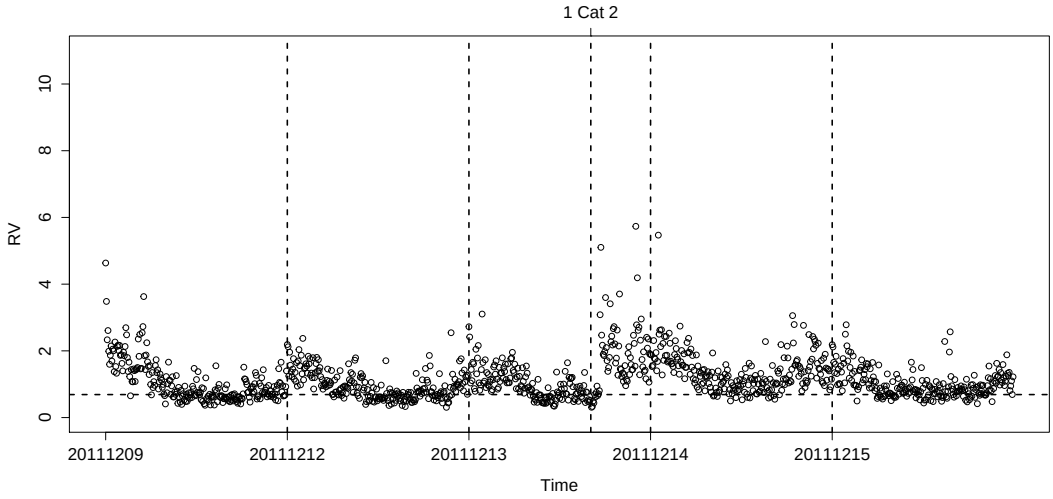

Figure 3.11: RRV by block, 12/09/2011 - 12/15/2011 (FMTWR, pool 250)

The remaining four members of the "Gang of Nine" each has one Cat 2 bad block and no other large RRVs. I plot each graph truncated to the range of $[0, 10)$ with the position of the Cat 2 bad blocks indicated by a vertical line. Figure 3.11 is the first example. The single Cat 2 bad block happened around 2pm on the third day, followed by a gap in the process. RRVs after the gap are significantly larger than before. On this day, the German Chancellor rejected the proposal of increasing the bail out amount to deal with the sovereign debt crisis in the Eurozone. The rest of the pool is quiet with most of the RRVs under 2.5.

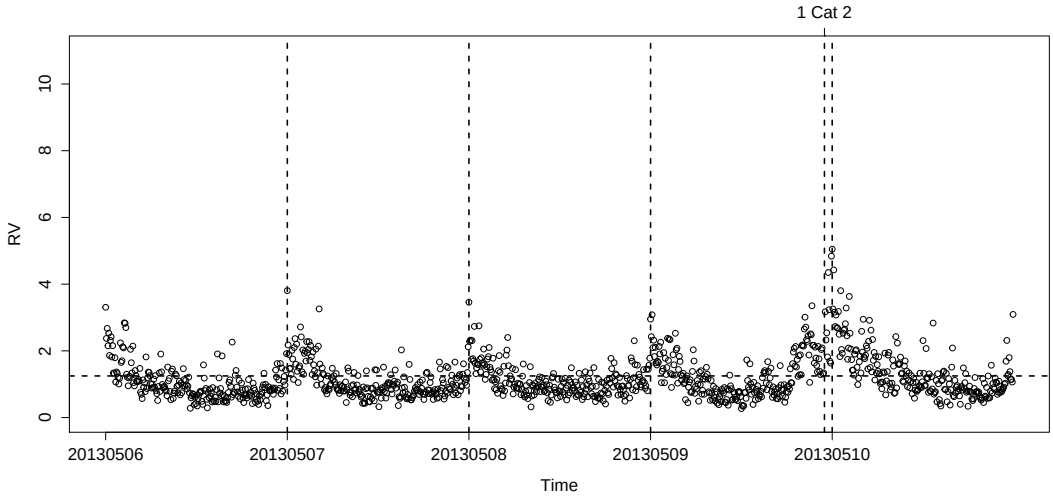

Figure 3.12: RRV by block, 05/06/2013 - 05/10/2013 (MTWRF, pool 320)

Pool 320 is shown in Figure 3.12. The Cat 2 bad block appears near the end of the fourth day with no after effect. No other RRVs are greater than 5.

The Cat 2 bad block for pool 324 and 368 both occur on the first day, as shown in Figure 3.13 and Figure 3.14. The estimate of $\widehat{\widehat{c}}$ is quite high in pool 368 with more than 80% of the RVs below $\widehat{\widehat{c}}$.

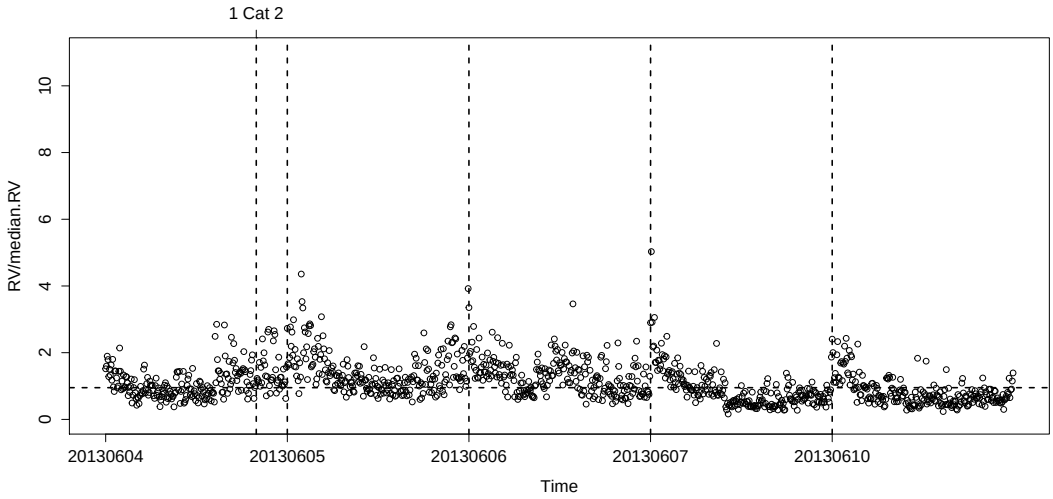

Figure 3.13: RRV by block, 06/04/2013 - 06/10/2013 (TWRFM, pool 324)

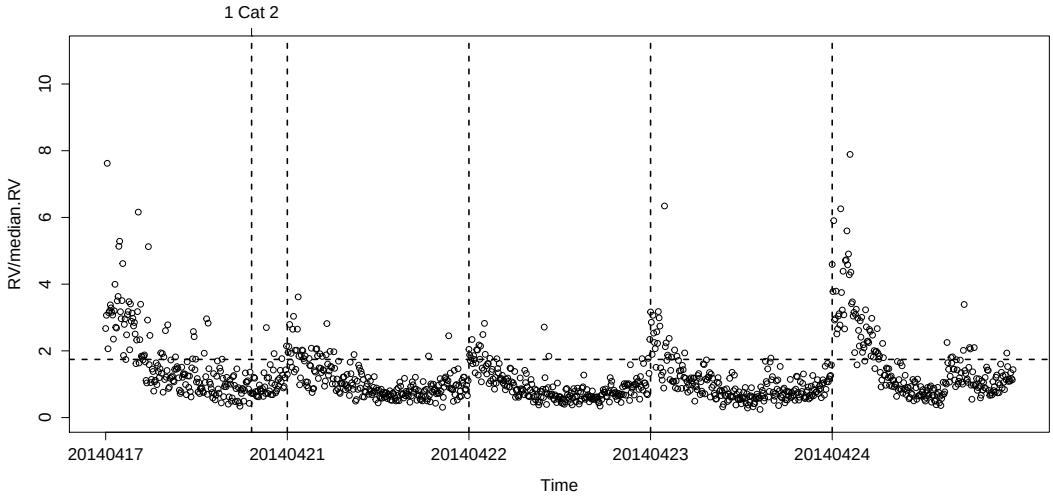

Figure 3.14: RRV by block, 04/17/2014 - 04/24/2014 (RFMTW, pool 368), truncated

Table 3.11: Parameter estimates of ten good pools with large jumps

Pool	$\widehat{\beta}$	$\widehat{\bar{c}}$	$\widehat{\gamma^2} \times 10^3$	jpvalue
6	0.17**	0.056***	7.25	0.27
42	0.19***	0.099***	5.21*	0.45
71	0.13***	0.093***	1.05***	0.86
133	0.11***	0.142*	4.24	0.36
351	0.065*	0.041***	0.96	0.74
250	0.06***	0.35***	2.91*	0.90
320	0.09***	0.041***	0.41	0.79
324	0.16***	0.073***	3.37***	0.86
368	0.11***	0.109***	1.12***	0.17
297	0.03*	0.067*	0.62	0.78

Table 3.11 presents the parameter estimates for all ten good pools with Cat 2 and Cat 3 bad blocks. None of the estimates are extremely large or small. The lower and upper quartile estimates of β for the 286 good pools are 0.07 and 0.13. Pool 6 and 71 have $\widehat{\beta}$ above the upper quartile. Pool 351 and 250 have $\widehat{\beta}$ below the lower quartile. The rest of the β estimates lie within the interquartile range. The lower and upper quartile estimates of $\bar{c}$ for the 286 good pools are 0.053 and 0.15. Only pool 250 has $\bar{c}$ above the upper quartile, and only pools 351 and 320 are below the lower quartile.

3.3.3 Good pools with many jumps

The previous section examined the RRV paths of good pools have Cat 2 and Cat 3 bad blocks. Table 3.6 shows that of the remaining pools, 121 good pools having Cat 1 bad blocks. In this section, I focus on good pools with many Cat 1 bad blocks.

Table 3.12 lists the 5 good pools having at least 7 Cat 1 bad blocks that will be discussed in this section. These 5 pools account for 66 of the 121 Cat 1 bad blocks, further evidence that bad blocks often tend to trigger cascades of jumps.

Table 3.12: Five good pools with many jumps

Pool	Time period	Cat 1	Cat 2	Cat 3
11	3/16/07-3/22/07	14	0	0
88	9/24/08-9/30/08	25	0	0
194	11/1/10-11/5/10	10	0	0
282	7/31/12-8/6/12	7	0	0
289	9/19/12-9/25/12	10	0	0

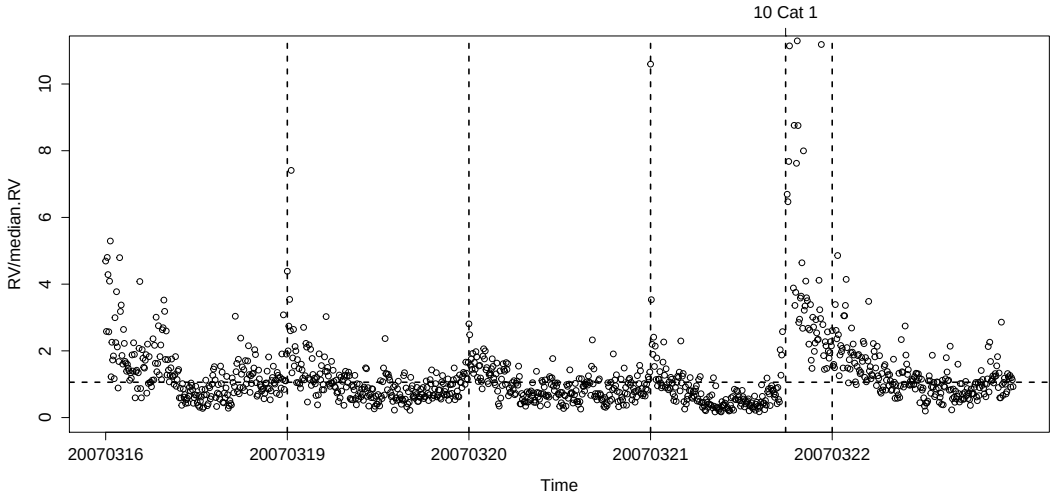

Figure 3.15: RRV by block, 3/16/2007 - 3/22/2007 (FMTWR, pool 11)

Three of the five pools are impacted by an FOMC announcement: Pool 11, 194 and 282, all labeled as "FOMC" in Table 3.8. They are shown in Figure 3.15, 3.16 and 3.17. For pool 11, I show a truncated graph of RRVs leaving out 10 Cat 1 bad blocks near the end of the fourth day, the day of the FOMC announcement. The pool has 4 other Cat 1 bad blocks, one near the beginning of the fourth day and three others shortly after the 10 Cat 1 bad blocks. In addition, there are 7 RRVs of magnitude in $[5, 10)$ following the Cat 1 bad blocks. Some other volatility jumps in $[2.5, 5)$ also occurred after them.

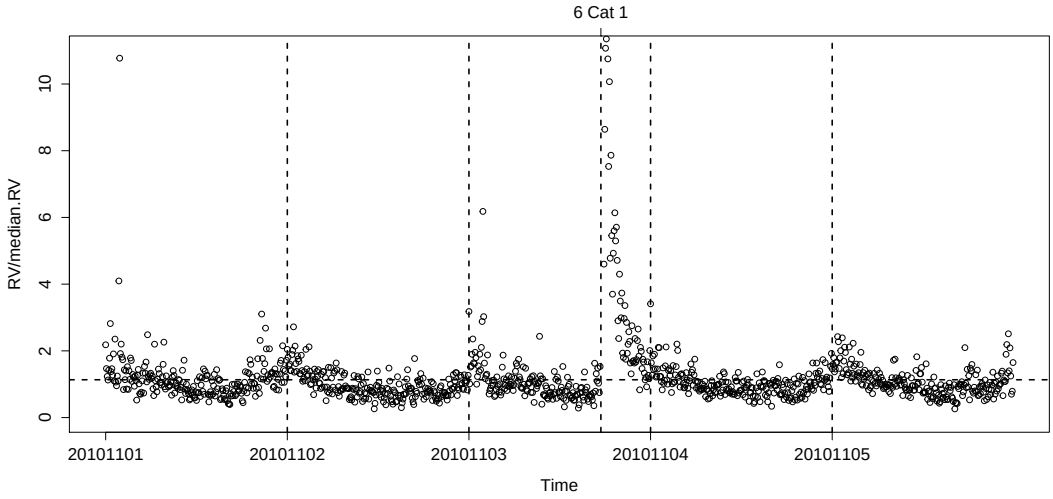

Figure 3.16: RRV by block, 11/1/2010 - 11/5/2010 (MTWRF, pool 194)

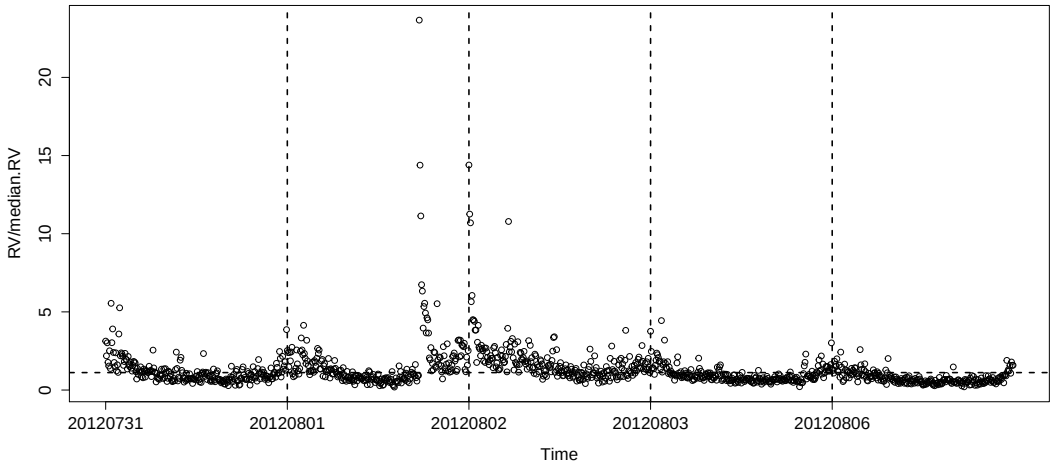

Figure 3.17: RRV by block, 7/31/2012-8/6/2012 (TWRFM, pool 282)

For pool 194, 9 out of the 10 Cat 1 bad blocks appear at the FOMC announcement time on the third day. Among these 9 bad blocks, 6 are outside the truncated graph and hence labeled on top. These bad blocks are followed by a volatility cascade lasting until the end of the trading day. Similarly, 3 of the 7 Cat 1 bad blocks for pool 282 appear at the announcement time on the second day. They are also followed by 11 RRVs in the range of

[2.5, 10). The other 4 Cat 1 bad blocks for pool 282 occurred at the beginning of the third day. The rest of the RRVs stay below 2.5 most of time.

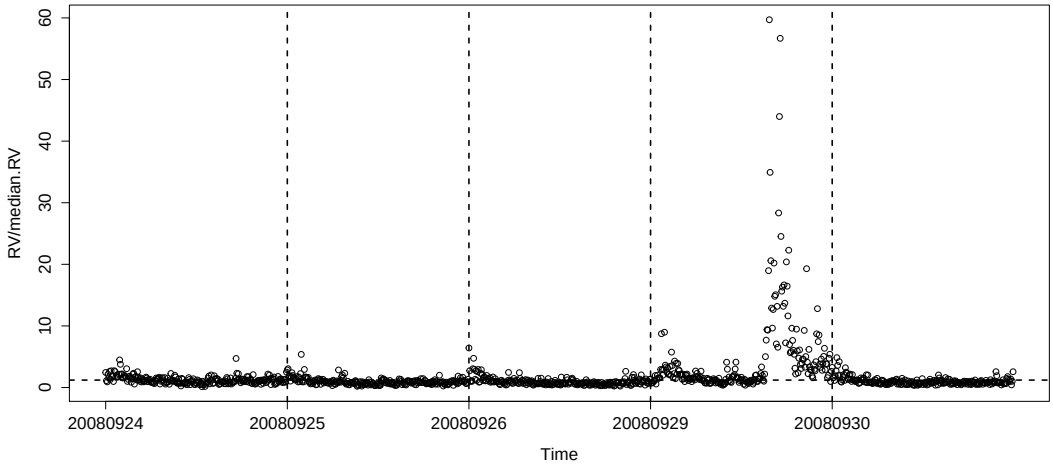

Figure 3.18: RRV by block, 9/24/2008 - 9/30/2008 (WRFMT, pool 88)

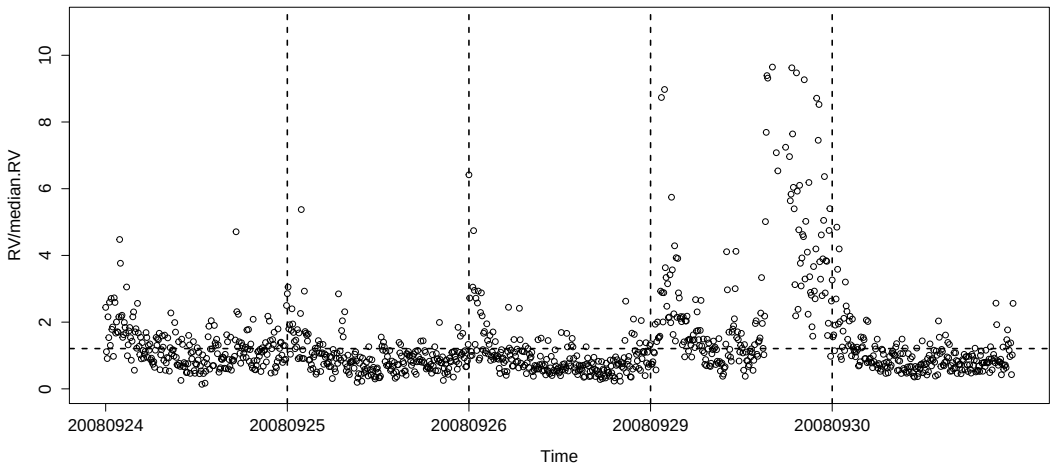

Figure 3.19: RRV by block, 9/24/2008 - 9/30/2008 (WRFMT, pool 88),truncated

The remaining two pools: pool 88 and 289 are impacted by irregular market activities. Pool 88 is labeled as "Largest dive of DJIA" in Table 3.8 because on 9/29/2008, the Dow

Jones index recorded the largest drop in its history. It declined by 777 points when congress denied the bailout plan of $700 billion to buy up bad debts and rescue the financial industry. All of the 25 Cat 1 bad blocks of pool 88 appeared on this day nearing the close of the market. Again, the rest of the RRVs are mostly below 5.

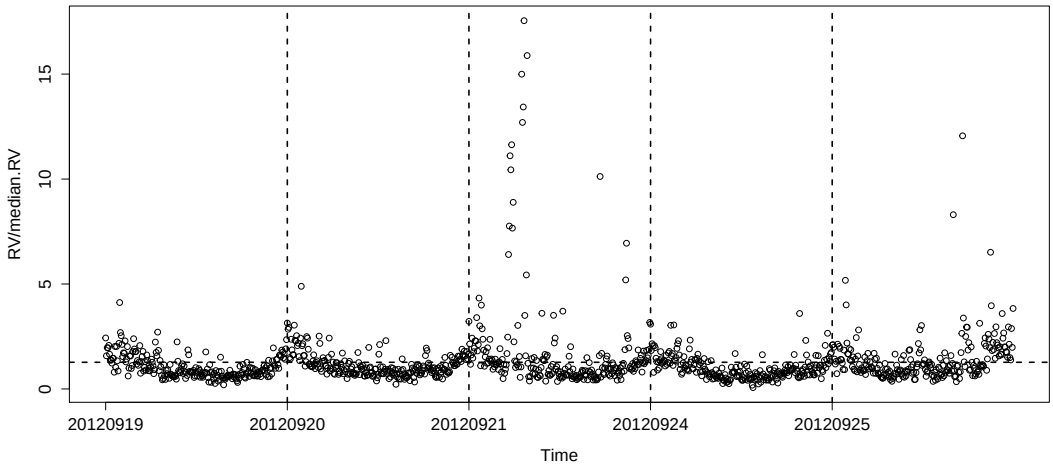

Figure 3.20: RRV by block, 9/19/2012-9/25/2012 (WRFMT, pool 289)

RRVs of pool 289 are shown in Figure 3.20, 8 out of the 10 Cat 1 bad blocks appeared starting at 10AM on the third day along with 5 jumps in $[5, 10)$. This occurred when Apple recorded a historically high sales of their new product, the iPhone 5. The other two Cat 1 bad blocks happened at the end of the third and fifth day.

Table 3.13: Parameter estimates of five good pools with many jumps

Pool	$\widehat{\beta}$	$\widehat{\bar{c}}$	$\widehat{\gamma^2} \times 10^3$	jpvalue
11	0.08**	0.049***	1.27	0.49
88	0.15***	0.43***	56.41	0.44
194	0.11***	0.094***	3.22	0.79
282	0.10***	0.067***	1.28	0.15
289	0.19***	0.053***	4.86	0.37

Table 3.13 gives the parameter estimates of these five pools. Similar to the good pools with Cat 2 and Cat 3 bad blocks, these estimates stay mostly within the interquartile range of parameter estimates for all 286 good pools.

3.3.4 Some other good pools

So far we have discussed 18 good pools, most from or before the financial crisis. To balance the choice of pools over the sample period, I examine some good pools in the post financial crisis era. Using Table 3.6, I try to pick pools having more than two Cat 1 bad blocks.

Table 3.14 provides information about these pools, extracted form Table 3.8. I also present the parameter estimates of these pools in Table 3.15. Pool 121 has a large estimate of $\bar{c}$ as it is from the financial crisis. The remaining estimates of both β and $\bar{c}$ lie within the interquartile range of estimates for all 285 good pools most of the time.

Table 3.14: Other good pools

Pool	Time period	Cat 1	Cat 2	Cat 3
121	5/21/09-5/28/09	4	0	0
159	2/23/10-3/1/10	0	0	0
184	8/20/10-8/26/10	3	0	0
389	9/17/14-9/23/14	5	0	0
395	10/29/14-11/4/14	5	0	0

Table 3.15: Parameter estimates of the other good pools

Pool	$\widehat{\beta}$	$\widehat{\bar{c}}$	$\widehat{\gamma^2} \times 10^3$	jpvalue
121	0.14***	0.24***	3.75**	0.48
159	0.08***	0.12***	1.16**	0.45
184	0.09***	0.14***	1.15*	0.51
389	0.11***	0.034***	0.64	0.77
395	0.16***	0.056***	3.60**	0.99

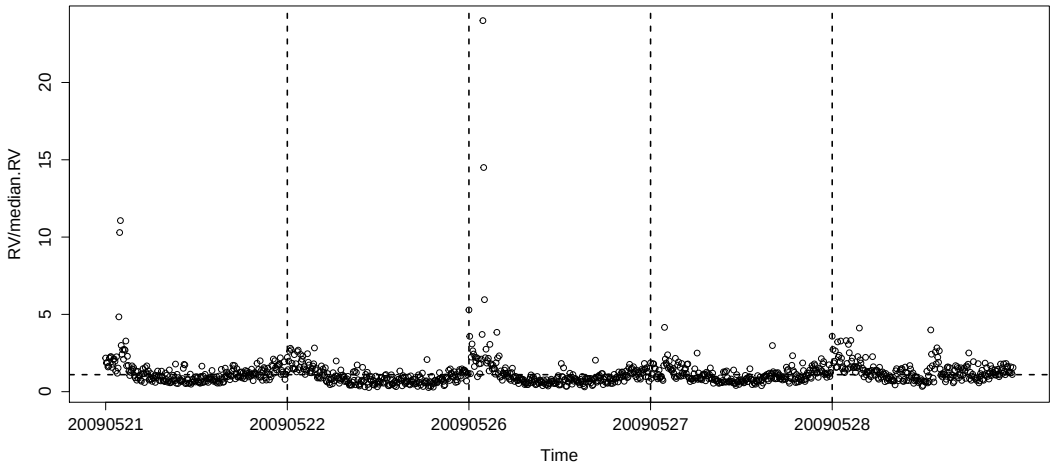

Figure 3.21: RRV by block, 5/21/2009-5/28/2009 (RFMTW, pool 121)

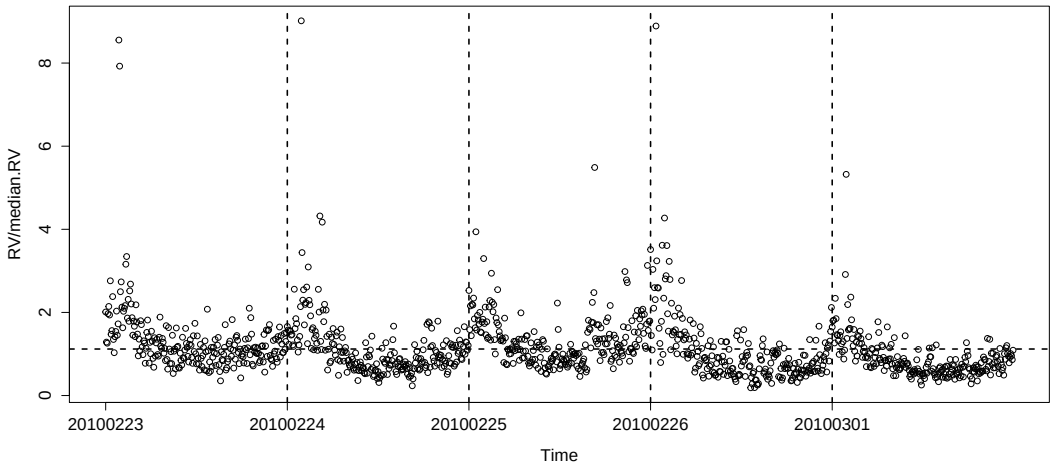

Figure 3.22: RRV by block, 2/23/2010-3/1/2010 (TWRFM, pool 159)

Because most of the RRV plots look very similar to ones discussed in previous sections, I do not comment on the common patterns among these plots such as the high RRVs near the beginning of a trading day.

Figure 3.21 for pool 121 has two Cat 1 bad blocks at the beginning of the first day and

2 others at the start of the third day. The rest of the RRVs are below 5.

RRVs of pool 159 are shown in Figure 3.22. There are no bad blocks in this pool but 6 middle sized jumps lie within $[5, 10)$. The rest of the RRVs look similar to other good pools: At the beginning of each trading day, we see high RRVs in the range of $[2.5, 5)$. The middle part usually stays close to but less than 1. RRVs near the end of the day go slightly up. In pool 159, more than 70% of the RVs are lower than $\widehat{\bar{c}}$, presumably reflecting the influence of the volatility jumps at beginning of each trading day on the estimate of the asymptotic mean $\bar{c}$.

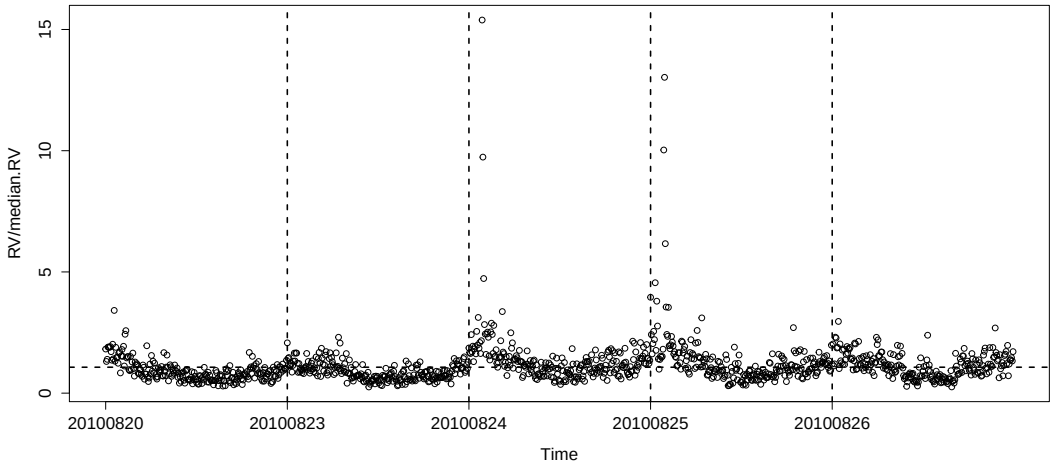

Figure 3.23: RRV by block, 8/20/2010-8/26/2010 (FMTWR, pool 184)

Figure 3.23 shows pool 184. There are 3 Cat 1 bad blocks in this pool. They appeared at the beginning of the third and fourth day. Most of the RRVs above 2.5 in this pool are from the beginning of each trading day.

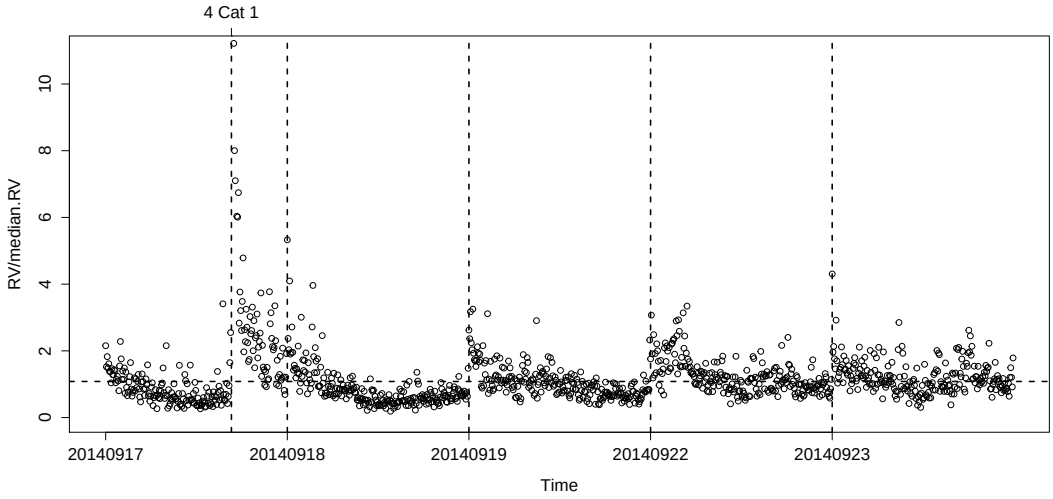

Figure 3.24: RRV by block, 9/17/2014-9/23/2014 (WRFMT, pool 389)

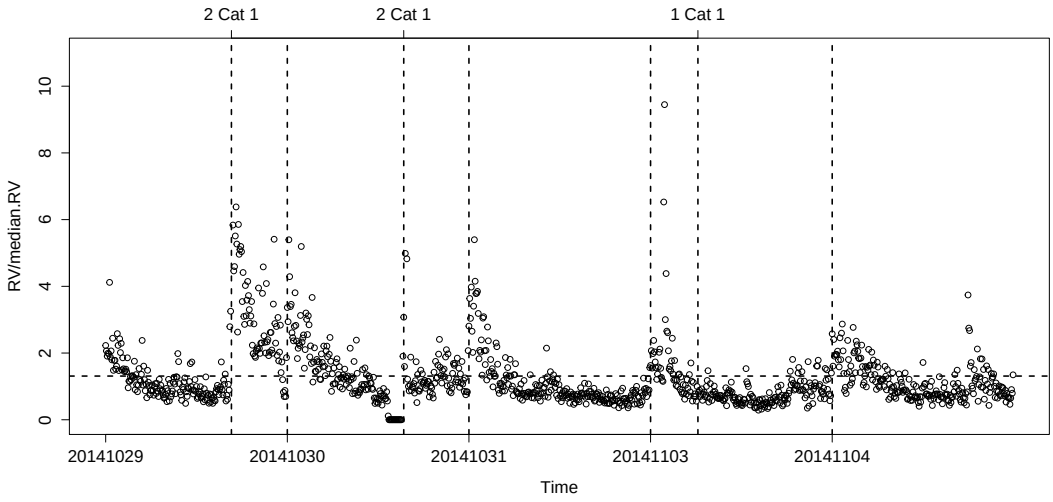

Figure 3.25: RRV by block, 10/29/2014-11/4/2014 (WRFMT, pool 395)

The remaining 2 pools, 389 and 395, are each impacted by a FOMC announcement. Like other "FOMC" pools discussed before, pool 389 has a volatility cascade right after the announcement time occurring on the first day. All of the bad blocks in this pool at the start of this cascade and 4 of them lie outside the range of the truncated Figure 3.24.

Pool 395 has a more complicated story. There are 5 Cat 1 bad blocks in this pool, two appearing at the FOMC announcement time on the first day. These two bad blocks trigger a series of middle sized volatility jumps in the range of $[2.5, 6.5)$. RRVs in the next day are very volatile. The trading stopped for around 10 minutes in the middle of the day followed by a series of volatility jumps which contains two more 2 Cat 1 bad blocks lying outside the range of this truncated figure. The last Cat 1 bad block occurred around 10AM on the fourth day. This day has 3 distinctive RRV jumps in the range of $[4, 10)$ at the market opening. Similar to other pools impacted by volatility jumps, more than 70% of the RVs in pool 395 are lower than the pool estimate of $\bar{c}$.

3.4 Examining RRVs for bad pools

So far, we have focused on the path of RRV for good pools. We have seen some common patterns in these RRV plots that could help us understand the reaction of Heston model to large jumps in the volatility process. Bad blocks are accompanied by a cascade of volatility jumps. The remaining RRVs stay below 2.5 most of the time but are often higher at the beginning of a trading day. The pool estimate of $\bar{c}$ is likely to be higher than the median RV when jumps happen. I now examine RRV for the 12 bad pools listed in Table 3.8.

3.4.1 Bad pools with category 3 bad blocks

As in the case for good pools, I start with with Cat 3 bad blocks. As Table 3.7 shows all 44 Cat 3 bad blocks occur in just 6 bad pools. These 6 pools are listed in Table 3.16 with information extracted from Table 3.8. I described these pools as "The Great Six".

Table 3.16: Six bad pools having large RRVs

pool	Time period	Cat 1	Cat 2	Cat 3
8	2/23/2007-3/1/2007	98	78	30
45	11/15/2007-11/21/2007	1	0	1
128	7/13/2009-7/17/2009	0	0	1
137	9/15/2009-9/21/2009	1	8	9
169	5/5/2010-5/11/2010	17	11	1
222	5/23/2011-5/27/2011	4	5	2

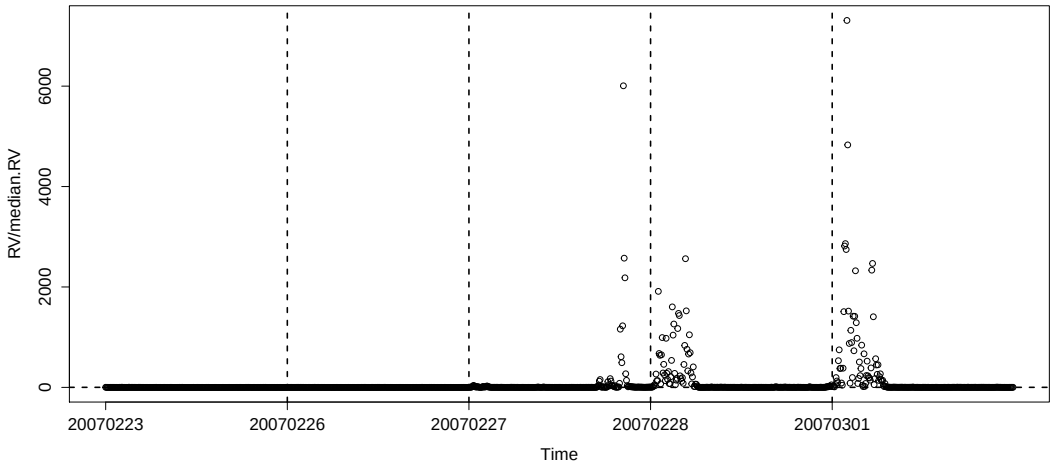

Figure 3.26: RRV by block, 2/23/2007 - 3/1/2007 (FMTWR, pool 8)

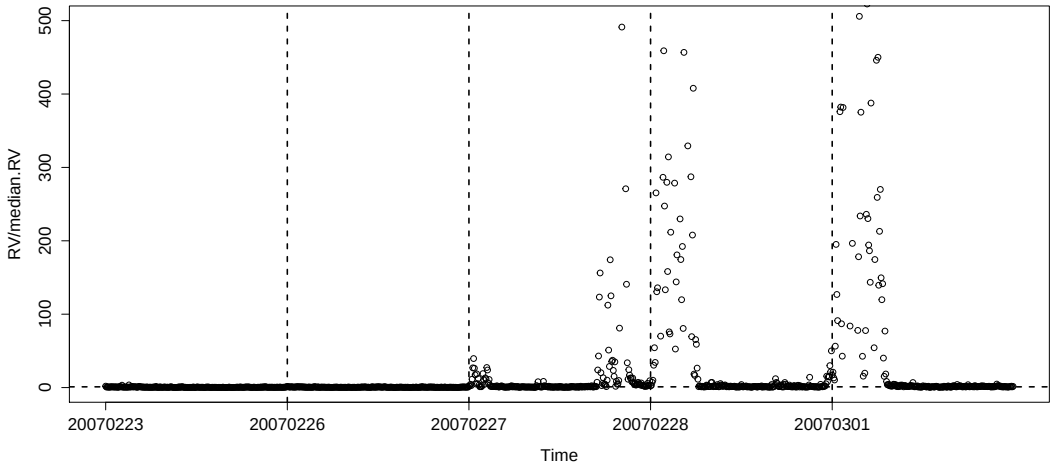

Figure 3.27: RRV by block, 2/23/2007 - 3/1/2007 (FMTWR, pool 8),truncated

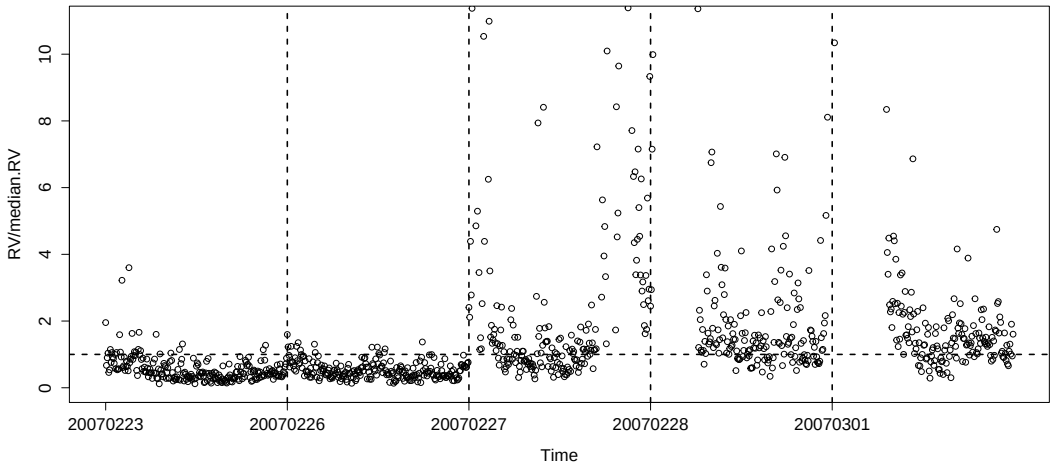

Figure 3.28: RRV by block, 2/23/2007 - 3/1/2007 (FMTWR, pool 8),truncated

Figure 3.26 presents the first member of "the Great Six", labeled in Table 3.8 as "Worst pool". It has the largest number of bad blocks among all pools. This pool includes February 27, 2007, when the S&P 500 Index dropped 3.5% following a 9% sell-off in China's stock market the night before.

There are 98 Cat 1, 78 Cat 2 and 30 Cat 3 bad blocks in this pool. The largest RRV is 7368. Figure 3.26 shows the untruncated graph of RRV for this pool.

To investigate the structure of RRV in detail for pool 8, I did two truncations in Figure 3.27 and 3.28. Because $\widehat{\bar{c}}$ is typically poorly estimated in bad pools, in this section, the horizontal dashed line indicates $RRV = 1$.

Comparing these graphs we notice that all 30 Cat 3 and 78 Cat 2 bad blocks happen at the end of the third day, the beginning of the fourth day and the beginning of the last day. For the 98 Cat 1 bad blocks, 14 occured at the beginning of the third day, the rest of them accompanied with Cat 2 and Cat 3 bad blocks.

The pool can be divided into two parts: the first part includes the first two trading days where 99% of the RRVs stay below 2.5. The second part includes the last three days during and after the shock. Even in this part, 60% of the RRVs are below 2.5 despite the presence of 184 bad blocks. This is because between shocks the volatility process quickly reverts back toward its mean, as can be seen in Figure 3.28. The gaps in Figure 3.28 are due to the large jumps outside the range of this plot. This suggests that if we remove all the 290 RRVs are above 2.5 and combine the remaining ones to form a new pool, the estimation of the Heston model could be improved. I will investigate that possibility later.

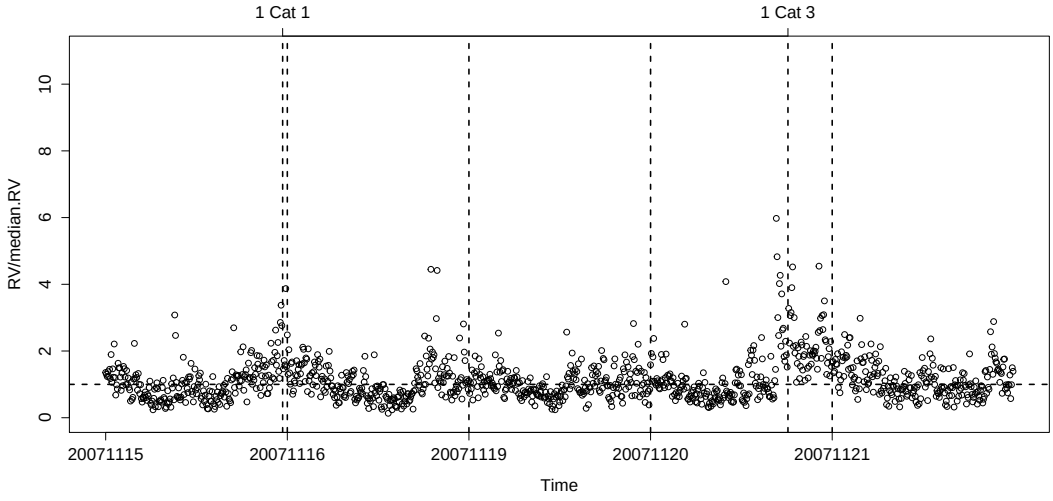

Figure 3.29: RRV by block, 11/15/2007 - 11/21/2007 (RFMTW, pool 45),truncated

Figure 3.29 plots the RRVs of pool 45. There is 1 Cat 3 bad block near the end of the fourth day in the midst of a volatility cascade. There is also 1 Cat 1 bad block at the end of the first day. I labeled their positions on top of the graph and use vertical dashed lines to emphasize their locations. All other RRVs are below 6 and most concentrate around the median. On 11/20/2007, the major market indices are dragged down by bad performances of financial stocks while investors worried about an incoming financial crisis.

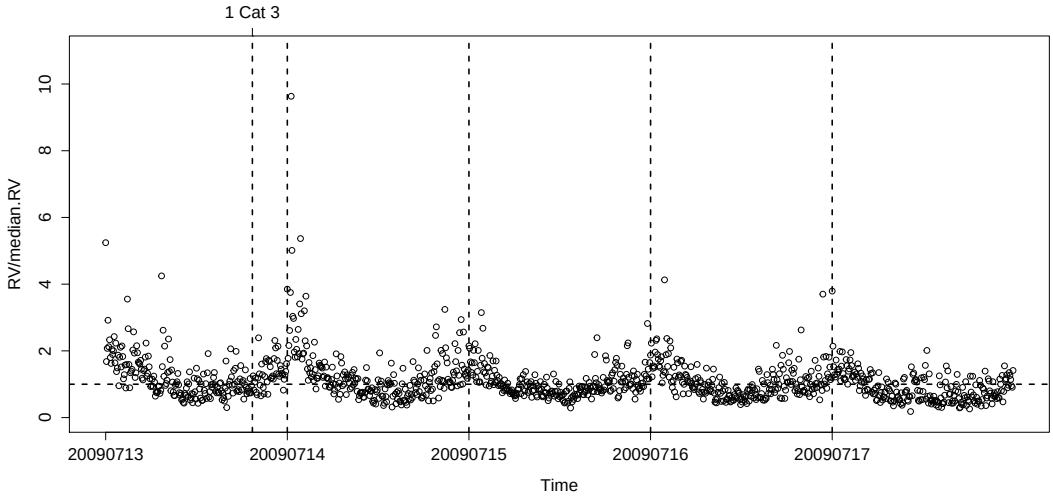

Figure 3.30: RRV by block, 7/13/2009 - 7/17/2009 (MTWRF, pool 128),truncated

Pool 128 has one bad block of Cat 3. I plot the pool in Figure 3.30 taking out the bad block, which occurred near the end of the first day. I label the position of the bad block with a vertical dashed line. Only 4 other RRVs are above 5. The remaining RRV plot looks very much like a plot for a typical good pool.

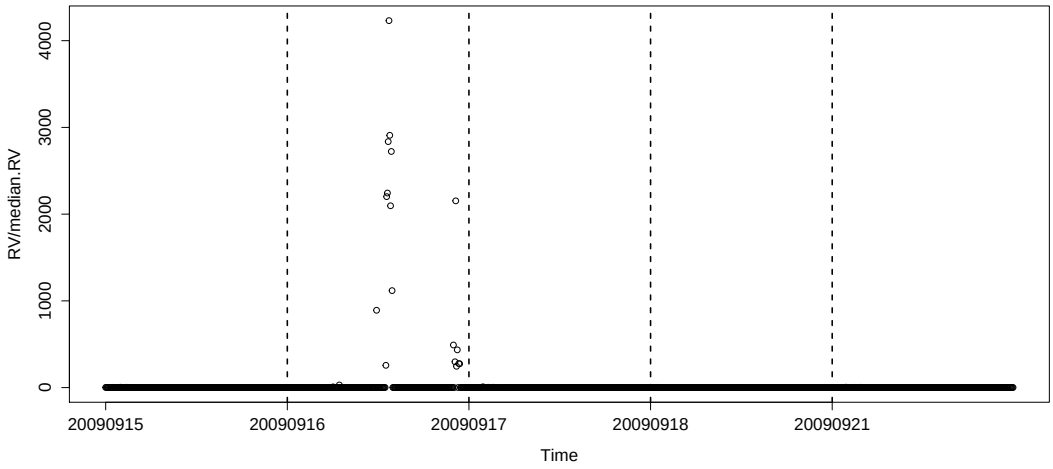

Figure 3.31: RRV by block, 9/15/2009 - 9/21/2009 (TWRFM, pool 137)

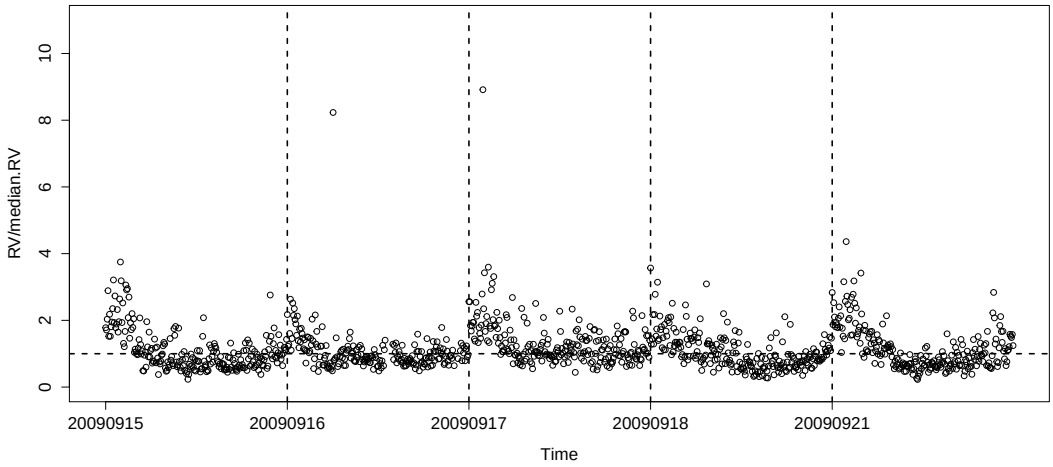

Figure 3.32: RRV by block, 9/15/2009 - 9/21/2009 (TWRFM, pool 137),truncated

Pool 137 is an interesting case as it has 9 Cat 3 bad blocks and 8 Cat 2 bad blocks, but only 1 Cat 1 bad block. I truncated Figure 3.31 to get Figure 3.32, which allows me to observe the bottom structure. Comparing these two graphs we see that the large RRVs are concentrated in two volatility cascades happening in the middle and end of 9/16/2009: The first one has 8 Cat 3 RRVs and 2 Cat 2 RRVs. The other has 1 Cat 3 RRV and 6 Cat 2

RRVs. RRVs inside each cascade happened consecutively. The only Cat 1 bad block happen before the two cascades on the same day. In Figure 3.32, we see most of the RRVs except these bad blocks are below 5, again looking very much like the pattern for a good pool.

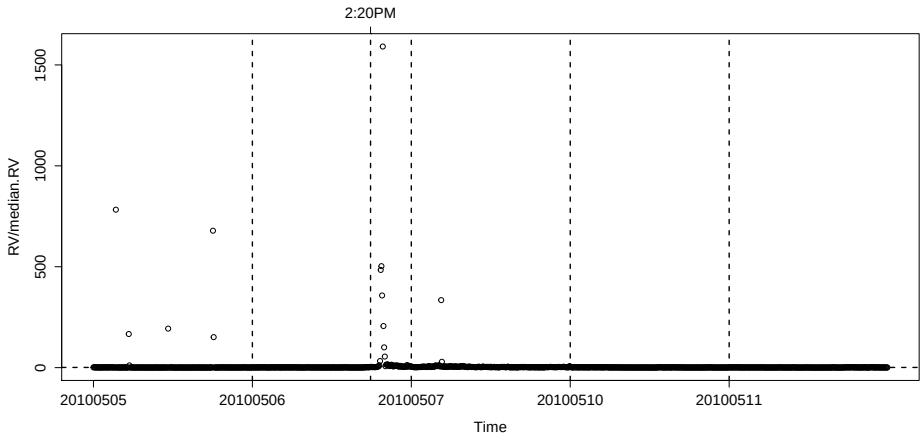

Figure 3.33: RRV by block, 5/05/2010 - 5/11/2010 (WRFMT, pool 169)

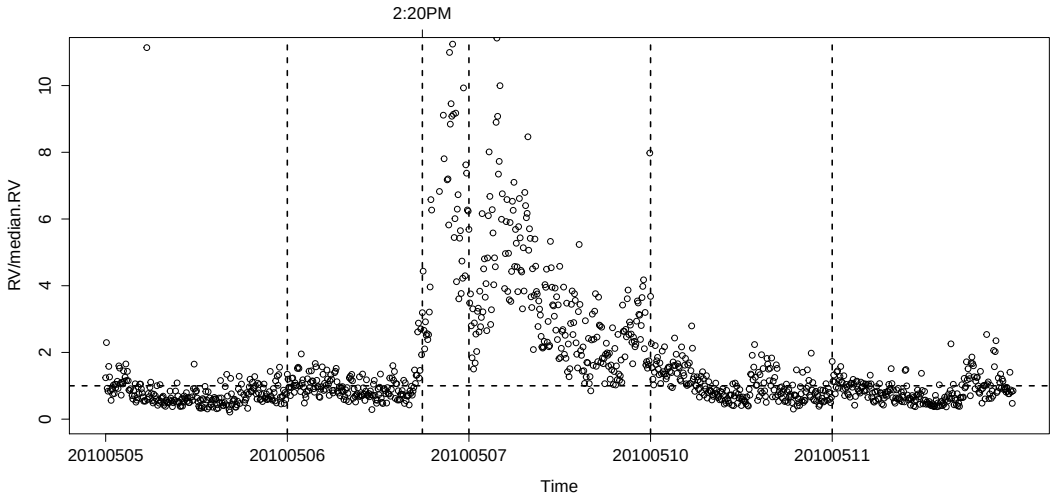

Figure 3.34: RRV by block, 5/05/2010 - 5/11/2010 (WRFMT, pool 169),truncated

Figure 3.33 and 3.34 display the sixth member of "the Great Six": pool 169. The Flash Crash happened on 5/6/2010 around 2:20PM in this pool. During the crash, the $S\&P$ 500

index tumbled by 3% and reverted back to the level before the crash within 20 minutes. This resulted in high stock price volatility until the end of the next day.

The impact of the crash can be witnessed from the RRV plots in Figure 3.33 and 3.34. There are in total 17 Cat 1, 11 Cat 2 and 1 Cat 3 bad blocks. Among them, 5 Cat 2 and 1 Cat 1 bad blocks happened on 5/5/2010, the day before the crash. One Cat 3, 5 Cat 2 and 13 Cat 1 bad blocks happened during the crash, and 1 Cat 2 and 3 Cat 1 bad blocks happened right after the crash. This was followed by a huge volatility cascade from 2:20PM on 5/6/2010 until the end of 5/7/2010, shown in Figure 3.34.

Similar to pool 8, RRVs outside of crash period stay fairly close to the median, indicated by the horizontal dashed line looking very much like the RRVs of a good pool. This invites the question of what could happen if we delete all the 300 RRVs in the crash period and reestimate the model. The Heston model should provide a well explanation for the remaining blocks. Detailed results of such an estimation will be discussed later.

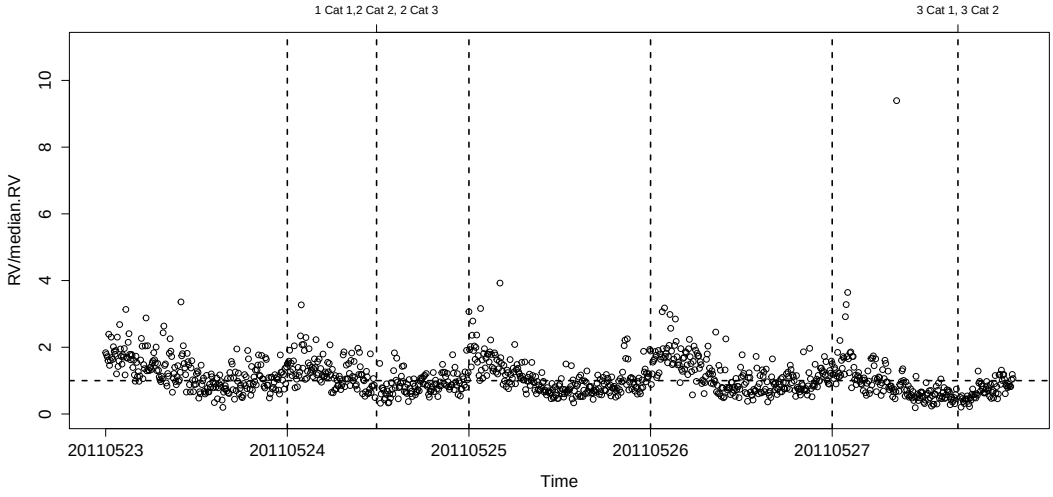

Figure 3.35: RRV by block, 5/23/2011 - 5/27/2011(MTWRF, pool 222), truncated

Figure 3.35 shows pool 222. There are 11 bad blocks in this pool, concentrated in two places. One Cat 1, 2 Cat 2 and 2 Cat 3 bad blocks happened right in the middle of the second day. The other 3 Cat 1 and 3 Cat 2 bad blocks occurred on the last day. These bad

blocks did not trigger volatility jumps in $[5, 10)$. Except for the bad blocks, the pattern of RRVs look like a good pool.

Table 3.17: Parameter re-estimation for six bad pools after "surgery"

Pool	$\widehat{\beta}$	$\widehat{\bar{c}}$	$\widehat{\gamma^2} \times 10^3$	jpvalue	median(RV)	blocks remaining
8	0.04	0.068***	117.7**	0.48	0.077	886
45	0.13***	0.19***	3.33***	0.85	0.17	1168
128	0.15***	1.1***	14.9***	0.38	0.99	1169
137	0.13***	0.13***	1.70***	0.73	0.11	1152
169	0.14***	0.21***	2.3***	0.59	0.24	870
222	0.11***	0.073***	0.73***	0.93	0.066	1159

After examining the path of these pools, I perform some "Surgery" on the RV sample and reestimate the Heston model. The surgery is not intended to be a general technique for dealing with jumps, but rather to provide some evidence that the Heston model describes the continuous component of the intraday volatility process even when jumps are present.

Table 3.17 present the estimation results for "the Great Six" after "Surgery". The last column of the table shows the median RV of the pool. For pool 8, I remove the 284 RVs when their RRVs are above 2.5 and combine the remaining blocks into a new pool. In the estimates for this new pool, $\bar{c}$ and γ^2 are significant. The estimation of β is not significant but has a z score of 1.33. I remove all the RVs during the Flash crash for pool 169. In other words, I exclude 300 RVs between 2:20PM on 5/6/2010 and 4:30PM 5/7/2010. I also get rid of the 5 bad blocks from 5/5/2010. This time all the parameter estimates become significant and model specification is good as well[4]. Moreover, the $\bar{c}$ estimate is 0.21, very close to the median RV of the pool.

[4]I ignore the overnight returns and treat RVs in the new pool as if they were from the same trading day in the estimation.

For the remaining four members of "the Great Six", I simply remove all the bad blocks. It turns out that all the parameter estimates are significant at 1% level and model specification are good. Meanwhile, all the $\bar{c}$ estimates are close to the median of RVs for the entire pool.

3.4.2 Bad pools with many jumps

The previous section covers the 6 bad pools that contain all the Cat 3 bad blocks for bad pools. I now discuss the other 6 bad pools in Table 3.8. Three are pools with many bad blocks, which are discussed in this section.

Table 3.18: Three bad pools with many jumps

pool	Time period	Cat 1	Cat 2	Cat 3
26	7/3/2007-7/10/2007	14	0	0
87	9/17/2008-9/23/2008	19	1	0
144	11/3/2009-11/9/2009	46	28	0

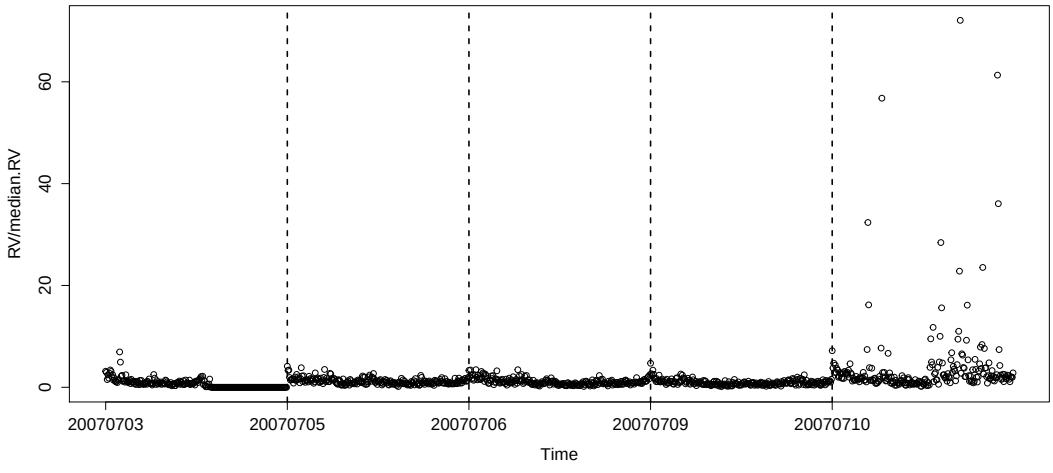

Figure 3.36: RRV by block, 7/3/2007 - 7/10/2007(TRFMT, pool 26)

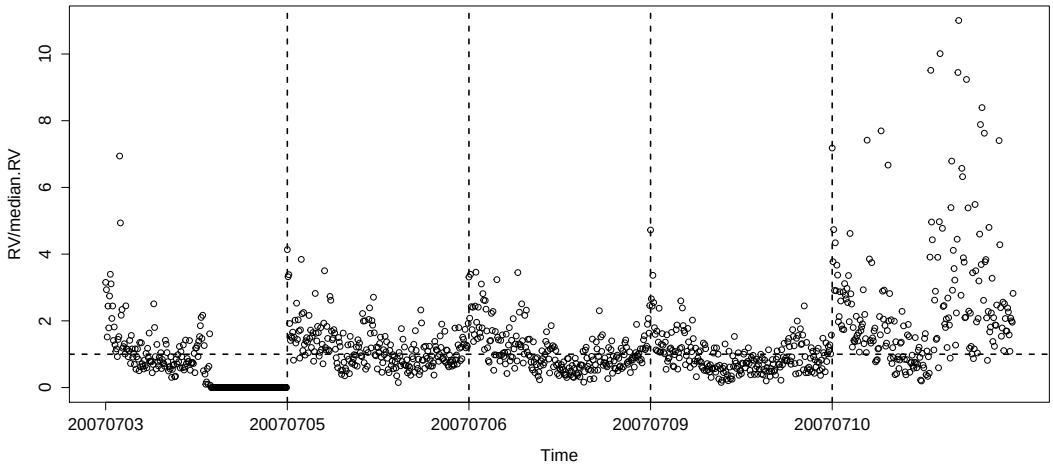

Figure 3.37: RRV by block, 7/3/2007 - 7/10/2007(TRFMT, pool 26), truncated

Figure 3.36 and 3.37 display the RRVs of pool 26. This pool is labeled as "Bernanke effect" because of the market reaction to a speech by Ben Bernanke on inflation on 7/10/2007. All 14 Cat 1 bad blocks occurred on this day, 11 right after the speech began at 1PM[5]. When Ben Bernanke gave little sign that the Fed would lower the interest rate in his speech, there was a large sell-off in the stock market.

[5]The first day of this pool shows the effect of half-day trading because the following day is a national holiday

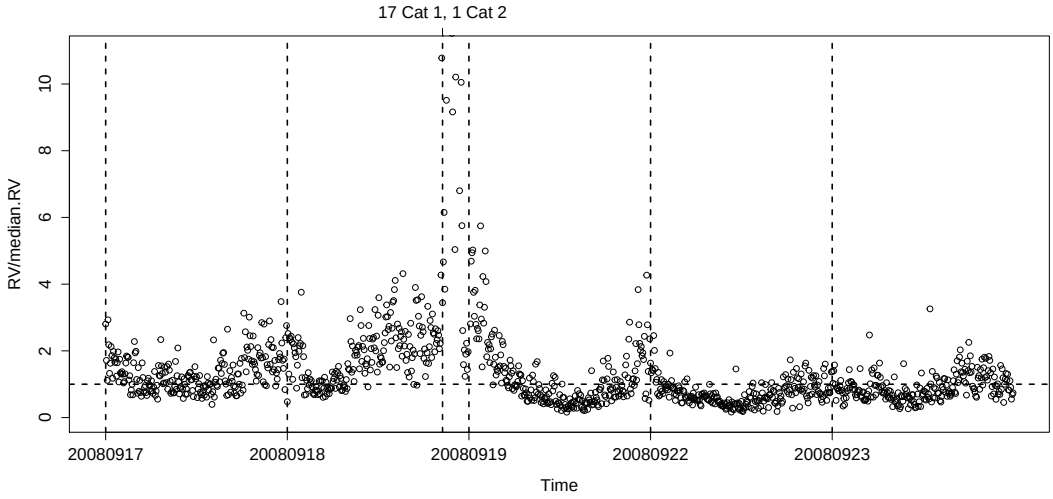

Figure 3.38: RRV by block, 9/17/2008 - 9/23/2008(WRFMT, pool 87), truncated

Figure 3.38 shows pool 87: labeled as the "Beginning of the financial crisis" in Table 3.8. This is the first day of the period we called the financial crisis in Chapter 1. The burst of volatility at the end of 9/18/2008 reflects the 410-point gain of the DJIA index in reaction bail-out plan to absorb money market bad debts that was submitted to the Congress. All of the 19 Cat and 1 Cat 2 bad blocks come from that time. They are accompanied by a series of middle-sized volatility jumps in $[5, 10)$.

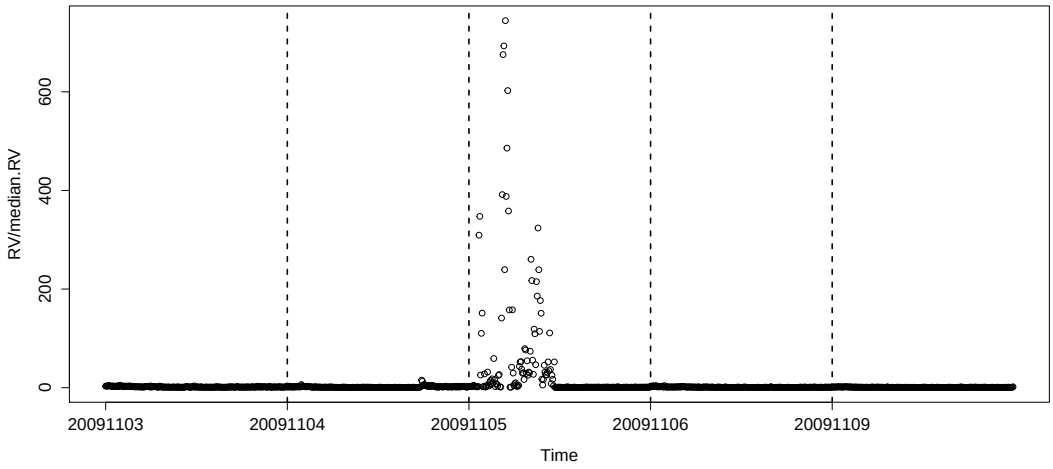

Figure 3.39: RRV by block, 11/03/2009 - 11/09/2009(TWRFM, pool 144)

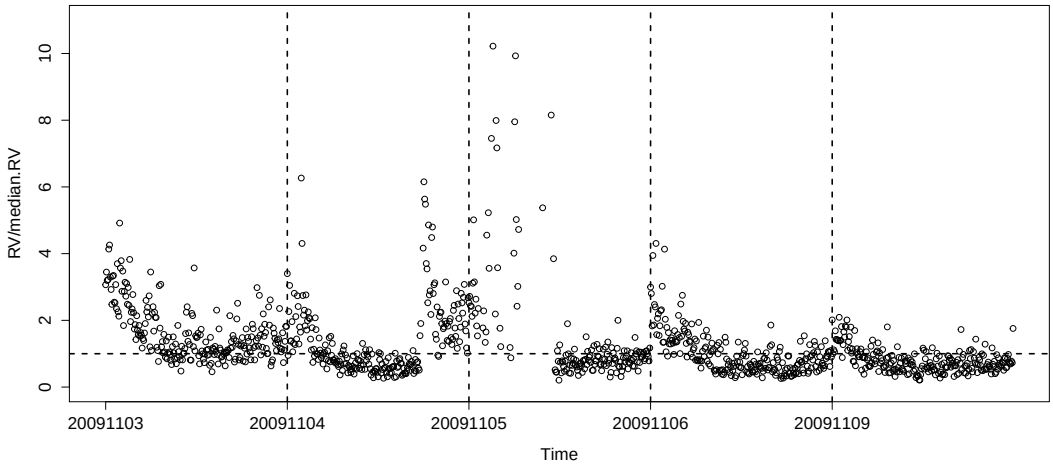

Figure 3.40: RRV by block, 11/03/2009 - 11/09/2009(TWRFM, pool 144), truncated

The last of the three is pool 144, which is plotted in Figure 3.39 and 3.40. There are many bad blocks in this pool so I truncate the graph to display the bottom structure. All 28 Cat 2 and 46 Cat 1 bad blocks appeared near the beginning of the third day. On this day, the DJIA index reclaimed 10,000 for the first time after the financial crisis. The market rallied when the government reported a bigger-than-expected drop in jobless claims.

3.4.3 Bad pools without large RVs

We have covered all the bad pools in Table 3.8 having bad blocks. In this last subsection, I now present some interesting bad pools without bad blocks.

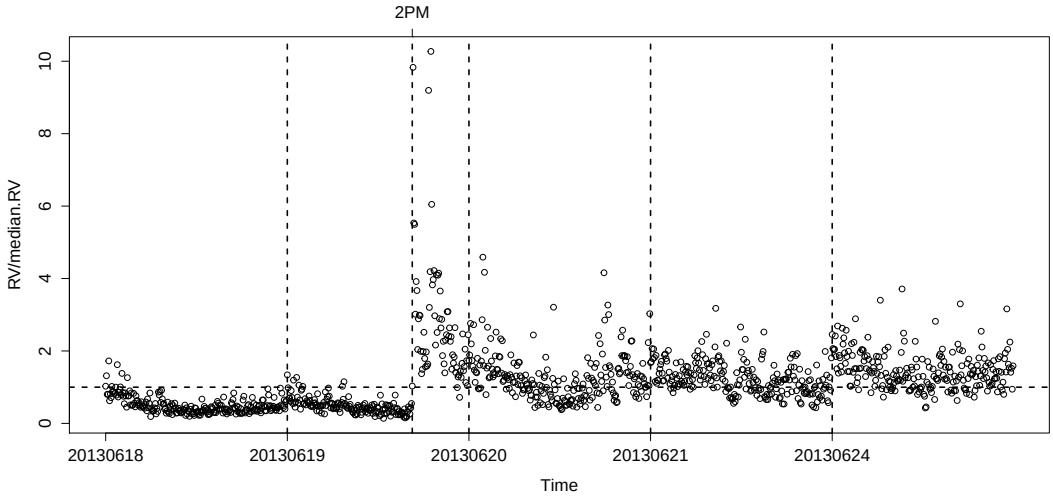

Figure 3.41: RRV by block, 6/18/2013 - 6/24/2013 (TWRFM, pool 326)

Table 3.19: Re-estimating Pool 326

	before	after
$\widehat{\beta}$	0.047*	0.128***
$\widehat{\bar{c}}$	0.05***	0.13***
$\widehat{\gamma^2}$	0.19	2.93*
jpvalue	0.73	0.65
median RV	0.04	0.13

Figure 3.41 plots a bad pool that is impacted by an FOMC announcement that happened at 2PM on the second day. Although there is no bad block in this pool, there is a clear

volatility cascade at the announcement time. Before the cascade, RRVs stay below 1 most of the time. After the cascade, the average level of volatility is considerably higher.

In fact, treating the volatility cascade as the start of a new pool, we could break this bad pool into two pools. Table 3.19 presents the estimation results of the two new pools, labeled "before" and "after". Both of the two new pools are good pools and the β and $\bar{c}$ estimates stay within the interquartile range of estimates for all good pools. The estimates of $\bar{c}$ are close to the median RVs of the two subpools.

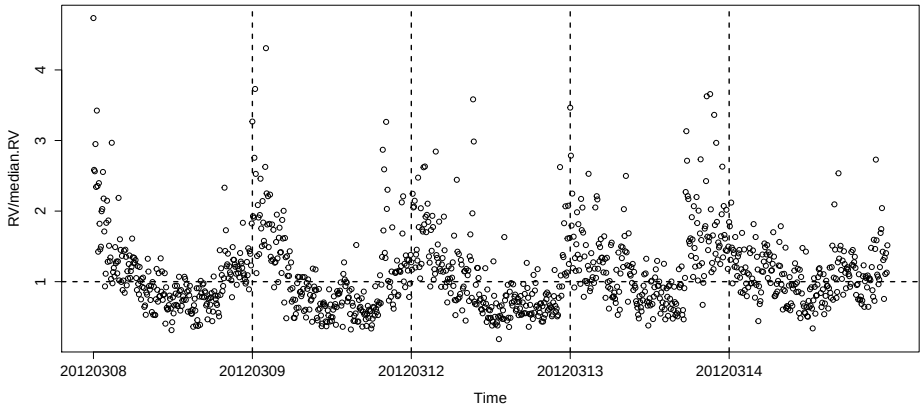

Figure 3.42: RRV by block, 3/8/2012 - 3/14/2012 (RFMTW, pool 262)

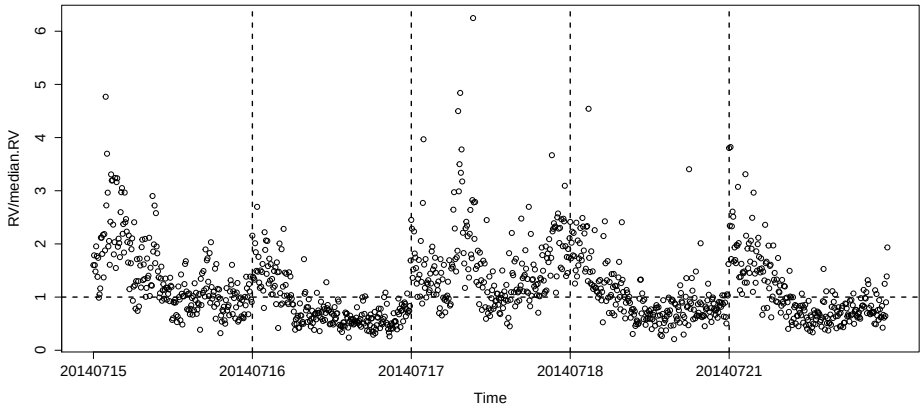

Figure 3.43: RRV by block, 7/15/2014 - 7/21/2014 (TWRFM, pool 380)

The bad pools, pool 262 and pool 380, are plotted in Figure 3.42 and 3.43. Both of the pool show high volatility at the beginning of each trading day. After the market opens, RVs quickly revert back to the mean and stay quiet mostly throughout the rest of the day. There is a volatility cascade on the third day of pool 380, at the time when Israel invaded Gaza. The DIJA plunged by 1.5% because of the event.

3.5 Good pools without bad blocks

This chapter so far has focused on large relative RVs that are 10 or higher. The evidence is convincing that these RRVs contain jumps in price or volatility. In this section, I focus instead on good pools without bad blocks.

Table 3.20: Parameter estimates of good pools

	all			without bad blocks		
	$\widehat{\beta}$	$\widehat{\bar{c}}$	$\widehat{\gamma^2}/10^3$	$\widehat{\beta}$	$\widehat{\bar{c}}$	$\widehat{\gamma^2}/10^3$
median	0.10	0.081	1.11	0.10	0.085	1.00
lower quartile	0.07	0.053	0.64	0.07	0.055	0.57
upper quartile	0.13	0.15	2.31	0.13	0.15	1.86
median standard error	0.031	0.006	0.52	0.031	0.005	0.38
mean	0.11	0.14	1.97	0.11	0.14	1.51
median z-score	3.16	15.11	2.33	3.17	17.05	2.53

Table 3.20 compares parameter estimates of the 286 good pools and the 155 good pools without bad blocks. There is not much difference in the order statistics of $\bar{c}$ and β estimates for good pools with and without bad blocks. However, taking out large jumps helps to improve the precision of parameter estimates. On the other hand, the order statistics of the volatility-of-volatility parameter estimates are smaller for good pools without bad blocks

than for all good pools.

Table 3.21: Distribution of middle sized jumps in good pools

	all	without bb	with bb
$[5, 10)$ (per pool)	1291 (4.51)	352 (2.27)	939 (7.17)
$[2.5, 5)$ (per pool)	13875 (48.51)	6166 (39.78)	9709 (74.11)

We have seen earlier in this chapter that large RRVs are often accompanied by a series of middle sized RRVs, RRVs larger than 2.5 but less than 10. Table 3.21 contrasts the number of RRVs in the intervals $[2.5, 5)$ and $[5, 10)$ in good pools with and without bad blocks. The number per pool is shown in parenthesis. In the introduction to this chapter I argued that 2.5 is the natural threshold of outliers for the RRV distribution. The table shows that RRVs in the range of $[5, 10)$ are much more likely to appear in good pools that contain RRVs larger than 10. The number of RRVs in the interval $[5, 10)$ per pool for good pools with bad blocks is 7.17 but only 2.27 for good pools without bad blocks.

Now I would like to show some examples of good pools with no bad blocks. Figures 3.44 to 3.51 plot the path of RRVs for 8 good pools without bad blocks. I use two horizontal dashed lines to indicate 2.5 and 5, and another horizontal dashed line to indicate the level of $\widehat{\bar{c}}$ relative to the median RV of the pool. In these figures very few RRVs lie in $[5, 10)$ and RRVs in the range of $[2.5, 5)$ are typically concentrated at the beginning of a trading day. Table 3.22 summarizes the number of RRVs in $[5, 10)$ for these pools. We see most of them have less than 5 cases. The estimates of $\bar{c}$ are very close to the median RV of the pool as well.

Overall, the market usually starts with high volatility at the beginning of each day and quickly reverts to the mean. Occasionally we observe small volatility jumps in the middle of the day. For example on 7/21/2010 in pool 179, the S&P 500 tumbled by 14 points right after a speech by Fed Chairman Ben Bernanke at 2PM. The market reverts back to equilibrium after the event.

Table 3.22: Number of RRVs in $[5, 10)$, good pools without bad blocks

pool	3	43	106	159	179	203	308	345
count	5	1	2	6	2	1	4	3

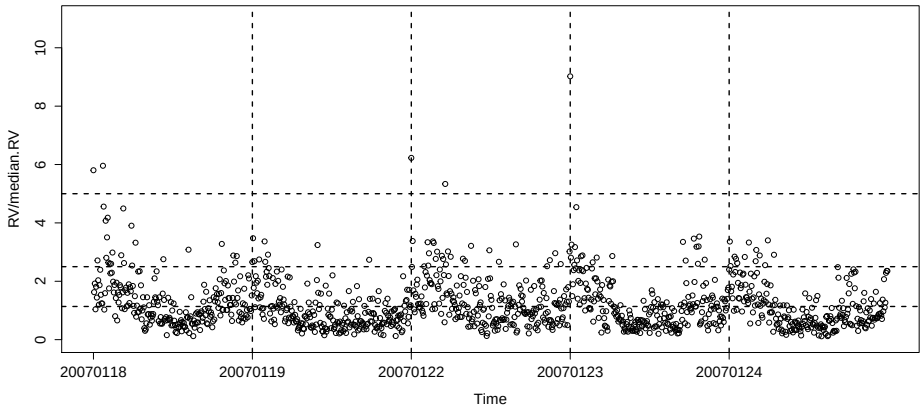

Figure 3.44: RRV by block, 1/18/2007 - 1/24/2007 (RFMTW, pool 3)

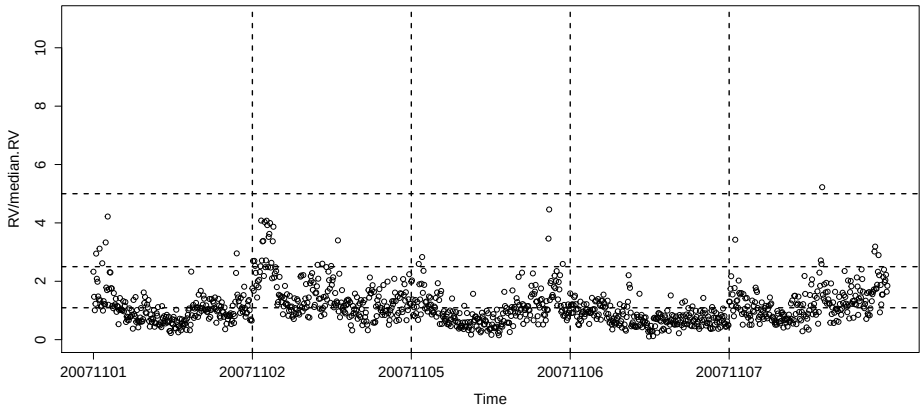

Figure 3.45: RRV by block, 11/01/2007 - 11/07/2007 (RFMTW, pool 43)

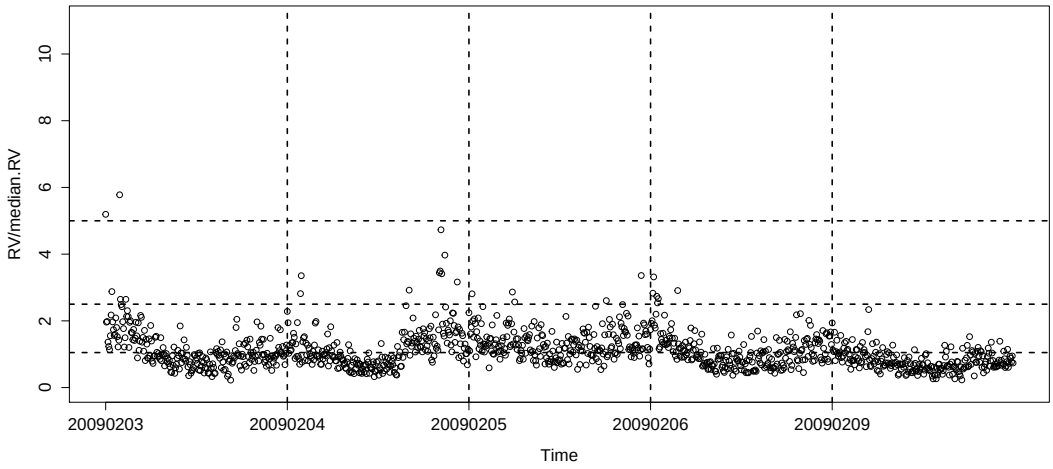

Figure 3.46: RRV by block, 2/3/2009 - 2/9/2009 (TWRFM,pool 106)

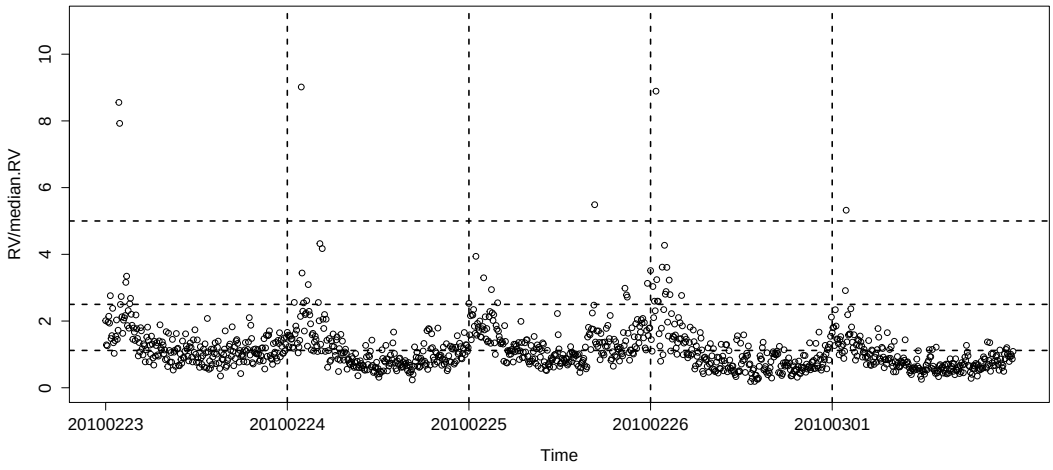

Figure 3.47: RRV by block, 2/23/2010-3/1/2010 (TWRFM, pool 159)

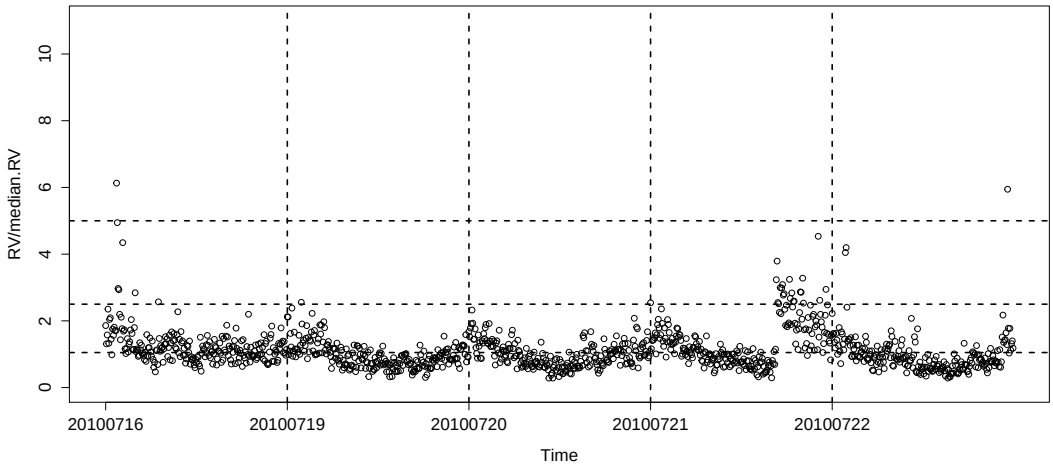

Figure 3.48: RRV by block, 7/16/2012 - 7/22/2010 (FMTWR, pool 179)

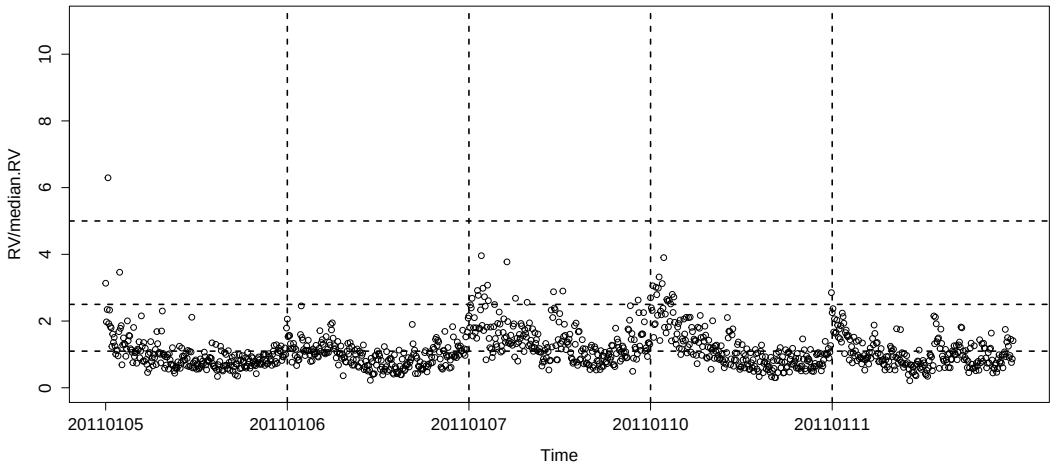

Figure 3.49: RRV by block, 1/5/2011 - 1/11/2011(WRFMT, pool 203)

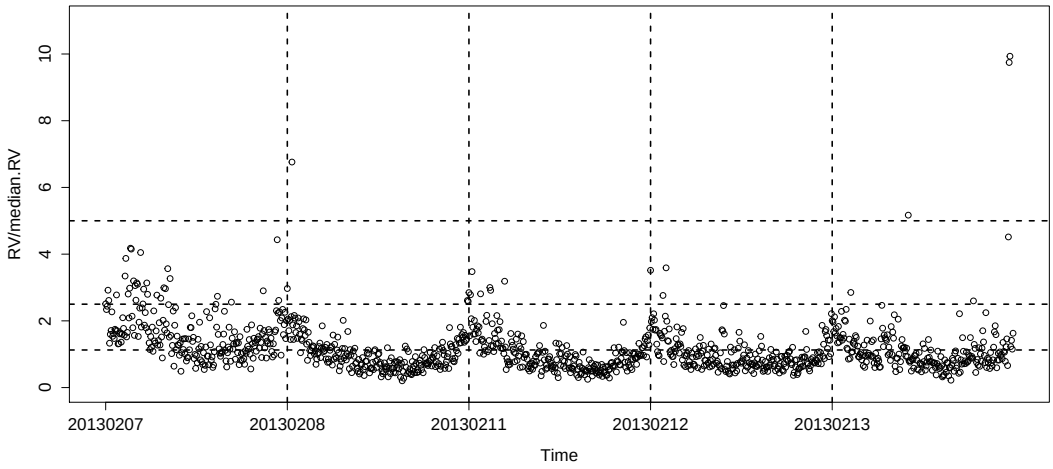

Figure 3.50: RRV by block, 2/7/2013 - 2/13/2013 (RFMTW, pool 308)

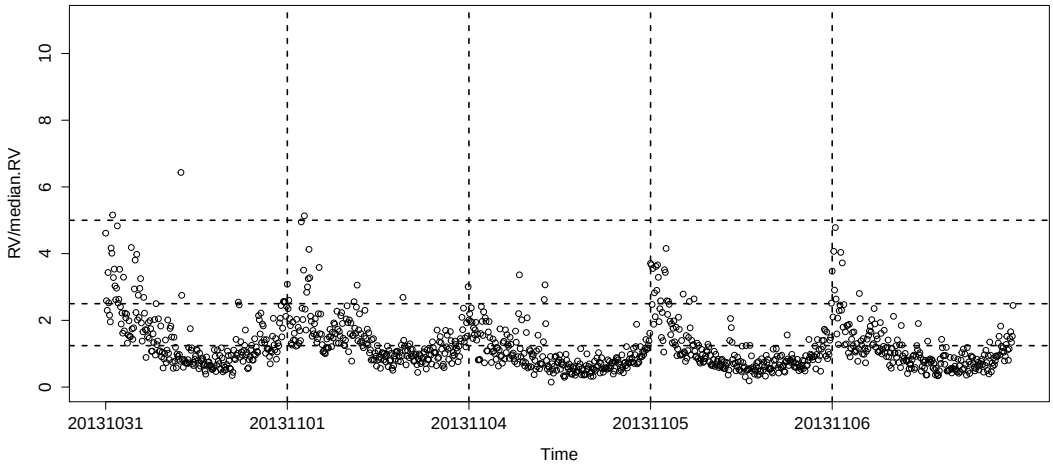

Figure 3.51: RRV by block, 10/31/2013 - 11/06/2013 (RFMTW, pool 345)

Figure 3.52 plots the average RRV for each block over our 8-year sample period for the 155 good pools without bad blocks. The graph coincides with the "U-shape" pattern often mentioned in the literature of realized volatility. The Heston model provides an explanation for the decline of realized volatility at the beginning of the day: The realized volatility process takes time to reach the equilibrium after the market opens. Although the average

RRV summarizes the pattern, the Heston model also describes the dynamics in the volatility process.

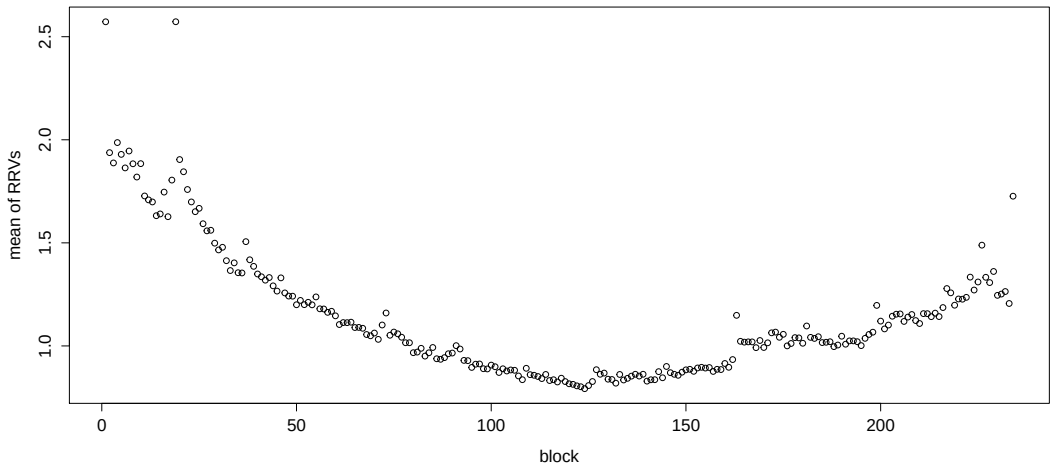

Figure 3.52: Average RRVs for good pools without bad blocks

3.6 Conclusion

This chapter examines the path behavior of 100-second relative RVs to find evidence for jumps in the Heston model. My conclusions are as follows:

- Jumps exist. Although most relative realized RVs are not large, many pools have at least one RRV above 10.
- Jumps are much more likely to appear in bad pools than good pools. Bad pools have four times more bad blocks per pool than good pools. Removing blocks with large relative RVs in bad pools can improve the estimation results.
- Large jumps often trigger cascades of smaller jumps. These cascades are usually attached to specific economic events. Examples including the Flash Crash and FOMC announcements. The duration of these cascades reflects the severity of the information shock. For instance, it took more than one day for the market volatility to settle after

the Flash Crash. However, the market volatility often stays high for less than half of a trading day after a FOMC announcement.

- Volatility typically stays high at the beginning of a trading day, which suggests that the Heston model requires time to reach equilibrium.

- Measuring realized volatility over 100-second intervals provides useful information about the path behavior of the volatility process. The literature on market microstructure noise suggests that stock prices should be sampled once every 5 minutes. As the plots of relative RVs in this chapter demonstrate, 100-second RVs computed using prices sampled once a second are useful not only in estimating the parameters of the Heston model but also in identifying departures from the model.

REFERENCES

Aït-Sahalia, Yacine, and Jean Jacod (2014), *High-Frequency Financial Econometrics* (Princeton University Press).

Anderson, Torbin, Tim Bollerslev, Francis X. Diebold and P. Labys, 2000, Great Realizations, *Risk* 13, 105–108.

Bryan Ellickson, Benjamin Hood, Tin Shing Liu, Duke Whang, and Peilan Zhou. Stocks in the Short Run. *Unpublished Manuscript*, Department of Economics, UCLA, 2012.

Bollerslev, Tim, Hao Zhou, 2002, Estimating stochastic volatility diffusion using conditional moments of integrated volatility, *Journal of Econometrics*, 109, 33-65.

Bergantini, Daniele (2013), Moment-based estimation of stochastic volatility, *Journal of Banking & Finance* 37, 4755-4764.

Corradi, Valentina and Walter Distaso (2006), Semi-parametric comparison of stochastic volatility models using realized measures, *Review of Economic Studies* 73, 635-667.

Cox, John, Jonathan Ingersoll, and Stephen Ross, 1993, A theory of the term structure of interest rates, *Econometrica* 53(2), 385–407.

Feller, William, 1951, Two singular diffusion problems, *Annals of Mathematics* 54(2), 173–182.

Garcia, Rene, Marc-Andre Lewis, Sergio Pastorello and Eric Renault (2011), Estimation of objective and risk-neutral distributions based on moments of integrated volatility, *Journal of Econometrics*, 160, 22-32.

Heston, Steven, 1993, A closed-form solution for options with stochastic volatility with applications to bonds and currency options, *Review of Financial Studies* 6, 327–343.

Mykland, Per and Lan Zhang, 2009, Inference for continuous semimartingales observed at high frequency, *Econometrica* 77(5), 1403–1445.

Protter, Philip, 2004, *Stochastic Integration and Differential Equations* (Springer-Verlag, New York).

Shreve, Steven, 2004, *Stochastic Calculus for Finance: II* (Springer-Verlag, New York).

Sun, Miao (2016), Modeling Volatility Using High Frequency Data, Ph.D. thesis, Department of Economics, UCLA.

Whaley, Robert, 1993, Derivatives on market volatility: Hedging tools long overdue, *Journal of Derivatives* 1, 71–84.

Whaley, Robert, 2009, Understanding VIX, *Journal of Portfolio Management* 35 (Spring), 98–105.